CHARACTERIZATION, COMPOSITION AND SOURCE IDENTIFICATION
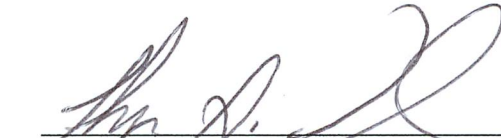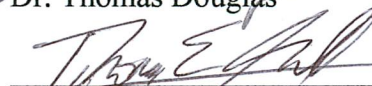
OF IRAQI AEROSOLS

By

Jennifer Michelle Bell

RECOMMENDED:

_____
Dr. Thomas Douglas

_____
Dr. Thomas Gill
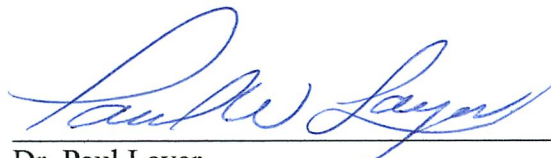
_____
Dr. Thomas Kuhn
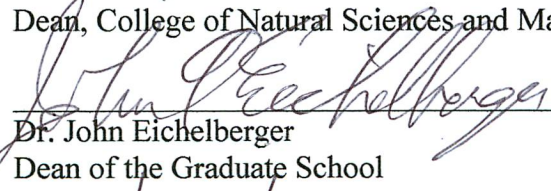
_____
Dr. William Simpson
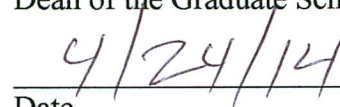
_____
Dr. Catherine Cahill
Advisory Committee Chair

_____
Dr. William Simpson
Chair, Department of Chemistry and Biochemistry

APPROVED:

_____
Dr. Paul Layer
Dean, College of Natural Sciences and Mathematics

_____
Dr. John Eichelberger
Dean of the Graduate School

_____
4/24/14
Date

CHARACTERIZATION, COMPOSITION AND SOURCE IDENTIFICATION

OF IRAQI AEROSOLS

A

DISSERTATION

Presented to the Faculty

of the University of Alaska Fairbanks

in Partial Fulfillment of the Requirements

for the Degree of

DOCTOR OF PHILOSOPHY

By

Jennifer Michelle Bell, B.S., M.P.A. M.S

Fairbanks, Alaska

May 2014

Abstract

Soldiers that are deployed overseas are breathing ambient air containing concentrations of fine particulate matter known to cause adverse effects to human health. A study initiated in 2008 was designed to determine the concentrations and compositions of fine particulate matter in Baghdad, Iraq. This study used a Davis Rotating drum Unit for Monitoring (DRUM) aerosol impactor to continuously collect size (eight stages between 0.09 and 10 microns in aerodynamic diameter) and time (hour and a half resolution) resolved aerosol samples for mass concentration and elemental composition analyses. Results of this study show that fine particulate matter is associated with geogenic and anthropogenic source emissions. Trace metal concentrations combined with vanadium (V) can be correlated to industrial and urban source emissions, while lead (Pb) is associated with geogenic and anthropogenic sources. The mass loadings on the finest size fractions (0.09-0.26) of the DRUM aerosol impactor (0.09-0.34 microns) correlated with the mass loadings of coarse particles (2.5-10.0 microns) as both had similar elemental mass ratios, and thus were interpreted as having a common geogenic source. Brittle fragmentation theory was incorporated in this study to assist in explaining particle behavior and was effective at explaining particle breakdown in no wind/low wind situations. The aerosol particle samples collected during this study contained high total soil mass concentrations in all size stages. However, a peak in mass concentration was observed within the ultrafine (0.09-0.26 microns) stage that is not consistent with current hypotheses about the size distribution of mechanically produced soil particles through brittle fragmentation theory. The production of soil particles cannot fully be explained by brittle fragmentation theory during high wind scenarios. It is more likely that a combination of processes (brittle fragmentation, saltation, long-range transport, and midair collisions during high wind conditions) occur that result in excess mechanical grinding to

produce ultrafine soil particles during high wind scenarios. A calibration study was conducted on the 8-stage DRUM aerosol impactor to ensure that the production of ultrafine particles was not a result of brittle minerals (calcium sulfate, sodium bicarbonate, and finely ground quartz) breaking down in the sampler. Mineral particles were not observed on the smallest size fractions under either 'wind' (4.1 m/s) or 'high wind' (8.3 m/s) conditions. This fact confirmed that the particles were not breaking down into smaller particles than observed in the initial size distribution characterized by an optical particle counter. These findings suggest that the increases in soil element concentrations on the DRUM stages seen in data sets from Iraq and White Sands, NM, are not a product of particle fragmentation during sampling. The production of these particles are important in that the fine particulate matter concentrations frequently exceed military exposure guidelines of 65 μg m^{-3} and individual constituents, such as lead, exceed U.S. national ambient air quality standards designed to protect human health.

Table of Contents

List of Figures

List of Tables

Chapter 1 Introduction

1.1　　History of Air Pollution

Anthropogenic degradation of air quality is not a new phenomenon tied strictly to the industrial revolution. Ancient records indicate that as early as 900 BC, King Tukulti complained of a noticeable smell in the air from the small asphalt-mining town of Hit, located in the vicinity of our present day Iraq. The "smell" was associated with the hydrogen sulfide fumes emitted when mining ulmeta rocks (Brimblecombe, 1995). In 1306 King Edward of England initiated the first air quality measures—he banned the burning of coal when his mother, Queen Eleanor, fled Nottingham Palace after succumbing to fumes emitted from its combustion (Evelyn, 1995; Hopke, 2009).

King Edward's ban was the first documented attempt at regulating air quality to protect human health. Over the next few centuries correlations were made between the degradation of air quality and a rise in morbidity rates in affected areas. The most noted of these involved the emission and trapping of sulfur dioxide over Meuse Valley, Belgium, Pennsylvania, US, and London, England.

1.1.1　Meuse Valley, Belgium—1930

The Meuse Valley, between the towns of Huy and Liège, was once considered the most industrialized area of Europe (Nemery et al., 2001). The Valley was heavily lined with steel mines, zinc smelters, fertilizer and explosive plants, and glass manufacturers that emitted significant quantities of sulfur dioxide, sulfuric acid, and fluoride gases directly into the atmosphere (Bell and Davis, 2001). Emissions of industrial pollutants coupled with 5 days (December 1-December 5, 1930) of thick fog, promulgated by anticyclonic conditions and a temperature inversion, resulted in the accumulation of sulfur containing particles (1-4 μm in

1

diameter) over the Valley. By December 3, hundreds of people living in small fishing villages along the river began exhibiting signs and symptoms of respiratory distress (Nemery et al., 2001). The final few days of the smog event resulted in the deaths of more than 60 people, 10 times the town's normal morbidity rate (Firket, 1936).

1.1.2 Donora, Pennsylvania—1948

Similar to the Meuse Valley Incident, the first severe air pollution episode recorded in the United States, October 27 to October 30, 1948, was caused by the release of industrial pollutants that had become trapped within an anticyclonic inversion (Hopke, 2009). The three day event ended with 20 dead and 6000 ill (Hopke, 2009), increasing the small town's norm morbidity rate by 6 times (Davis, 2000; Schrenk et al., 1949).

1.1.3 London, England—1952

The most noted early air pollution episode was the London Smog of 1952. At a peak measurement of 4.46 mg/m^3 (Scott, 1953), 5-19 times greater than normal particulate matter (PM) concentrations (Bell and Davis, 2001), the 1952 episode brought issues pertaining to air quality to the forefront of public scrutiny and contributed to the establishment of regulatory controls on industrial emissions.

The region's typical foggy and humid weather conditions were worsened by a temperature inversion, resulting in unusually colder temperatures from December 5-9, 1952. Air quality had declined due to coal combustion to heat private homes. The demand for heat in private homes magnified the average amount of smoke and soot normally released from the daily operations of power plants and factories. As a result the stagnant air masses over London trapped large quantities of sulfur oxides (SO$_x$) in the atmosphere. Government reports indicate that the sulfur-enriched fog was responsible for 3,000 more deaths than normal (Ministry of

Health, 1954). It is estimated that between the months of January and February over 8,000 people died from complications due to respiratory and cardiac related illnesses brought on by foul air (Ministry of Health, 1954). This was approximately 3 times the expected morbidity rate (Ministry of Health, 1954).

1.2   Health Effects Associated with Long Term Exposure to Poor Air Quality

Epidemiological investigations that study the effects of chronic and acute exposure to air pollution in populations living in/around industrial areas find significant correlations between the aerosol particle exposure and decline in human health (Bates, 1992; Schwartz and Marcus, 1994; Seaton et al., 1995). Research conducted at 14 locations shows increases in morbidity with increasing particulate concentrations (Bates, 1992; Schwartz and Marcus, 1994; Seaton et al., 1995). The documented rise in insurance claims (Bell and Davis, 2001) for individuals admitted to the hospital due to exacerbation of respiratory and cardiac illnesses during peak particulate events (Dockery et al., 1989) strongly affirm that illness and air quality are related (Seaton et. al., 1995). There are also known increases in morbidity associated with short-term exposure to inhalable (≤ 10 μm) particulate matter and exposure to air pollutants (Katsouyanni et. al., 1995). Particulate matter is a complex mixture of extremely small solid particles (acids, dust, organics, metals, soil) and liquid droplets. The Environmental Protection Agency (EPA) defines fine particulate matter as particles and droplets with an aerodynamic diameter of 2.5 microns ($PM_{2.5}$). Coarse inhalable particles are defined as having aerodynamic diameters larger than 2.5 microns but smaller than 10 microns (U.S. Environmental Protection Agency accessed at www.epa.gov/air/caa/).

To understand the effects on human health associated with poor air quality, it is necessary to discuss particle size in relation to respiratory illnesses. An analysis conducted

across six eastern U.S. cities indicated that an increase of 10 μg/m^3 in fine particulate matter correlated with a 1.1% increase in mortality, a 3.3% increase in chronic obstructive pulmonary disease, and a 4.0% increase in pneumonia related deaths (Schwartz et al., 1996).

Most experts agree that particulate matter with an aerodynamic diameter of ≤10 μm (PM$_{10}$) is responsible for a decline in human health; however, there is disagreement as to the pollution level that first causes significant impacts (Dockery and Pope, 1994). Pope et al. (1995) suggested concentrations exceeding 150 μg/m^3 may be responsible for a 7% decrease in lung function and a 1-10% increase in respiratory symptoms (e.g., cough, lower respiratory symptoms, and asthma attacks). Schwartz et al. (1996) showed a correlation between a 30 μg/m^3 increase in PM$_{10}$ and a 12% increase in asthma related hospital visits. Thurston et al. (1992) found a 1.9% to 2.1% increase in asthma hospital admissions for each 10 μg/m^3 increase in daily mean PM$_{10}$. Pope et al. (2002) showed 10 μg/m^3 increases in annual average PM$_{10}$ correlated with an increase in overall mortality of 4%, cardiopulmonary mortality of 6%, and lung cancer mortality of 8%. Increased incidences of illness associated with degraded air quality have led to tighter controls on emission with the passing of and subsequent amendments to the U.S. Clean Air Act of 1963.

1.3   Clean Air Act

Established in 1963, the Clean Air Act (CAA) provided the legal justification for the Secretary of Health, Education, and Welfare (HEW) to intervene when the pollution problems of a given state endangered the health and well-being of the population of another state (U.S Environmental Protection Agency accessed at www.epa.gov/air/caa/). At the time of its passage, the Act was exclusively concerned with pollution emitted from stationary sources (U.S Environmental Protection Agency accessed at www.epa.gov/air/caa/). The passage of

subsequent amendments refined the CAA to include air quality criteria that both state and local government were to achieve and the time frame during which the achievements were to be made. The subsequent Clean Air Act of 1990 encompassed a broader spectrum of polluting sources - including emission criteria/objectives for area and mobile sources (U.S. Environmental Protection Agency accessed at www.epa.gov/air/caa). The Clean Air Act required the EPA to establish National Ambient Air Quality Standards (NAAQS: 40 CFR part 50) for pollutants considered environmentally harmful. The NAAQS identified six criteria pollutants (U.S. Environmental Protection Agency accessed www.epa.gov/air/criteria.html) for which both primary and secondary standards have been established; Table 1-1 identifies the NAAQS pollutants pertinent to this dissertation.

Primary standards are stringent to ensure that safety factors for the protection of individuals at risk (the elderly, children, and those with pre-existing respiratory illnesses) are included in public health objectives. Secondary standards are more general and are designed to protect public welfare, animal health, and aesthetics (U.S. Environmental Protection Agency accessed at www.epa.gov/air/criteria.html). The 24-hour mass standards for fine particulate matter ($PM_{2.5}$) were reduced in 2006 as a means of protecting U.S. citizens from short and long-term aerosol exposures (Federal Register, 2006). Although the U.S. EPA has designed these standards to protect citizens within its jurisdiction, it does not regulate the air quality of U.S. military personnel deployed abroad.

1.4   Acute Lead Toxicity

Another aspect of air pollution encountered in Iraq is airborne lead (Cahill, 2009). Acute lead symptomatic poisoning is life threatening and is a result of acute toxicity via inhalation or ingestion. Persons inflicted with acute symptomatic poisoning are likely to experience

abdominal colic, constipation, fatigue, anemia, peripheral neuropathy and alterations of central nervous system (CNS) functions (Cullen et al., 1983). The illness can progress to acute encephalopathy with coma, convulsions, and papilledema (optic disk swelling caused by increased cranial pressure; Cullen et al., 1983). Acute lead encephalopathy may result in irreversible neurological and behavioral disorders (Byers and Lord, 1943).

1.5   U.S. Military Exposure Guidelines and the USACHPPM

In 1996, the U.S. Army Center for Health Promotion and Preventive Medicine (USACHPPM), a military support organization consisting of toxicologists, environmental health risk assessors, physicians, industrial hygienists, chemists, and environmental engineers, issued the Technical Guide (TG) 230 Version 1.3–Chemical Exposure Guidelines for Deployed Military Personnel (USACHPMM RD 230, 2013). To ensure a safer working environment, the goal of the USACHPPM was to create preventive medicine guidelines for wartime soldiers' chemical exposures (USACHPPM RD 230, 2013). By 1997, the USACHPPM received additional funding from the Army Office of the Surgeon General (for Nuclear, Biological, and Chemical issues) to address delayed and/or prolonged health effects experienced by veterans from chemicals that did not pose an immediate threat to life during deployment.

By monitoring low-level exposures of military personnel to radiation and chemicals, the Department of Defense continues to take steps to ensure the health of its military personnel under Forced Health Protection (FHP). USACHPPM determined military exposure guidelines (MEGs) based on chemical contact and sensitivities deployed soldiers would likely experience. These numbers are based on upper confidence limits of acquired data, and include uncertainty factors. The following assumptions were made when establishing the MEGs (USACHPPM RD 230, 2013):

- Deployed military populations consist of healthy and fit males and non-pregnant female adults – in such cases that a female learns of pregnancy following deployment and given that the greatest fetal concerns exist during the first trimester, toxicity and reproductive effects were considered, when available, for establishing guidelines.
- Military personnel are assumed to be between the ages of 18-55.
- The average deployed person weighs approximately 70-kg.

Since deployment could range anywhere from weeks to years, and exposures vary between jobs, scenarios were designed for both short-term and long-term exposures. Short-term MEGs do not cover acute exposure; rather, they are designated for a longer time frame (1-year). MEGs specifically identify 1-year as the target for short-term exposure as they are designated to ensure a protective working environment 24-hrs/day for 365 days (USACHPPM RD 230, 2013). Long term exposure has two classifications 1) a lengthier tour (>1year) and 2) multiple short-term exposures that are consecutive.

1.6   Air MEGs

Discussed below are the three health level classifications (minimal, significant, and severe), which are designated under the 1-hour air MEGs (USACHPPM RD 230, 2013):

- 1 hour Minimal Effects – Air concentrations exceeding this level could result in mild, non-disabling, transient, reversible effects.
- 1-hour Significant Effects – Air concentrations exceeding this level could begin to elicit irreversible, permanent, or serious health effects.
- 1-hour Severe Effects – Air concentrations exceeding this level could elicit life threatening or result in lethal effects for a small subpopulation.

Additional factors were included to make guidelines applicable to a deployed soldier's breathing environment (USACHPPM RD 230, 2013):

- Deployed soldiers will experience continuous exposure, that is, 24-hr/day – 365 days/yr.

- Deployed soldiers are physically more active than the general population and will likely have increased ventilation rates of 29.2 m^3/day. This exceeds the calculated ventilation of 20 m^3/day for non-military personnel.
- Under this calculation, ambient air is considered to be constant.

The deployed soldier's derived ventilation rate is based on probable activities (standing in a fox hole, guard duty, load carriage, dig defensive positions) and the expected duration of activities military personnel are likely to participate in on any given day. It is important to note that the calculated average is based on "normal" military operations and may vary based on the level of activity required for a given mission or mission location.

As a means of estimating the inhalation rate, the USACHPPM assumed the personnel spent 6-hours sleeping (inhalation rate (IR) = 0.4 m^3/hr), 4-hours eating and/or other sedentary activities (IR = 0.5 m^3/hr, EPA), 6-hours completing light duties (IR=1.2 m^3/hr, arithmetic mean of all light intensity activities), and 8-hours (IR= 2.2 m^3/hr, arithmetic mean for digging related tasks) engaging in moderate duties (USACHPPM RD 230, 2013). Inhalation rates were calculated based on a 70 kg male because men tend to have higher respiration rates than females (USACHPPM RD 230, 2013). These assumptions were used for deriving the weighted ventilation rate of 29.3 m^3/day shown in USACHPPM RD 230 (2013).

Given that active duty military personnel are assumed to have higher ventilation rates than the average person, the EPA threshold limit values (TLVs), shown in Table 1-2, were adjusted to meet military needs. It should be noted that the TLVs are higher than those suggested by the U.S. EPA because the MEGs do not include higher safety factors for the young, elderly, and immunosuppressed. Table 1-2 provides the TLVs used to develop MEGs for wartime soldiers.

The adjusted threshold limits used for development of MEGS are based on an extended 40-hr week (5 days/week exposure is assumed for members of the general working population, while 7 days/week are assumed for active duty soldiers). Increasing the hours of the work week will also increase the default ventilation rate (10 m^3/8 hrs) established by the Occupational Safety and Health Administration (OSHA) for allowable exposure to breathable workplace pollutants. Wartime soldiers live in their work environment; as such, they are continuously (24hr/day, 7days/week) exposed to workplace pollutants. Due to their increased exposure to ambient conditions, the MEGs were established to address their exposure levels, which increase the ambient default of 10 m^3/20 m^3 to 20 m^3/29.3 m^3/day.

1.7   Soil MEGs

Chemicals that adhere to soil particles can be inhaled as fugitive dust during storms and while digging. Fugitive dust is classified using soil MEGs. The ability of nonvolatile chemicals to liberate as fugitive dust during soil agitation is estimated using a Particulate Emission Factor (PEF) of 1.32 x 10^9 m^3/kg (USACHPPM RD 230, 2013). PEF parameters are derived from the U.S. EPA recommended default values and are not representative of geographical regions outside of the U.S. The absence of actual field data values in military war zones outside of the U.S. presents limitations for accurate predictions (USACHPPM RD 230, 2013). Since air MEGs are expressed in terms of the gaseous phase, soil MEGs were used to evaluate aerosols. Soil MEGs assume a body weight of 70-kg, exposure duration of 1-year, a target risk factor of 1x10^{-4}, an inhalation rate of 29.2 m^3/day, and a particle emission factor of 1.32x10^9 m^3/kg (USACHPPM RD 230, 2013).

1.8   Project Background and Justification

Recent reports have indicated that aerosol concentrations ($PM_{2.5}$) in military areas of operation are higher than the allowable 24-hour average mass-based standards established by the U.S. EPA in 2006 for the safety of U.S. citizens (Engelbrecht et al., 2009; Sheehy, 2008) and exceeds the MEGs (Engelbrecht et al., 2009) designed for the protection of soldier health. The Battlefield Environment Division of the Army Research Laboratory, in conjunction with the USACHPPM, has prioritized understanding the warfighter's aerosol environment through its commitment to obtain aerosol samples used for health impact studies in its "Aerosol Characterization for Soldiers' Health Initiative" (Sheehy, 2008). However, instrumentation limitations did not provide aerosol information of sufficient quality and quantity for medical and environmental health determinations (Weese, 2008). Aerosol data that can provide the information needed for medical health determinations and meet the time resolutions required for acute epidemiological studies needs to include information on the size, concentration, and chemical composition of the particulate matter (Cahill, 2009).

The focus of the aerosol characterization portion of the three-year Department of Defense (DOD) funded research project (Grants: W911NF-07-1-0346, W911NF-08-1-0318, and W911NF-09-0543) was to develop analytical protocols for characterizing biological aerosols collected using ground-based or UAV-based cascade impactor aerosol samplers, and to expand the use of DRUM aerosol impactors in other military interest areas for the purpose of aiding environmental, human health, and source determination studies. As a component of this research program, the purpose of this dissertation's research was: 1) to characterize the chemical composition of Iraqi aerosols utilizing an 8-stage cascade DRUM impactor; 2) to determine the

predominate sources of dominate aerosols within the region; and 3) to understand the behavior of aerosols found in Iraq.

1.8.1 Vicinity

Iraq is located in the NE corner of the Arabian Peninsula and lies between latitudes 29° 5' and 37° 15' and longitudes 38° 45' and 48° 45' (Buringh, 1963; Sibrava, 2006). The general vicinity of Iraq is depicted in Figure 1-1. The country is bordered by the Taurus Mountains of Turkey to the north, Zagros Mountains of Iran to the east, Saudi Arabia to the south, and Jordan and Syria to the west and northwest (Sibrava, 2006). Physiograpically, Iraq is located in the Tigris and Euphrates drainage, near the center of the so-called "Fertile Crescent" of Mesopotamia (Figure 1-2), and is characterized by a topographical low extending from central Syria to Saudi Arabia (Sibrava, 2006). The country is divided into 5 physiographic regions unique in their hydrology, geology, and climate: Jezira, the Foothills, the Northern Desert, the Lower Mesopotamian Plain, and the Southern Desert (Buringh, 1963).

1.8.2 Iraq's Climate

Iraq is characterized as having a subtropical climate with a mean temperature of 73°F in Baghdad (National Oceanic and Atmospheric Administration accessed at www.ncdc.noaa.gov/oa/climate/afghan/iraq-narrative.html). It is known for its hot, arid, low-pressure summers that bring about strong Shamal (northeasterly) winds and cool, high-pressure winters that drive the Kous (southeasterly) winds (National Oceanic and Atmospheric Administration accessed at www.ncdc.noaa.gov/oa/climate/afghan/iraq-narrative.html). The strong Shamal winds are primarily responsible for the extreme dust events observed during the spring and summer. Strong Shamal winds carry large plumes of dust from the Taurus and Zagros mountains into the recessed plains of Iraq.

The dust clouds observed in Iraq are the result of low-pressure systems creating winds with sufficient energy for particles to break free of the topsoil and entrain in the passing storm (Thoppil and Hogan, 2010; Foda et al., 1985). The strong winds are most prevalent during daytime hours due to surface winds becoming less hindered by friction as the lower layers of the atmosphere are heated and mixed (Membery, 1983). Shamal winds can last one to five days and reach surface velocities of 15-20 m/s (Thoppil and Hogan, 2010). The strength of the Shamal winds is the result of differences in surface pressures over Saudi Arabia, the Gulf of Oman, and/or Pakistan (Ali, 1994). The vertical motion of the local air pressure systems determines the speed, direction, and thickness of the dust cloud (Ali, 1994). The lack of vegetation and availability of uninterrupted surfaces optimize the strong northwesterly Shamal winds and southeasterly Kous winds.

Area-wide dust storms carry fine particulate matter throughout Iraq. Soldiers and inhabitants of the region are continuously exposed to these storms. To characterize the aerosol content of air in the soldiers' operating environment, an 8-stage DRUM (Davis Rotating drum Unit for Monitoring) aerosol impactor was placed outside their working and living quarters in Camp Victory, Iraq, beginning February 14, 2008. The location of the DRUM impactors was chosen based on their proximity to the soldiers, who were responsible for collecting samples and maintaining the samplers.

1.9   Sampling Study – DRUM and Particle Separation

Ground-based, eight-stage DRUM impactors have been successfully used in remote areas, where frequent human intervention would otherwise be difficult, for the continuous collection of size and time-resolved aerosol elemental composition and mass concentration data (Cahill et al., 1985; Raabe et al., 1988; Cahill and Wakabayashi, 1993; Wetzel et al., 2003;

Collins et al., 2007). The DRUM impactors are advantageous as they continuously collect eight size fractions (5.0-10.0, 2.5-5.0, 1.15-2.5, 0.75-1.15, 0.56-0.75, 0.34-0.56, 0.26-0.34, and 0.09-0.26 μm in aerodynamic diameter) on Apiezon L™ coated Mylar™ strips and they are compatible with several non-destructive analytical techniques (beta–gauge for aerosol mass, ultraviolet-visible spectroscopy for optical absorption as function of wavelength, and synchrotron x-ray fluorescence for elemental composition; Cahill et al., 1999; Cahill, 2003).

Particles collected on the DRUM impactor (Figure 1-3) are passed through a succession of stages where the aerosol jet is directed through a nozzle onto a solid surface. Impaction, the physical distribution and deposition of particles, occurs as the collected aerosols are forced around a sharp bend stripping them from the high velocity jet. The efficiency of this process is a function of particle aerodynamic diameter, air velocity, and jet dimensions. The narrower the jet and higher the velocity, the finer the particles collected. Finer particles are collected on each successive stage of the impactor as the sample passes through the device by decreasing the nozzle size and increasing the air velocity for each successive impaction stage. The distribution of particulate matter between the stages provides a means for assessing the particle size distribution of the aerosol (Vincent, 2007).

Collection efficiency is degraded through the loss of particles from bounce or rebound (Vincent, 2007). That is, the elastic properties of both the particle and collecting surface are high during impaction resulting in the tendency of particles to bounce off the surface (Vincent, 2007). This is problematic as some particles, especially solid, gritty ones, may fail to be retained on impact. Particle loss can be important if only a small fraction of material is collected on the correct stage. Whether or not particle bounce occurs depends on many factors: the velocity of

impacting particles, particle size, particle surface properties, and the properties of the collecting surface (Vincent, 2007).

The elasticity of the particles on the Mylar™ is reduced with the addition of sticky substrates to enhance adhesion (Bench et al., 2002). This project utilized Apiezon-L™ to coat the Mylar™, which has proven advantageous due to its uniform projected density, efficient particle collection, reduced tendency for background noise in elemental analysis due to its purity, and its anti-bounce properties (Bench et al., 2002; Lawson, 1979.) If the impaction surfaces are not sticky, the resulting size distributions and mass median diameter values will be skewed towards smaller particle sizes (Dzubay et al., 1976).

To address concerns pertaining to impaction and whether brittle minerals would fragment upon impaction, resulting in a higher proportion of finer particles within the DRUM, a DRUM impaction study was conducted and included in Chapter 4 of this dissertation. The purpose of this study was to eliminate concerns that larger particles may fragment into smaller particles during impaction. This fragmentation would be problematic, as it would result in a misrepresentation of the particle being sampled and the true mass of individual size fractions. Results from this study indicate the sampler is performing correctly and that all particles were collected in the correct size fractions.

1.10   Analytical Techniques

1.10.1 Synchrotron X-Ray Fluorescence

Synchrotron X-Ray Fluorescence (S-XRF) performed at the Advanced Light Source at Lawrence Berkeley National Laboratory in Berkeley, California was chosen for the analysis of the particulate matter samples, as it is a non-destructive technique widely accepted for aerosol analysis (Barberie et al., 2013). The ability of the synchrotron beam to excite x-ray emission

from a sample while maintaining sample integrity for repeat analysis is advantageous given the small quantities of sample collected on the DRUM impactors and the uniqueness of a given sample (Barberie et al., 2013).

A synchrotron generates a brilliant, broad-spectrum (including infrared, visible, and ultraviolet light, and x-rays) electromagnetic radiation beam, called synchrotron radiation, that can contain a flux of x-rays many orders of magnitude greater than that produced by a conventional x-ray tube. Electrons emit synchrotron radiation when they are forced by magnetic fields to change directions at close to the speed of light. As the magnets of the synchrotron steer the electrons in a circle of evacuated tubes hundreds of meters in diameter, the synchrotron radiation is given off tangentially from the circle (Owens, 2012). At specific points along the circle, the synchrotron radiation is steered down a beamline to encounter a sample placed in its path. When the synchrotron radiation hits the sample, it ejects inner electrons from the atoms in the sample. The vacancies caused by the ejected electrons are filled with outer shell electrons (Pecharsky and Zavalij, 2009) that cascade down to fill the voids and x-rays characteristic of the change in energy between the outer shell and inner shell energies are released. These x-rays are collected using a detector, subjected to curve-fitting programs for known elemental x-ray energies, and compared with thin film standards to result in final elemental concentrations (Barberie et al., 2013).

This data was collected using the Advance Light Source's polarized polychromatic-beam 18keV bending magnet beamline 10.3.1 developed by University of California at Davis DELTA Group for analyzing the DRUM impactor's low mass aerosol samples (Barberie et al., 2013). The polychromatic, or white, beam is advantageous because it allows for the simultaneous analysis of multiple elements. The high beam intensity and low background resulting from the

synchrotron beam's polarization provide the high signal to noise ratios required to quantify the elemental concentrations in low mass samples (Barberie et al., 2013).

1.10.2 Beta Gauge

The β-gauge was used to measure the total mass of aerosols collected during the loading process. The β-gauge works by measuring the change in the intensity of β-particles passing through a blank Mylar™ tape compared to one that is loaded with the sample (Husar, 1974; Friedlander et al., 1981; Chueinta and Hopke, 2001). Friedlander et al. (1981) used the Beer's law expression (Equation 1.1) to draw correlations with intensity and the number of β-particles passing through the sample.

$$I = I_\circ e^{-mx}$$

<div align="right">1.1</div>

where,
$I_\circ =$ incident particle flux,
$I =$ exiting particle flux
$x =$ areal density in mg/cm^2
$m =$ mass attenuation coefficient in cm^2/mg

The general design of the β-gauge is fairly simple, consisting of a β source, detector, and a filter holder. Ideally, the β source spectrum and the mass thickness will not exceed the energy of the β source (Chueinta and Hopke, 2001). This project utilizes ^{63}Ni ($E_{\beta max} = 67$ keV and $E_{avg} = 17$ keV) as it has a low energy beta spectrum and a fairly long half-life of 96 years (ICRP Report 72, 1995). The long half-life ensues stability; as a result, decay corrections are not necessary. Further, stable beta sources encourage green practices within the laboratory as we would not be required to continually purchase new sources, nor have we created excess waste from depleted sources.

1.11   Thesis Review/Approach

The purpose of the research described in this thesis was to obtain, using DRUM aerosol impactors, particulate matter samples suitable for health impact studies, characterize the aerosol's size distributions and chemical compositions, and determine the sources of observed particulate matter using meteorological analyses and known aerosol emissions (e.g., local wind trajectories and smelting industries). As a result of this research, three papers will be submitted to peer reviewed publications: 1) one on the chemical composition of Iraqi aerosols; 2) one on the geochemical fragmentation seen within Iraqi aerosols; and 3) one on an experiment designed to study impaction and fragmentation in an 8-stage DRUM aerosol impactor. However, it also is useful to put the results of these investigations into the broader context of the literature on aerosol research in the region and wind blown dust. Therefore, this chapter summarizes some of the key research findings and techniques previously used to characterize Iraqi aerosols and wind blown dust.

1.12   Heavy Metal Aerosols

It is believed that over the duration of the Gulf War, an estimated 300 tons of depleted uranium, a by-product of the ^{235}U radionuclide enrichment process for nuclear weapons and reactors, were dropped over 20,000 km^3 of Kuwait and southern Iraq from aircraft rounds and tank-fired shells (US AEPI, 1995a). Metallic uranium used in military operations is considered to be insoluble, however, long-term exposure to the elements (air/water) can slowly result in its oxidation to its +4 and ultimately +6 state(s) (Bem and Bou-Rabee, 1997).

Particulate matter collected during a high atmospheric dust concentration event caused by regional wind contained a high concentration of uranium, 0.24 ng/g (Bem and Bou-Rabee, 1997) in contrast to the normally observed values of approximately 0.1 ng/g (Bem and Bou-Rabee,

1997). Once in the air, small particles of uranium oxides (UO_2, UO_3, and U_3O_8) can be introduced into the human body via the inhalation of aerosols. Of the uranium inhaled, up to 1% can be retained in the kidneys (ICRP-72, 1995). Uranium toxicity is similar to that of other heavy metals; it is capable of forming stable complexes with biological ligands of low molecular mass and disrupting the re-absorption of glucose and amino acids (Priest, 2001).

In 2001 the Lebanese Ministry of the Environment reported that more than 2400 tons of heavy metal (Pb, Cd, Mn, Zn, Se, and As) laden industrial waste was generated annually in Lebanon (Inhorn, 2004). The presence of abnormally high levels of heavy metals in the air in Lebanon is suspected to be the cause of observed decreases in male fertility (Auger et al., 1995; Benoff et al., 1997; Telisman et al., 2000). It is believed that 10-15% of all Middle Eastern couples are infertile (Serour, 1996), with Lebanon representing 60-70% of the total infertile population (Inhorn et al., 2008). The pollution levels were worsened further by the continued practice of improperly disposing of medical, industrial, and household wastes (Hamdan, 2002).

Improper disposal of wastes was not unique to Lebanon. Recent news articles have highlighted concerns regarding wartime soldiers' exposure to plumes of smoke in Iraq from active burn pits used to dispose everything from batteries to medical waste (Kennedy, 2009). However, to date, no concrete evidence exists linking burn pits emissions to adverse health effects amongst wartime soldiers (Lyles, 2011). For data to exhibit any conclusive results, an independent burn pit study would need to be conducted. That is, samplers would need to be employed upwind and downwind of local burn pits to get a better understanding of the emissions from the burn pit as well as the background concentrations and types of aerosol. A better understanding of the background aerosols and different types of combustion emissions is required because there are high concentrations of aerosols throughout the Middle East. For

example, dust is present virtually everywhere within the Middle East (Engelbrecht et al., 2009; Awadh, 2012; Misconi and Navi 2010; Al-Hurban and Al-Ostad, 2010) and local combustion sources (burn pits, smelters, manufacturers, etc.) are located throughout the Arabian Peninsula.

The Shamal winds are responsible for: 1) the large concentrations of aerosols lofted during Iraqi dust storms; 2) the long-range transport of mineral dust (Awadh, 2012; Clarke et al., 2001; Yang et al., 2001; Moore et al., 2003), 3) the increased erosion along the predominant wind paths; and 4) the significant reductions in visibility that occur when high concentrations of mineral dust are present in the atmosphere. The best way to ascribe major wind events to specific source regions is through the use of meteorological backward trajectory analyses.

1.13   Backward Trajectories and the Use of HYSPLIT

Computational meteorological trajectories have greatly improved in accuracy since their introduction in the 1940s. Today, calculated trajectories are widely used within environmental sciences for describing the likely path a particle has taken (Abdalmogith and Harrison, 2005; Escudero et al., 2006; Cong et al., 2007; McGowan and Clark, 2008; Cahill et al., 2010). However, the particle path is limited by the accuracy of the trajectory (Pack et al., 1978). The Eulerian and Lagrangian models differ in how the particle is considered as it travels. The Eulerian model utilizes a fixed set of points in space to describe how the air flows, while the Lagrangian model studies individual air particles as they move through time and space (Stohl, 1998). Lagrangian particle dispersion models are generally preferred among atmospheric scientists for simulating physical and chemical processes (Stohl, 1998).

The Hybrid Single-Particle Lagrangian Integrated Trajectory (HYSPLIT_4) is an atmospheric dispersion model that mathematically interpolates the likely path taken by an aerosol parcel along backward (where has the particle been) and forward (where will the particle

19

go) trajectories. It has been used in numerous studies worldwide to link aerosol deposition with source region identification (Abdalmogith and Harrison, 2005; Escudero et al., 2006; Cong et al., 2007; McGowan and Clark, 2008; Cahill et al., 2010). HYSPLIT requires input datasets of meteorological data. There are four vertical coordinates that meteorological data can be useful to the HYSPLIT_4 model: pressure-sigma, absolute-pressure, terrain-sigma, or a hybrid absolute-pressure-sigma coordinate system (Draxler and Hess, 1998). HYSPLIT is considered a hybrid in that it uses concepts from both the Eulerian (fixed grid) and Lagrangian models (advection and diffusion) in its computation (Draxler and Hess, 1998). HYSPLIT was originally designed to assist the Bureau of Meteorology (BoM) in determining the likely direction a hazardous airborne contaminant would transport after emission (Draxler and Hess, 1998). Once the trajectory is calculated, particle composition can be hypothesized based on emission sources known to be unique to a given region's geological and topographical characteristics.

1.14   Aeolian Dust Models

Aeolian processes may be defined as the ability of wind to shape the surface of the Earth through erosion, transport, and deposition. Alfaro and Gomes (2001) and Shao (2001) use size resolved dust flux measurements to describe processes that lead to dust emissions. In doing so, the source soil is used to determine particle characteristics and likely downwind aerosol concentrations. The accuracy of physical based models for dust emissions is dependent on correctly representing soil source profiles and their behavior during erosion, transport, and dispersion (Uno et al., 2006; Yin et al., 2007; Reid et al., 2008). Butler et al. (2012) suggest that spatial variability is important when studying airborne soil particle size distributions and that studies should examine the distance a plume travels to estimate the particle size distribution in a dust cloud; larger source areas are more likely to have finer dust concentration profiles

downwind of them due to greater transport distances across the source areas. In contrast, Kok (2011a; 2011b) suggested particle size distributions follow a power law and considered the development of the distribution to be a scale-invariant process. Kok (2011b) selected data from leading saltation theorists to draw correlations with his brittle fragmentation model and validate his theory that particle size distributions are independent of wind velocity.

1.15   Brittle Fragmentation

Brittle fragmentation is currently one of the leading hypotheses used to describe particle breakdown. Particle fragmentation is the rendering of a material into multiple pieces by applying a strain to the material, such as a chemical or mechanical load (Astrom, 2006). Using this definition, brittle fragmentation is defined as the break-up of a brittle material.

Fragmentation can be continuous or instantaneous (Astrom, 2006). Continuous fragmentation implies the slow mechanical breakdown or decomposition of particles through the processes of grinding and crushing (e.g., mining and milling). Instantaneous fragmentation occurs quickly and is associated with violent processes that favor critical crack velocity (e.g., earthquake). Both instantaneous and continuous fragmentation destroys smooth crack surfaces through the simultaneous breakup of unstable cracks. This can lead to the propagation of crack branches and dust fragments along the crack or fraction paths (Astrom, 2006; Fineberg and Marder, 1999). Astrom and Timonen (1997) suggest the initial propagation of cracks, and their subsequent branching, may not be from related events; rather, the fragmentation may be the result of random nucleation and/or uncorrelated events/locations. Astrom and Timonen (1997) propose that unstable main cracks create large fragments that form a damage zone in which smaller fragments become entrapped, filling the void space. Sharon and Fineberg (1996) hypothesize that smaller fragments are likely to be found closest to main cracks while larger

fragments are created from crack branching. As branches merge with multi-generational cracks, 2D models show that fragments may continue to breakup, even beyond what was believed to be the level of "maximum" fragmentation (Linna et al., 2004; Astrom et al., 2004).

Among leading theorists, much debate exists as to the role particle bombardment and saltation has on fragmentation. Alfaro and Gomes (2001) argue that increasing saltating impact energies produce more disaggregation resulting in smaller particles. They quantify this effect by suggesting the role wind velocity plays on a saltating particle's energy is essentially squared. Kok (2011a, 2011b) argues that saltator impact speed and impact energy are independent of wind velocity. To validate his theory, Kok (2011a, 2011b) calculated the mean aerosol dust diameter by number (D_N) and volume (D_V) from several published size-resolved vertical dust flux measurements (Equation 1.2).

$$D_N = \int_{D_{low}}^{D_{up}} D \frac{dN}{dD} dD \Big/ \int_{D_{low}}^{D_{up}} \frac{dN}{dD} dD$$

$$D_V = \int_{D_{low}}^{D_{up}} D \frac{dV}{dD} dD \Big/ \int_{D_{low}}^{D_{up}} \frac{dV}{dD} dD$$

$$1.2$$

where, N and V correspond to the number of emitted aerosols at a given diameter (D) and D_{low} (1.2 microns) and D_{up} (8.4 microns) represent the overlap of aerosol size ranges from published data sets. According to Kok (2011b) equation 1.2 assumes the sub-bin distribution follows the power law for 2.0-10.0 micron diameter dusts (Gillette, 1974).

To determine if our samples followed the power law and agreed with Kok's model (2011b), we applied the theory of brittle fragmentation to the aerosols sampled in Iraq. In doing so, the soil concentration was determined for each aerosol diameter (d) range sampled by the DRUM impactor using the techniques described in Malm et al. (1994) assuming the density (ρ) of soil was 2.5 g/cm^3. Equation 1.3 demonstrates the calculations used for determining

dV/dlogD.

$$[soil] = 2.20[Al] + 2.49[Si] + 1.63[Ca] + 2.42[Fe] + 1.9[Ti]$$
$$dV = \frac{[soil]}{\rho} \qquad 1.3$$

Once dV was determined, dV/dlogD could be calculated using the log of the diameter range for each size fraction, during its respective 1.5-hour sampling interval, the results were imputed and normalized within the brittle fragmentation model. The data was further categorized within the model to separate local, Shamal, and Kous wind events. This distinction was chosen to investigate the impact of long-range transport and wind velocity. The results of these analyses are presented in Chapter 3.

Scientists question whether ultra-fine soil particles can be generated. However, experts do suggest that fragmentation can result from saltation. Sow et al. (2009) suggests that changes to the aerodynamic roughness length during high velocity winds may result in brittle fragmentation for particles less than 5 microns. Nickling et al. (1999) found significant particle size variability in bulk dust concentration profiles between individual events suggesting there is considerable variation in particle size emissions between distinct events. Li et al. (2009) stated that over several seasons, wind erosion changes the particle size distribution of parent soils due to changes in wind and surface conditions. Combining brittle fragmentation with other hypotheses for fine dust aerosol generation and observations of fine dust in the atmosphere leads to the conclusion that fine particles found in desert dust storms may result from the combination of several factors. The results of this combination are examined in Chapter 3.

1.16   Authorship

This dissertation is the result of my thesis investigations. Several investigators have provided me with technical assistance, scientific guidance, and advice including: Catherine F.

Cahill, William R. Simpson, Thomas Gill, Thomas Douglas, Thomas Kuhn, Sean Egan, and Jasper Kok. Their efforts will be acknowledged through co-authorship and acknowledgement on the papers resulting from Chapters two through four of this thesis are as follows: I am the primary author on all papers. The first paper, Chapter 2, will have Catherine Cahill as a co-author. The second paper, Chapter 3, will have Catherine Cahill, Thomas Gill and Sean Egan as co-authors. The final paper, Chapter 4, will have Sean Egan and Catherine Cahill as co-authors. Catherine Cahill provided scientific guidance for the papers. Thomas Gill provided assistance with the interpretation of the soil modeling results. Sean Egan assisted with MatLab programming and experimental implementation.

1.17   Figures

Figure 1-1. A general vicinity map of Iraq. The green and red place markers depict the Taurus and Zagros Mountains ranges of Turkey and Iran, respectively. Baghdad is represented with a blue thumbtack and Camp Victory is located in Baghdad. Image created from Google Maps: www.google.com
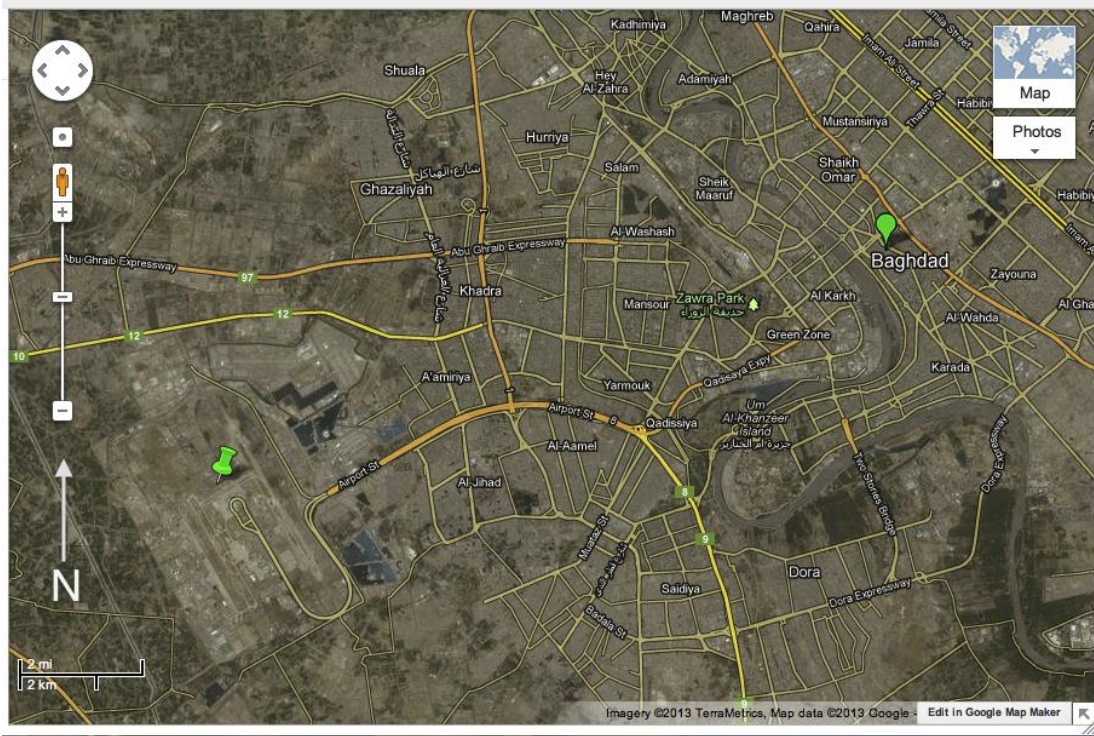
Figure 1-2. Camp Victory with respect to Baghdad. Camp Victory is indicated with a green thumbtack and Baghdad is represented with a place marker. Image created from Google Maps: http://www.google.com.
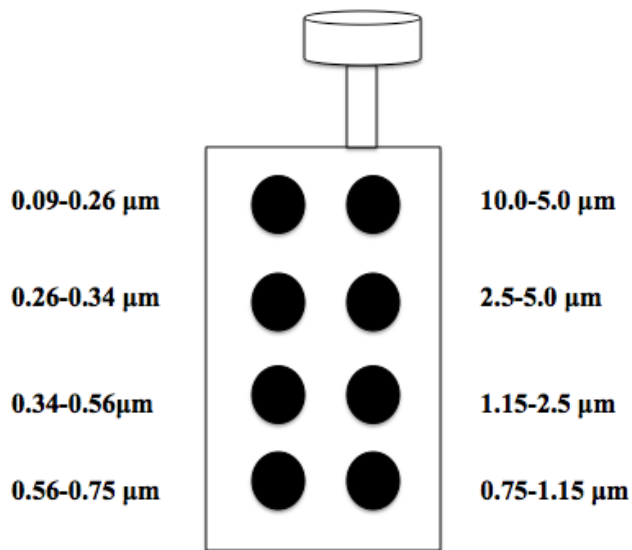
Figure 1-3. A schematic of the DRUM impactor and its size ranges.

1.18 Tables

Table 1-1. National Ambient Air Quality Standards[1].

Pollutant		Primary/ Secondary	Averaging time	Level	Form
Particle Pollution	PM$_{2.5}$	Primary	Annual	12 μg/m^3	Annual Mean, Average over 3 yrs
		Secondary	Annual	15 μg/m^3	Annual Mean, Average over 3 yrs
		Primary & Secondary	24-hr	35 μg/m^3	98th percentile, Average over 3 yrs
	PM$_{10}$	Primary & Secondary	24-hr	150 μg/m^3	Not to be exceeded more than once per year on average over 3 yrs

[1] Table 1-1 and its references are reprinted from the U.S. Environmental Protection Agency. www.epa.gov/air/criteria.html (accessed December 11, 2009).

Table 1-2. Threshold Limit Values. These values are adjusted to meet the Military Exposure Guidelines for Active Duty Soliders.[2]

Criteria Pollutant	TLV-Adj/TWA Adj.	Long Term MEGs
Lead (Pb)	0.001 mg/m^3	0.0015 mg/m^3
PM_{10}	0.24 mg/m^3	0.07 mg/m^3
$PM_{2.5}$	0.07 mg/m^3	0.04 mg/m^3

[2] Table 1-2 was accessed and reformatted from the USACHPPM RD 230.

Chapter 2 An Analysis of Source and Source Regions and Chemical Composition of Iraqi

Aerosols[2]

2.1   Abstract

Studies have shown that soldiers deployed in the Middle East are breathing ambient air containing concentrations of fine particulate matter known to cause adverse effects to human health. A study initiated in 2008 was designed to determine the concentrations and compositions of fine particulate matter and quantify the fine particulate matter exposures for soldiers currently deployed in Baghdad, Iraq. This study used a DRUM aerosol impactor to continuously collect size (eight stages between 0.09 and 10 microns in aerodynamic diameter) and time (hour and a half resolution) resolved aerosol samples for mass concentration and elemental composition analyses. Results of this study show that there is fine particulate matter associated with both geogenic and anthropogenic source emissions. The presence of Pb with S, Cl, and Br can be correlated to the use of leaded fuels within Baghdad. Trace metal concentrations combined with V can be correlated to fuels and/or local mining and smelting operations. Aerosol collected on the finest size fractions of the DRUM aerosol impactor (0.09-0.34 microns) correlate well with coarse particles and elemental soil ratios implying a geogenic source. Lead concentrations observed during this study (2.0 ug m^{-3}) exceed the U.S. national ambient air quality standard for lead (0.15 ug m^{-3}) designed to protect human health.

2.2   Introduction

Recent studies have reported high concentrations of aerosols throughout the Middle East, including Iraq, particularly during dust storms (Al-Hurban and Al-Ostad, 2010; Engelbrecht et

---

[2] Bell, J.M.; Cahill, C.F. An analysis of source and source regions and chemical composition of Iraqi aerosols. University of Alaska Fairbanks, Fairbanks, Alaska. In preparation for submission to the American Chemical Society, 2014.

al., 2009; Al-Dabbas et al., 2012; Misconi and Navi, 2010; Awadh, 2012; Shahsavani, et al., 2012). High aerosol concentrations are problematic because they effectively scatter light and reduce visibility (Saeed and Hassam, 2010; Awadh, 2012), affect the radiative budget of the earth (Liao, et al., 1999), damage military vehicles (Engelbrecht et al., 2009), and adversely affect human health (Pope et al., 1995. Seaton et al., 1995; McClellan, 2000; Bell and Davis, 2001; MacNee and Donaldson, 2003; Derbyshire, 2007; Szema et al, 2010; King et al., 2011; WHO, 2012a; Morman and Plumlee, 2013). Reported aerosol concentrations throughout the Middle East commonly exceed current standards such as the National Ambient Air Quality Standards (NAAQS) and Military Exposure Guidelines (MEGs). The NAAQS (U.S. Environmetnal Protection Agency accessed at www.epa.gov/air/criteria/html) and MEGs (USACHPPM RD 230, 2013) for particulate matter with aerodynamic diameter of less than 2.5 microns ($PM_{2.5}$) are 35 µg m^{-3} and 65 µg m^{-3} per 24-hour average, respectively. These standards were designed to protect human health because short term exposure to high concentration of airborne particulates have been correlated to increased mortality in infants and young children, inflammation of lung tissue, increased incidences of heart attacks, increased emergency room visits in people with pre-existing lung illnesses, and death from respiratory related diseases (Dominici et al., 2002; Pope and Dockery, 2005; Ghio et al., 2000; Van Der Eeden et al., 2002). Long-term exposures to high concentrations of airborne particulates have been correlated with increased incidences of hospital admissions to individuals with suppressed immune systems, cardiovascular and respiratory diseases, and premature death (Pope et al., 1995; Seaton et al., 1995; Bell and Davis, 2001; MacNee and Donaldson, 2003).

In desert environments, specifically Iraq (Al-Dabbas et al., 2012) and the Middle East, hospitals are inundated with respiratory patients during regional dust storm events (Prospero,

1999; Al-Frayh et al., 2001; Thalib and Al-Taiar, 2012). Sanders et al. (2005) found that respiratory illness was the second largest cause of hospital admissions for deployed personnel. Incidences of asthma (Szema et al., 2010), desert lung syndrome (Derbyshire, 2007; Morman and Plumlee, 2013) and desert pneumonia (Hammond et al., 1989; Middleton, 2001; Griffin, 2007; Al-Dabbas et al., 2012) are frequently reported as respiratory related illnesses among deployed U.S. military personnel in the Middle East.

Engelbrecht et al. (2009) sampled total suspended particulate matter (TSP), particulate matter less than ten micrometers in aerodynamic diameter (PM_{10}), and $PM_{2.5}$ for 24 hours once every six days across the Middle East, including in Baghdad, Iraq. The authors observed high concentrations of soil particles during dust storms. To fully characterize each sampling area, and to understand soil particles being sampled, bulk soil was collected from the 15 sampling sites, throughout Iraq and the Middle East, and compared to dust particulate matter. Results from their study suggested there are elemental ratio differences between soil found within the Arabian Desert and other desert regions (Engelbrecht et al., 2009; Awadh, 2012). Specifically, Engelbrecht et al. (2009) noted higher concentrations of calcium (Ca) and magnesium (Mg) and reported lower concentrations of silicon (Si) at all sites within the study area. This finding is significant in that it establishes a tracer for potentially differentiating Arabian Desert aerosols from dusts from other sources, and from the global background dust aerosols.

Engelbrecht et al. (2009) also noted elevated levels of trace metals during non-dust storm periods. Field reports suggest that elevated trace metals may correlate to monitoring site locations and their proximity to open burn pits where garbage, medical waste, batteries, and other hazardous and non-hazardous materials are discarded into excavated pits and combusted. Engelbrecht et al. (2009) and others (Schmaltz, 2008; Al-Khafaji, 2009; Al-Dabbas et al., 2012)

33

noted that the sources of non-dust trace metals were predominately anthropogenic and attributed these emissions to the continued use of leaded fuel in motor vehicles, engine combustion processes associated with oil, gasoline and natural gas, and regional smelting operations. Iraq has significant oil resources with many active refineries. Al-Baiji Oil Refinery, the largest refinery in Iraq, is located in the town of Baiji, 130 miles north of Baghdad (Al-Jebouri and Younis, 2012). This refinery is linked to significant pollution events and is likely a continued source of anthropogenic trace metal emissions. Al-Jebouri and Younis (2012) discusses the use of vanadium (V) as a tracer for anthropogenic source emissions from oil refinery operations. In addition to ambient particulate matter sampling, atmospheric models have noted increases in sulfur dioxide and nitrous oxide concentrations (Radi et al., 2007). These studies have correlated well with increased emission of combustion gases and the steady rise in local industries (Radi et al., 2007). Iraq, and its surrounding countries have a long mining history of carbonate hosted ore deposits such as: lead (Pb), zinc (Zn), and copper (Cu). The mining of these deposits has continued into the present (Ayhan and Ersayar 1985; Koptagel et al., 2006) and may be an additional anthropogenic source of ultra-fine mineral dust, mineral ash, and trace metal emissions. Aerosols from these mining and mineral processing industries likely have unique metal to non-metal chemical composition that can be used, in addition to air mass back trajectory modeling, to attribute aerosols in potential source regions.

The Enhancement Particulate Matter Surveillance Program (Engelbrecht et al., 2009) was a preliminary study designed to address immediate concerns regarding soldier health and abrasion to moving parts in machinery and vehicles due to high particle concentrations trapped within lubricants. However, this study had significant drawbacks in that it did not provide sufficient data to meet the time resolution necessary for epidemiological determinations.

34

Immediate issues presented with Engelbrecht et al. (2009) were the use of low volume one day in six samplers. Dust storms moving through Iraq deposit vast amounts of organic and inorganic aerosols into the region; a low volume sampler would readily overload or shut off before the sampler became overloaded.

Their study was further limited through the use of three different substrates for sample collection: Teflon™ membrane (T), Quartz fiber (Q), and Nuclepore filters (N). The use of different filters on varying sampling days limited the elements being sampled on a given sample day, the quantity of the sample collected, and their reproducibility. The brittleness of the Q filter media proved unreliable during gravimetric analysis. Many of these samples were ignored because the edges of the filters were brittle and would frequently break off resulting in sample loss. The choice of sample media also limited the length of collection. The T and Q samples were set for 24-hr run times while the N sample would only collect for 2-hrs (counted as 24-hr sampling period) to ensure it did not become overloaded. Collecting samples for only 2 of 24 hours on every sixth day would miss diurnal effects and not fully represent local drainage, thereby missing key wind patterns important for identifying source and source regions. Additionally, it allowed for the possibility of missing significant pollution events altogether, as well as individual dust storms, which last for a day or portions thereof. Further, sampling every sixth day and rotating through three different sampling media meant that different numbers of each type of filters were taken each month.

Al-Dabbas et al. (2012) used large plastic bins to collect deposited dust samples from the top of buildings in several cities (Baghdad, Ramadi, Kut, Basra, Naraf, Karbala, Hilla, and Tikrit) throughout Iraq. In doing so, they were able to collect a larger mass of aerosols (approximately 0.5 kg) without overloading collection bins; however, collection was limited by

the size of the aerosol and its ability to settle quickly. The main objective of their study was to characterize regional dust storms and identify source regions likely to impact Iraq and the Middle East. A benefit to the large collection of aerosols was that it provided an understanding of the overall types of trace metals and clays inherent to the region. However, that study was unable to make mass concentration, size, and time determinations on the aerosols sampled. Thus, they were unable to distinguish between the samples and how they were related to wind events. Nor were they able to draw correlations between sources and source regions.

Shahsavani et al. (2012) utilized a Grimm model 1.177 Aerosol Spectrometer optical particle counter to collect one day in six samples and samples on dusty days between April and September 2010 in Ahvaz, Iran. On each of the dusty days measurements were taken every 30 minutes over a twenty-four hour period. During this period they sampled a total of 82 days (72 of these days were classified as dusty). Results from Shahsavani et al. (2012) confirmed the findings of Draxler et al. (2001) that showed high concentrations of PM_{10} aerosols (>3,000 $\mu g/m^3$) entering Ahvaz from Iraq, Saudi Arabia, and Kuwait. Much of the aerosol was attributed to Iraq because the Iraqi soil is easily lofted due to unstable desert surfaces from war efforts, significant desert plateaus, drought, deforestation, improper land use, etc (UNEP, 2003). Shahsavani et al. (2012) used a scanning electron microscope (SEM) to analyze samples that were collected on fiberglass filters from a high volume sampler to verify the findings of Engelbrecht et al. (2009) that showed higher Ca and lower Si in Iraqi soils than were present other desert regions. Similar to Engelbrecht et al. (2009), Shahsavani et al. (2012) was limited by the duration of collection (every 30 minutes during dusty days and 24-hours/6 days) and the low number of samples collected.

The study presented here addresses the limitations of the previous studies cited above. Specifically, to overcome inherent problems associated with one day in six samplers we used an 8-stage DRUM aerosol impactor to obtain size and time resolved samples of aerosol mass and elemental composition. We report on continuous 3-week sampling campaigns designed to better understand the temporal variation of Iraqi aerosols and to provide sufficient data for epidemiological studies.

2.3   Experimental Methods

2.3.1   Sampling Site

The monitoring site was located at Camp Victory in Baghdad, Iraq. Samplers were placed outside of both the soldiers' office and living quarters. Baghdad is located within the Tigris and Euphrates drainage at the foot of the Taurus and Zagros Mountain Ranges (Figure 2-1). Camp Victory (Figure 2-2) is located 5-km from Baghdad International Airport and 16-km west of Downtown Baghdad.

Iraq is classified as a having a subtropical, semi-arid climate and is known for its hot, dry summers with daytime temperatures exceeding 100 °F and nighttime temperatures remaining around 80 °F (Ali, 1994). Evening temperature inversions occur as cool air masses are trapped below warmer air (Mohammed, 2013). The temperature inversions are broken by winds exceeding 7.7 m/s and by heat from the morning sun. Humidity inversions occur during daytime hours as the sun rises and the temperature inversion disappears (Ali, 1994).

Winters are typically short (December and January) and mild, with 5 to 10 inches of precipitation and temperatures generally above freezing (Ali, 1994; Qatar, 1990; MEPA, 1989). Winter rainstorms are the result of frontal systems caused by the migration of cyclones over the Arabian Peninsula from the Mediterranean Sea (Ali, 1994). Intensified thermal highs result in

37

low visibility and foggy conditions over the Tigris and Euphrates rivers that typically burn off by mid-afternoon.

During the summer months visibility is worsened by the lack of precipitation and the lofting of fine silt from the Tigris and Euphrates riverbeds and evaporated lakes (Al-Farrajii and Harvey, 2000; NOAA accessed at www.ncdc.noaa.gov/oa/climate/afghan/iraq-narrative.html). The dry summer climate combined with steep pressure gradients produce strong northwesterly winds that loft large quantities of dust during sandstorms (Thoppil and Hogan, 2010; Ali, 1994). Strong Shamal winds carry large plumes of dust from the Taurus and Zagros mountains into the recessed plains of Iraq (Figure 2-3). The dust cloud is a result of low-pressure systems creating winds with sufficient energy for particles to break free of the topsoil and entrain into the passing storm (Thoppil and Hogan, 2010; Foda et al., 1985). The energy from the strong winds are most prevalent during daytime hours due to surface winds becoming less hindered by friction as the lower layers of the atmosphere are heated and mixed (Membery, 1983). Shamal winds can last 1-5 days and reach surface velocities of 15-20 m/s (Thoppil and Hogan, 2010). Increases in wind velocities are generally a result of differences in surface pressures over Saudi Arabia, the Gulf of Oman, and/or Pakistan (Ali, 1994). The vertical motion of the local air pressure systems determines the speed, direction, and thickness of the dust cloud (Ali, 1994). The lack of vegetation and availability of uninterrupted surfaces optimize the strong northwesterly Shamal winds and southeasterly Kous winds. Dust storms in this region are significant in that they: 1) result in a tremendous amount of aerosols that reduces visibility (Figure 2-3) (Jassim and Buday, 2006; Thoppil and Hogan, 2010); and 2) increased erosion along Shamal wind paths (Jassim and Buday, 2006).

2.3.2   Aerosol Sampling and Analysis

Size and time-resolved measurements of aerosol size and composition were continuously collected at the site every three weeks starting on February 14, 2008, using an 8-stage DRUM aerosol impactor (Figure 2-4) (Raabe et al., 1988; Cahill and Wakabayashi, 1993). The DRUM impactor is advantageous as it collects samples in smaller size fractions than traditional $PM_{2.5}$ filter methods. In doing so, the differences in particle size, composition, and potential health effects can be determined. The aerosol samples were collected on eight Apiezon L^{TM} coated Mylar^{TM} strips each corresponding to a specific size fraction collected by the sampler. The eight size fractions were 5.0-10.0, 2.5-5.0, 1.15-2.5, 0.75-1.15, 0.56-0.75, 0.34-0.56, 0.26-0.34, and 0.09-0.26 μm in aerodynamic diameter.

The strips rotate underneath a nozzle that deposits aerosols of the correct aerodynamic diameter onto the sample strip. The DRUM was programmed to concentrate an initial aerosol peak to mark the start of sampling by collecting aerosols for six hours before beginning its normal 8-mm per day rotation. A blank of 6-mm is collected in the middle of the sample run by advancing the sample strip. This blank is represented as a gap in the data set. The gap allows for a more efficient match of peaks of corresponding fractions. At the conclusion of the three-week sampling event the sampler concentrates the sample again.

The aerosols were analyzed with 1.5-hour resolution for mass concentration using elemental composition (27 selected elements between Mg and Pb: see Table 2-1) using synchrotron x-ray fluorescence (Cahill et al., 2010; Cahill et al., 1985) at the Lawrence Berkeley National Laboratory Advanced Light Source. Synchrotron x-ray fluorescence is a non-destructive technique, so the samples can be archived and reanalyzed later.

2.4   Meteorological Modeling

The National Oceanic and Atmospheric Administration Air Resources Laboratory's Hybrid Single Particle Lagrangian Integrated Trajectory Model, HYSPLIT (Draxler and Rolph, 2013; Rolph, 2013), was used to compute archived backward meteorological trajectories from the global data assimilation system (GDAS, 2006-present). Parameters used for all the trajectory calculations were starting elevations of 500, 1000, and 1500 meters above ground level with trajectory lengths between 24 and 76 hours. Trajectory heights were chosen based on the likelihood of the particle to touch ground in route to the site. The length of time each trajectory was run was based on the duration of a given wind event. As previously mentioned Shamal winds can last for 24 hours up to 5 days. Backward trajectories show where the aerosols, collected at the site at a specific time, may have originated and the path they took as they were transported to the site.

2.5   Results and Discussion

Figure 2-5 depicts four of the eight size fractions for the element calcium (Ca) and shows how Ca concentrations vary with size, due to changes in the dust profile over time. Larger particles would settle out more quickly resulting in the enrichment of the plume in smaller particles as the plume transports over longer distances. Once these particles are deposited to the surface, they can be resuspended and redistributed over Iraq with each subsequent dust storm. High Ca concentrations are expected as Iraq has significant calcite ($CaCO_3$) and gypsum ($CaSO_4$) mineral resources (Al-Dawachi, 2005; Al-Bassam and Huk, 2006; Awadh, 2012; Koh and Wakeley, 2011; Al-Dabbas et al., 2012) and dust storms are likely to loft anhydrous gypsum and calcite while passing over dry riverbeds, coastal sabkhas, and salt flats. Although the second size fraction (2.5-5.0 microns) appears to be the most concentrated, results from stage one, the

largest size fraction (5.0-10.0 microns), cannot be analyzed with any level of confidence. This is due to the significant mass loading that occurs during dust storms and the tendency of particulate matter to flake off when removing the aerosol laden Mylar[TM] strips from the sampling drum. However, the smaller fractions contain less aerosol mass so flaking does not occur on the lower stages. As a result, this study focused on aerosol particles smaller than 2.5 microns in aerodynamic diameter because these particles stick to the Mylar[TM] strips, are a health concern as this size fraction is capable of becoming embedded in the deepest part of the lungs (Weese and Abraham, 2009), and are associated with increased incidences of respiratory illnesses (Pope et al., 1995; Seaton et al., 1995; Schwartz et al., 1995).

The time series of aluminum (Al), calcium (Ca), silicon (Si), magnesium (Mg), iron (Fe), and titanium (Ti) shown in Figure 2-6 represents concentrations of elements in aerosols collected on stage six (0.34-0.56 μm) during a three week field campaign beginning February 13, 2009. This period was chosen because it provided a background of both dusty and non-dusty days for the soldiers working quarters, and was representative of other sampling periods.

Aerosols on stage six correlate well to one another in that peaks overlie in a "fingerprint" pattern. The fingerprint is indicative of key soil components (Al, Ca, Si, Mg, Fe and Ti) found within the earth's crust and desert soils (Faure, 1998). The crustal element abundances (27% Si, 16.3% Ca, 9.6% Al, 5.6% Mg, 8.4% Fe, and 0.2% Ti) in Figure 2-6 agree well with average abundances (28.2% Si, 4.5% Ca, 8.2% Al, 2.3% Mg, 5.6% Fe, and 0.56% Ti). Many previous investigations (Duce and Tindale, 1991; Uematsu et al., 1983; Taylor and McLennan, 1985; Measures and Brown, 1996) state that aluminum's crustal abundance is approximately 8% and is a useful indicator of mineral dust present in the air. Given aluminum has proven successful as a mineral dust indicator in the past and its crustal element ratios correlate well to the known crustal

element abundances, the fingerprint defined above is expected to be representative of desert soils.

Iraq has significant mineral resources and dust source areas enriched in Ca, Si, Mg, Al, Fe, and Ti (Al-Bassam and Huk, 2006). Changing elemental ratios may be attributed to aerosols lofting from desert soils and basins, mineral enriched deposits, unstable limestone and gypsum shelves, and enriched clay layers (Al-Bassam and Huk, 2006). However, the concentrations of individual elements will vary depending on the extent of erosion of particulaer soil surfaces, crusts, dry lakes, desiccated marshes, enriched deposits, mineral shelves or clay layers.

Scanning electron microscope (SEM) analysis was used in a previous study (Engelbrecht et al., 2009) to determine if ultra-fine particles (<0.5 microns) were present on one <2.5 micron filter from each site. According to this study, samples collected from Taji, Iraq and Kuwait differed from coarse fractions as they contained less of a geological signature (Si, Al, Mn, Fe, Ca, Mg), were more spherical than irregular, and contained products of combustion processes (carbon, sulfur, sodium, and chlorine). The present study's results differs from Engelbrecht et al. (2009) in that samples collected from Baghdad, Iraq routinely show geological signatures within the ultra-fine aerosols.

The results of Figure 2-6 (0.34-0.56 microns in aerodynamic diameter) are consistent with the time series in Figures 2-7 (1.15 - 2.5 microns) and 2-8 (0.26-0.34 microns), with the exception that Ca (Figure 2-7) tends to vary more in both size and time. Specifically, the ratio between Ca and Si seems to increase from 1:1 to 2:1 with particle size. The differences observed in Ca/Si ratios are likely due to various deposits of calcite, calcium-bearing clay minerals, and gypsum in desert soil surfaces, desiccated marshes, and coastal sabkhas. These findings are noteworthy as they suggest fragmentation of crustal surfaces into aerosol sizes smaller than

expected for brittle fragmentation of primary soil particles, differ from the findings of Engelbrecht et al. (2009), show the soil aerosol profile alters with transport, and demonstrate that source regions vary in clay, silt, evaporites, and crustal component concentrations. Further, this data set is unique in that most aerosol samplers cannot distinguish particles less than 2.5 microns and particles within this range are not generally attributed to soil (Whitby and Cantrell, 1976; Seinfeld and Pandis, 1998).

The wind rose in Figure 2-9 depicts wind patterns and velocities during the sampling period. It is noteworthy that Mg is more heavily influenced by Kous winds (Figure 2-10) than Shamal winds (Figure 2-11). As can be seen from the wind rose and the frequencies of wind speed (Figure 2-12), the sampling campaign in February 2009 had winds exceeding 5 m/s along both the Shamal (9%) and Kous (11%) drainage paths.

The regression lines for Ca, Fe, and Al were plotted with respect to Si for stage 0.34-0.56 microns (Figure 2-13) to demonstrate that other common crustal elements correlate with Si and are likely a product of soil components. Calcium does not correlate to as well as Al and Fe, which may be due to the different calcium-bearing minerals originating from both the lithosphere and hydrosphere. It should be noted that Ca tends to correlate better with Si when Si values are lower. In Iraq, mineral resources associated with Ca are calcite ($CaCO_3$), gypsum ($CaSO_4$; Al-Bassam and Huk, 2006), clay minerals such as montmorillonite $((Na,Ca)_{0.33}(Al,Mg)_2(Si_4O_{10})(OH)_2 \cdot nH_2O)$ (Al-Rawi et al., 1969) and the ions of calcium chloride ($CaCl_2$) and calcium bromide ($CaBr_2$) from sea salts (Bardoukia et al., 2003). Sea breezes from the Mediterranean are likely a source of seawater-derived emissions of Ca (Bardoukia et al., 2003). Sea salts are carried into Iraq predominately from the Mediterranean Sea with some influence from the Red Sea. Significant variations also are seen between Si and

Mg. This also may be due to Mg in sea salts, anthropogenic emissions from industrial processes (fertilizers), variable proportions of Mg-bearing minerals in Iraqi soil, and varying transport patterns. Figure 2-14 is a HYSPLIT backward trajectory showing a parcel of air crossing the Mediterranean prior to being carried into Baghdad.

Deviations from the regression line between a given element and silicon may be attributed to different wind directions bringing in other types of soil or anthropogenic source emissions (Figures 2-14 through 2-16). As previously stated, Engelbrecht et al. (2009) and others (Schmaltz, 2008; Al-Khafaji, 2009; Al-Dabbas et al., 2012) noted anthropogenic sources of non-dust trace metals and correlated sources to the continued use of leaded fuel in motor vehicles, combustion processes associated with oil, gasoline, and natural gas, and regional battery smelting operations. Specifically, Engelbrecht et al. (2009) states that the occurrence of Pb, Zn and other trace metals (As and Cd) correlate well to battery smelting operations. The February 19th peak (Figures 2-17 and 2-18) and the HYSPLIT trajectory (Figure 2-19) agree with Engelbrecht et al. (2009) in that concentrations of Cu, As, and Ni increase during local winds and are likely attributable to smelting operations. The presence of V (Figure 2-20) with Ni and Zn on February 18th combined with the corresponding transport pattern also validates Al-Jebouri and Younis (2012) claims that V is a useful tracer for anthropogenic source emissions from refineries, local smelting operations, and fossil fuel combustion processes.

The CIA World Factbook estimates the 2013 population for Iraq as approximately 31.8 million with 7.2 million of those people living in Baghdad. A population of this magnitude, combined with Baghdad being the capital of Iraq and the hub of air, rail, and road transportation (Mustafa and Mohammed, 2012), requires significant amounts of fossil fuel resources for daily household, business, and transportation needs. The wind rose for the March 2010 sampling

campaign (Figure 2-15) shows a higher occurrence of winds between 2.1-3.6 m/s (40.8%) and 3.6-5.7 m/s (37.4%). Figure 2-16 depicts the percentage of time that winds are in each range. The trace metals shown in Figures 2-17 and 2-18 are consistent with the HYSPLIT results in Figure 2-19 that show local winds and sources impacting the site. The presence of V with Ni and Zn in Figure 2-20 provide further evidence that the wind drainage during this time is predominately local.

The data shown in Figures 2-17, 2-18, and 2-20 are consistent with local wind events (Figure 2-19) and minimal influence from surrounding areas. The peak that occurred on March 18, 2010, was centered in the vicinity of Baghdad; therefore, the high Pb concentrations are likely a result of the trapping and accumulation of local combustion activities (tail pipe emissions, industrial combustion activities [Engelbrecht et al., 2009]), and Pb-Zn smelting activities (Carroll and Essik, 2008) within Baghdad's recessed basin under minimal wind conditions. Correlating Pb to S, Zn, and Br provides a fingerprint of anthropogenic emissions from leaded gasoline (Sturges and Harrison, 1986; Dowdell et al., 1994; Gribble, 2000). Bromine is associated with the tetraethyl lead, tetramethyl lead, and 1,2-dibromomethane (Lammel et al., 2002) compounds added to gasoline to reduce engine knocking. A study conducted by Lammel et al. (2002) suggests the ratio of Br/Pb in vehicular emissions is 0.4-0.5 in urban and rural sites. Zn may also be used as an anthropogenic source emission for motor vehicles since Zn comes from the normal wear of tires and brakes (Adachi and Tainosho, 2004).

A time series of Pb (Figure 2-21) was plotted to determine when Pb was at its maximum concentrations during this sampling campaign. The Pb time series shows peak concentrations on March 12th and the morning of the 18th. Figure 2-22 shows a time series of S with the most concentrated peaks occurring on stages 6 (0.34-0.56 μm) and 7 (0.26-0.34 μm), also on March

12th and 18th. A HYSPLIT analysis indicates that on both of these days winds entered Iraq from Jordan and Saudi Arabia. A smaller S peak on March 15th is influenced by the Red Sea, the Gulf of Aden, and Saudi Arabia as evidenced by HYSPLIT backward trajectories.

The time series of Cl (Figure 2-23) shows Cl is well represented in all size fractions, especially in the 2.5-5.0 micron size fraction. It is likely that this Cl signature is associated with sea salts from the Mediterranean Sea, salt flats, and coastal sabkhas. This conclusion agrees with HYSPLIT backward trajectories occurring between March 10th and 11th. Chlorine on stage 8 (0.09-0.56 microns) peaks on the 12th and 18th and aligns well with the Pb and S peaks noted above.

The time series of S and Cl were plotted with Pb (Figures 2-24 through 2-27), as these elements are commonly associated with leaded fuel (Novakov et al., 1972; Miller et al., 1972), coal smelting, mining ash, sea salts, and gypsum (Engelbrecht et al., 2009; Engelbrecht et al., 2013). The overlapping peaks of Pb with S (Figures 2-24 and 2-25) and Pb with Cl (Figures 2-26 and 2-27) are consistent with the elemental signature of the 1970s smog events within the Los Angeles (LA) basin (Novakov et al., 1972; Miller et al., 1972). Similar to LA, photochemical pollution episodes are worsened by Iraq's hot, sunny climate and its topographical low bounded by mountain ranges (Mustafa and Mohammed, 2012). The lack of local drainage results in the trapping and accumulation of diurnal lead-laden traffic pollution and the re-suspension of road dust, which also may be lead-contaminated. Mustafa and Mohammed, (2012) and others (Kanbour et al., 1987; Al-Quzweny, 1999) noted that spring (March, April and May) and fall (September, October, and November) were the most favorable months for the accumulation of air pollution, due to the lack of wind drainage in Baghdad. The accumulation of Pb (Figure 2-21) and the lack of sufficient drainage (Figure 2-19) during our March field campaign and

trajectory analysis are consistent with the findings of previous studies (Engelbrecht, et al., 2009; Schmaltz, 2008; Al-Khafaji, 2009; Al-Dabbas, et al., 2012). Figure 2-28 shows a three-week time series of Pb, Cl, Br, and S (0.75 to 1.15 microns) collected during the March 6, 2010 sampling campaign. Although S and Pb and S and Cl overly one another, there is no significant 0.4 to 0.5 ratio between Pb and Br.   However, Harrison and Sturges (1983) noted that the 0.4 to 0.5 narrowed to 0.11 to 0.59 in urban areas when atmospheric Pb and Br dominated traffic emissions.   Figures 2-28 and 2-29 suggests that 94% of the Pb associated with this field campaign is associated with sources other than gasoline.

The high concentrations of Pb observed in some of the samples (Stages 1-8) (Figures 2-21 and 2-24 to 2-28) are of concern as they exceed the NAAQS (150 ng m^{-3}) health-based standard for Pb.   Health-based standards were established for Pb due to its suspected carcinogenicity, increased incidences of mental retardation (Fulton et al., 1987; Campbell et al., 2000; Needleman, 2004; Papanikolaou et al., 2005) and aggression in children (McDonald and Potter, 1996), ability to accumulate in the skeletal system (Phillip and Gerson, 1994; Rabinowitz, 1991), and correlations to hypertension (Nawrot et al., 2002; Fanning, 1988; Schwartz, 1995; ATSDR, 2005; Staessen et al., 1994) and cardiovascular disease in adults (Schober et al., 2006; Böckelmann et al., 2002; Cheng et al., 1988; Kirkby and Gyntelberg, 1985; Kosmider and Petelenz, 1962). According to Hursh et al. (1969) approximately 95% of inhaled inorganic lead aerosols are absorbed from the bronchiolar and alveolar regions of the respiratory tract and 30-40% of this amount absorbs into the bloodstream (Phillip and Gerson, 1994).

The wind sector graph (Figure 2-30) and the wind rose (Figure 2-31) show the three-week May to June sampling campaign was strongly influenced by winds originating from Syria, Turkey, and the Mediterranean Sea. Figure 2-32 is an analysis of the predominant elements

associated with the 0.34 to 0.56 micron range (stage 6) beginning on May 29, 2010. The text boxes above each peak (Figure 2-32) assist in illustrating the individual wind events (Figure 2-33) and showing the origin of the air reaching the site during those events as determined by the HYSPLIT backward trajectories. The high S concentrations are likely associated with anthropogenic emissions from combustion activities (Figure 2-34) and the use of leaded fuels in Iraq and its surrounding countries. In addition to leaded fuel, the presence of chlorine may also be correlated to salt mining operations and the lofting of fine sediment from dried lakebeds as well as salty desert soils and coastal sabkhas. In absence of fuel emissions, S can also be associated with gypsum, natural S cycle from bacterial fixation, sea salt, coal smelting, and local industry.

2.6   Conclusions

This paper describes the results from a sampling campaign in Baghdad, Iraq, designed to collect continuous high temporal resolution, aerosol size and composition data for use in epidemiological studies. This study showed that Pb concentrations routinely exceeded U.S. NAAQS, which are health based standards designed to safeguard human health. The lead-laden aerosols are likely a result of anthropogenic source emissions from the continued use of leaded gasoline in Iraq, combustion activities, local smelting operations, and the lofting and transport of Pb enriched soil/deposits. Sulfur, when combined with lead, is a good source indicator of the use of leaded fuels and smelting industries, as well as geogenic emissions of gypsum-laden dust. Cl combined with Br and S indicates coastal and salt flat emissions and anthropogenic source emissions of leaded fuel and smelting activities. The presence and accumulation of V, in the absence of wind drainage, is a good indicator of local fossil fuel refining, fuel combustion, and smelting/mining activities. Soil element abundances were consistent across all aerosol size

48

fractions. Additionally, good correlations between the crustal elements / Si ratios and the soil aerosol abundance ratios indicate that there are geogenic crustal particles in the finest size fractions.

The presence of high concentrations of lead and other elements observed during this study suggest that there may be adverse health effects associated with the particulate matter breathed by soldiers deployed to Iraq. Epidemiological studies of the effects of the observed particulate matter concentrations and compositions will determine what, if any, adverse health effects might be expected due to long-term exposure to the aerosols in the Iraqi atmosphere.

2.7   Acknowledgments

2.8   Figures

Figure 2-1. A general vicinity map of Iraq. The green and red place markers depict the Taurus and Zagros Mountains ranges of Turkey and Iran, respectively. Baghdad is represented with a blue thumbtack and Camp Victory is located in Baghdad. Image created from Google Maps: www.google.com.

Figure 2-2. Camp Victory with respect to Baghdad. Camp Victory is indicated with a green thumbtack and Baghdad is represented with a place marker. Image created from Google Maps: http://www.google.com.
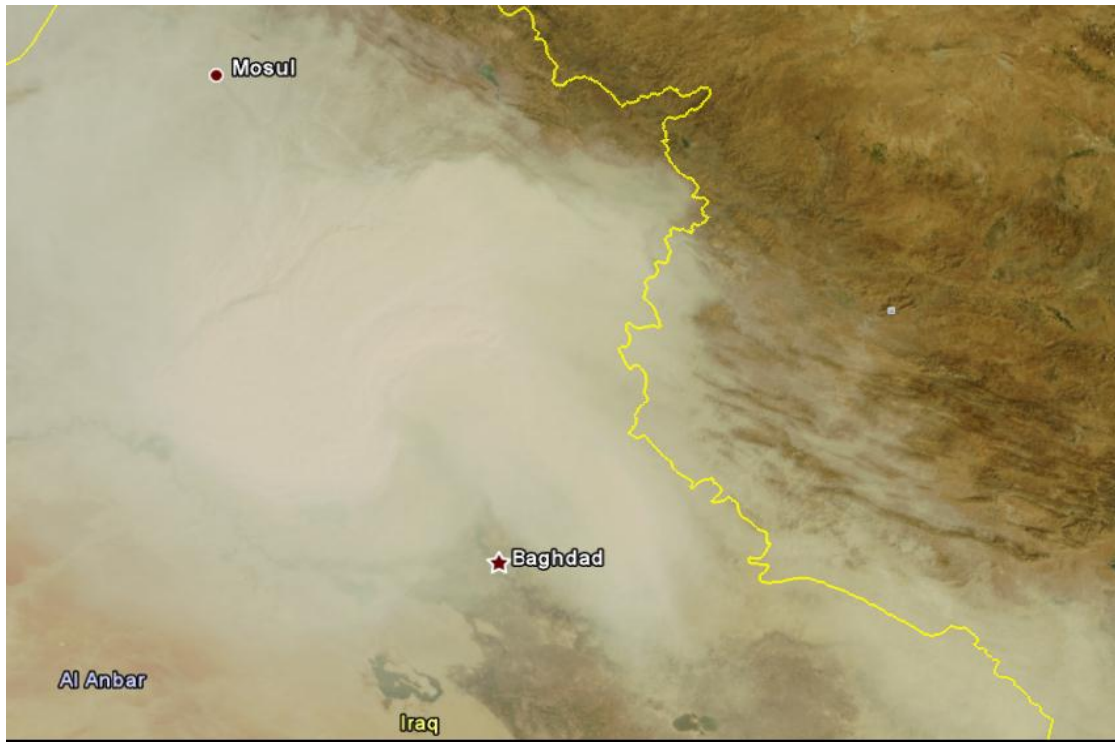
Figure 2-3. Shamal dust storm passing through Iraq. This Envisat/ASAR image is of a dust storm over Iraq occurring from September 12-15, 2008. The star marker indicates the approximate location of Baghdad with respect to the Storm. The image was taken by Envisat/ASAR passes on the 12th and 15th of September. ASAR images are generated from Level-0 (raw) and Level-1b products Envisat source Level-0 and Level-1b products are provided by ESA. Envisat/ASAR image courtesy of Earth Snapshot.

Figure 2-4. Photograph of a Davis rotating drum unit for monitoring (DRUM) aerosol impactor.
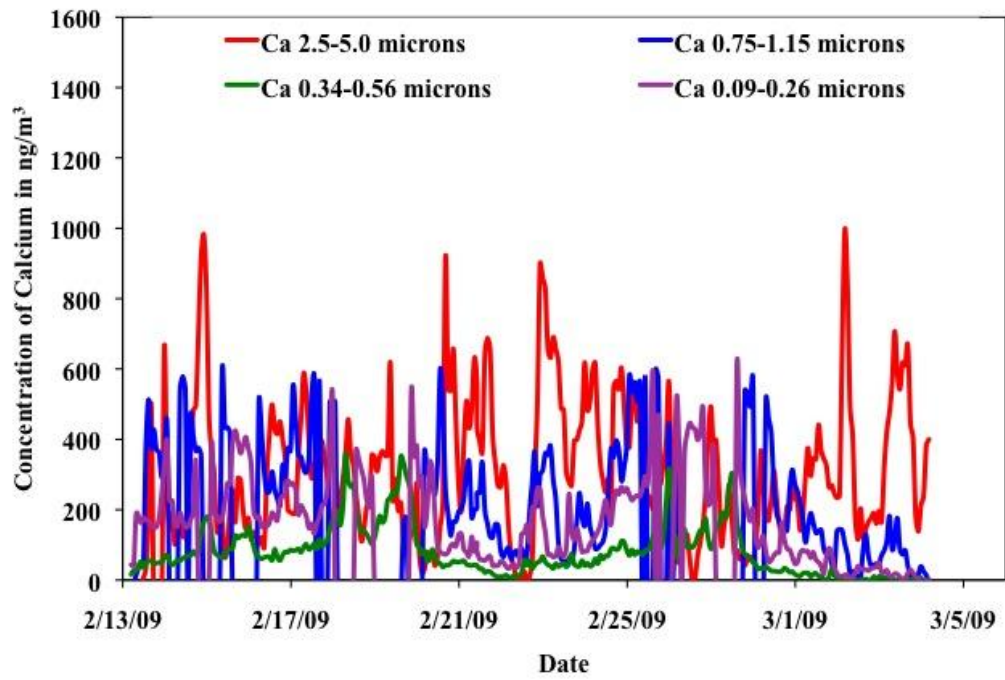
Figure 2-5. Time series of calcium showing the temporal variability of representative size fractions over a three-week period in February 2009.
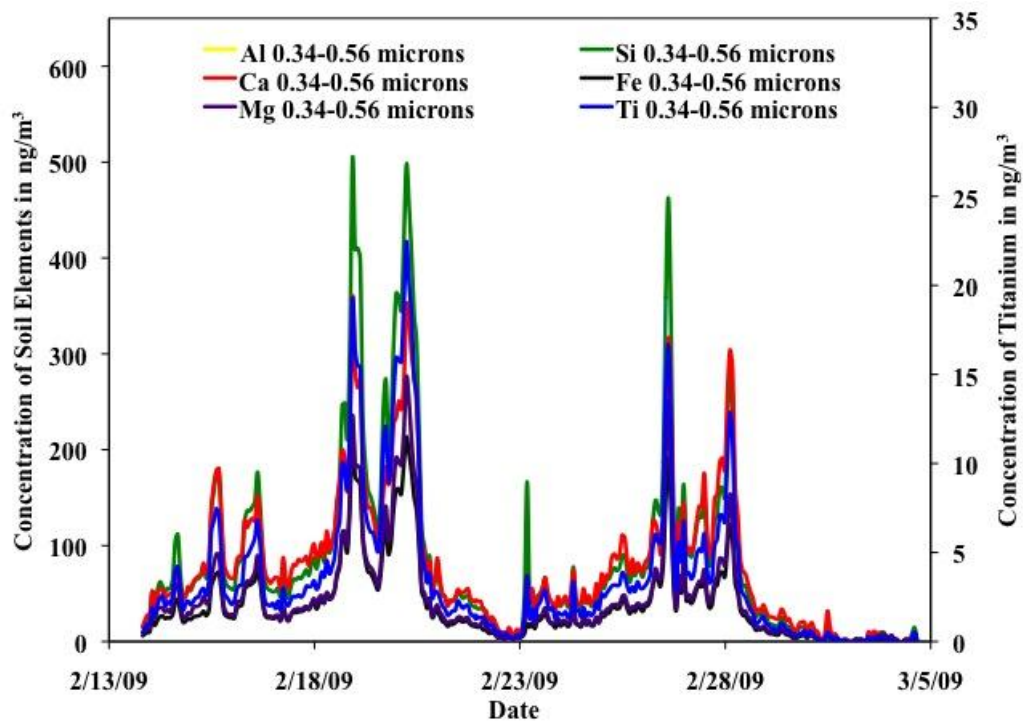
Figure 2-6. Time series of the soil elements Al, Si, Ca, Mg, Ti, and Fe in the 0.34-0.56 micron size fraction. The concentration of Ti is on the secondary axis. This figure shows the presence of soil within the fine aerosols.
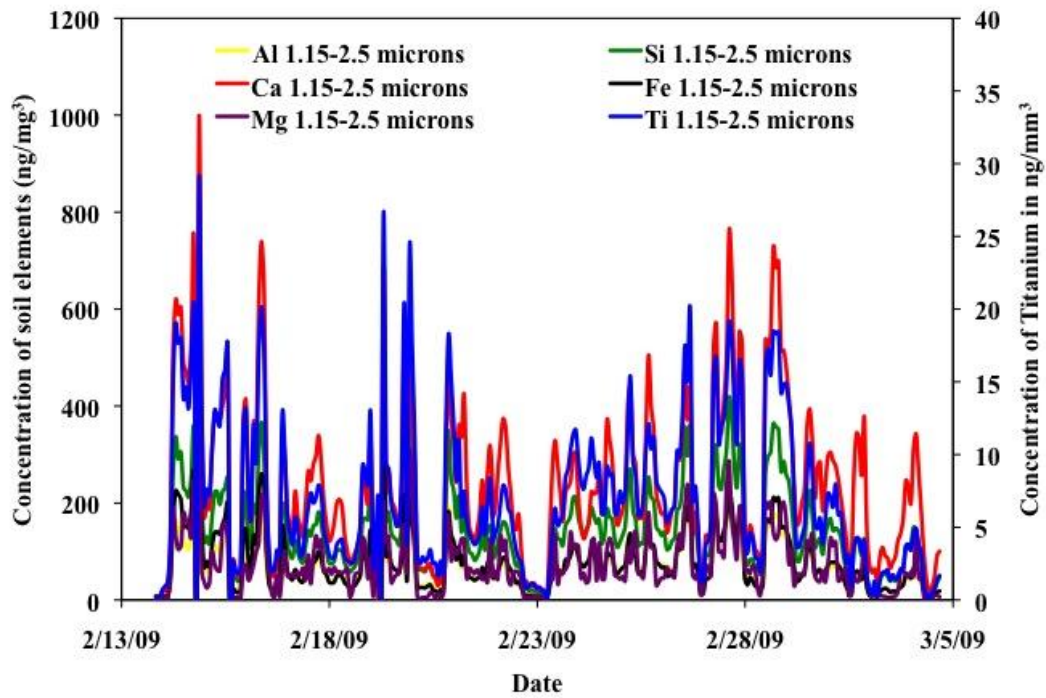
Figure 2-7. Time series of the elements Al, Si, Mg, Ca, Ti, and Fe in the 1.15-2.5 micron size fraction. The concentration of Ti is on the secondary axis.
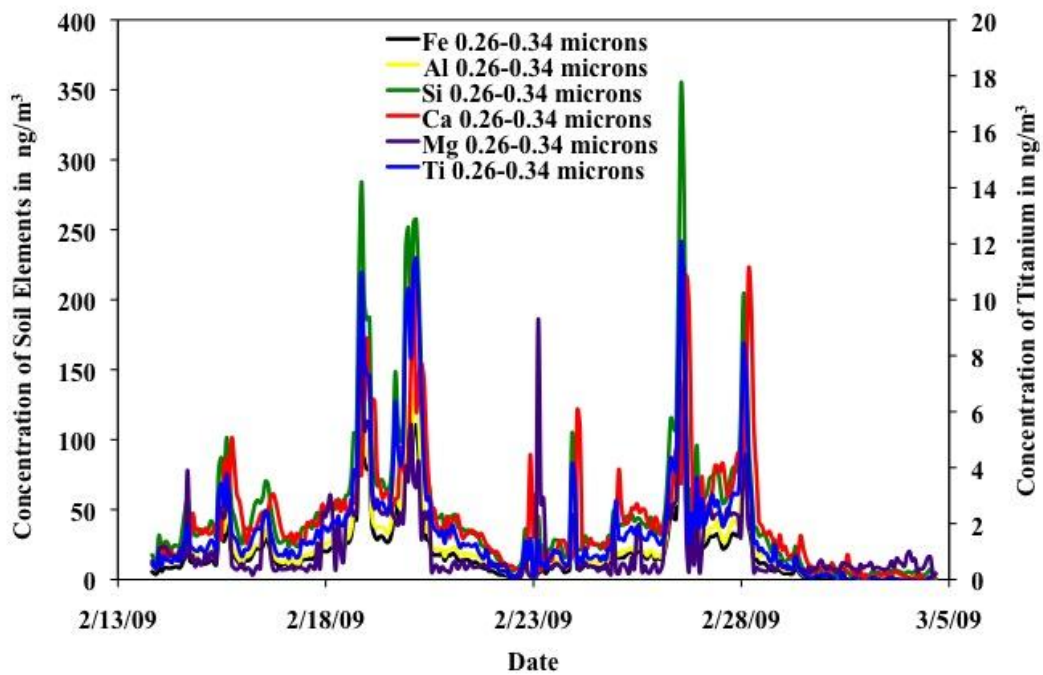
Figure 2-8. Time series of the elements Al, Si, Mg, Ca, Ti, and Fe in the 0.26-0.34 micron size fraction. The concentration of Ti is on the secondary axis.

Shamal
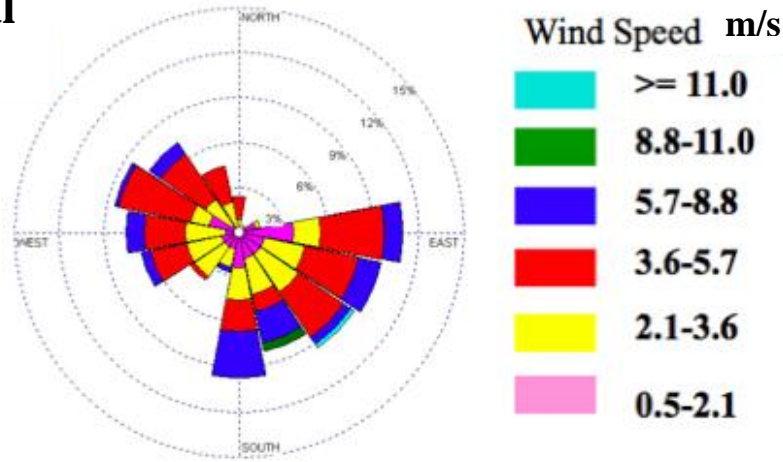
Kous

Figure 2-9. A wind rose for Baghdad, Iraq. Data for this wind rose was collected during a three-week sampling campaign beginning February 13, 2009. It can be noted from this figure that Shamal and Kous winds are the prevailing winds during this time. It can also be noted that 34% of the time wind speeds were between 2.1-3.6 m/s during both Shamal and Kous winds. Wind directions and wind velocity were compiled from data retrieved on September 21, 2013 from Weather Underground METAR KTZR at the Baghdad International Airport in Baghdad, Iraq. Camp Victory is 5km from Baghdad International Airport. The wind rose was compiled using WRPlot from Lakes Environmental.
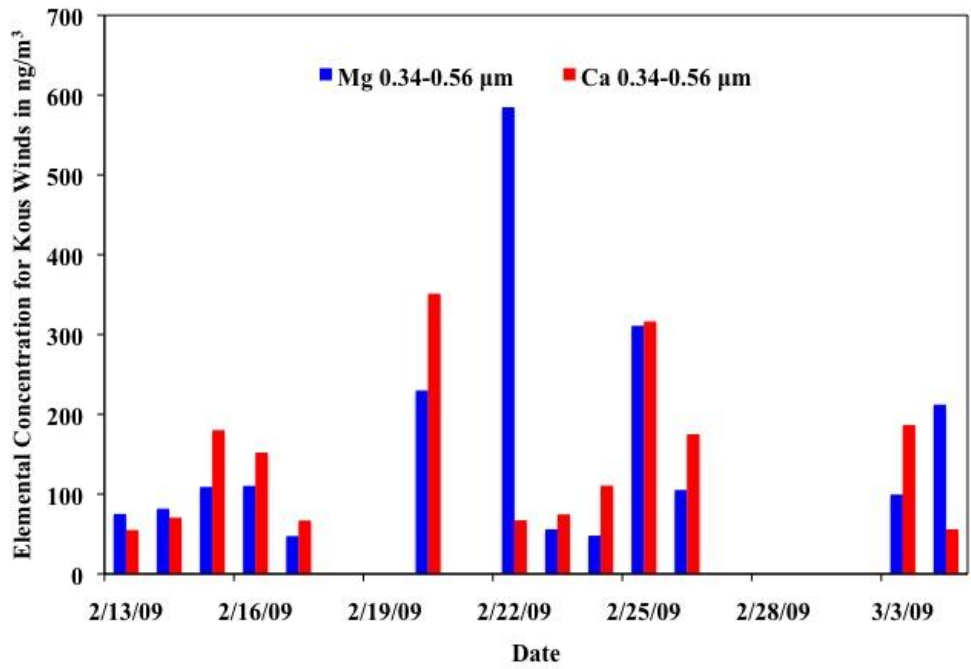
Figure 2-10. Time series of calcium and magnesium during Kous winds.

.
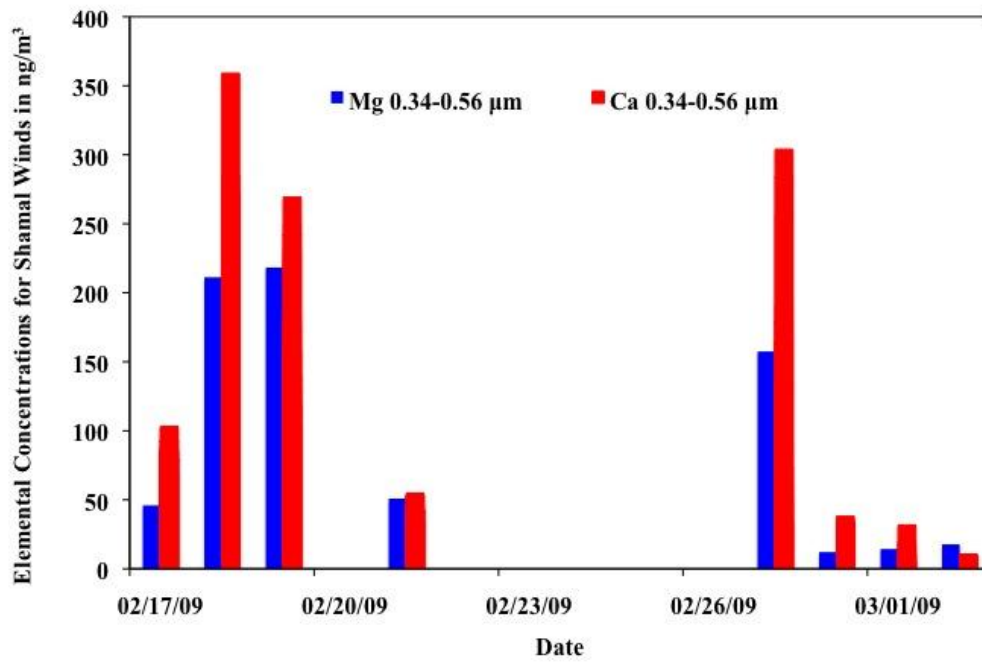
Figure 2-11. Time series of calcium and magnesium during Shamal winds.
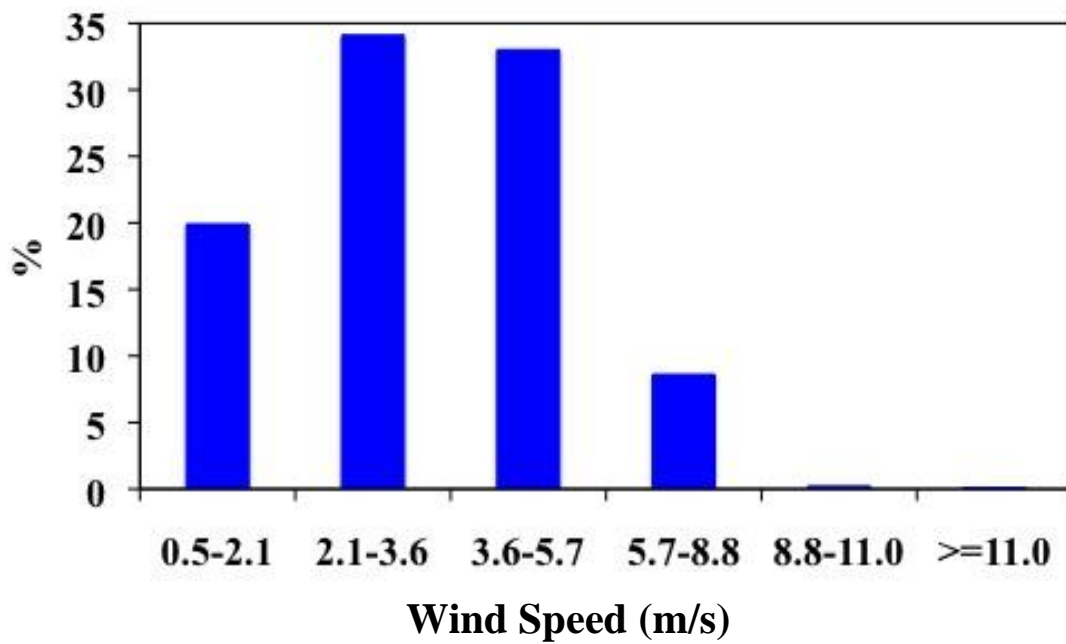
Figure 2-12. Wind speed ranges were collected for three weeks beginning February 13, 2009 from METAR KTZR at Baghdad International Airport. During this campaign typical winds ranged from 2.1 to 3.6 m/s (34.1%) and 3.6-5.7 m/s (33%) during both Shamal and Kous events.
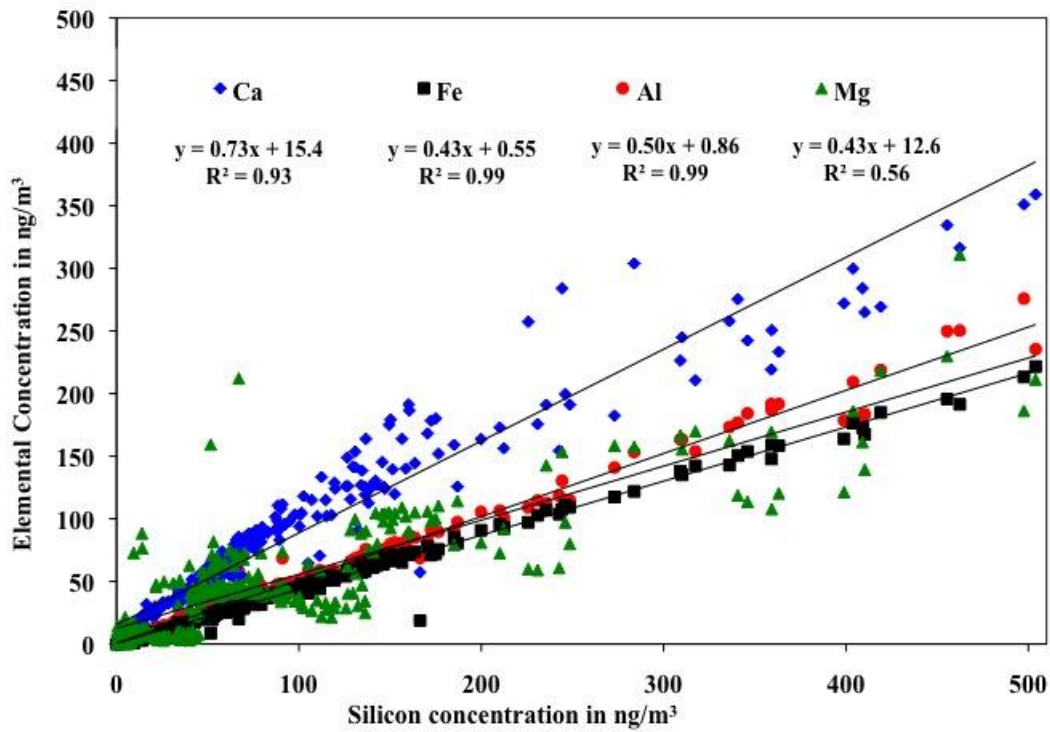
Figure 2-13. Variation of specific crustal elements as they correspond to Si in the 0.34-0.56 micron range during the February 13, 2009 sampling campaign. This figure demonstrates how well Ca, Fe, Mg, and Al correlate to Si. This indicates that these particles are from the same source and appear to be crustal soils within the 0.34 to 0.56 micron size fraction.
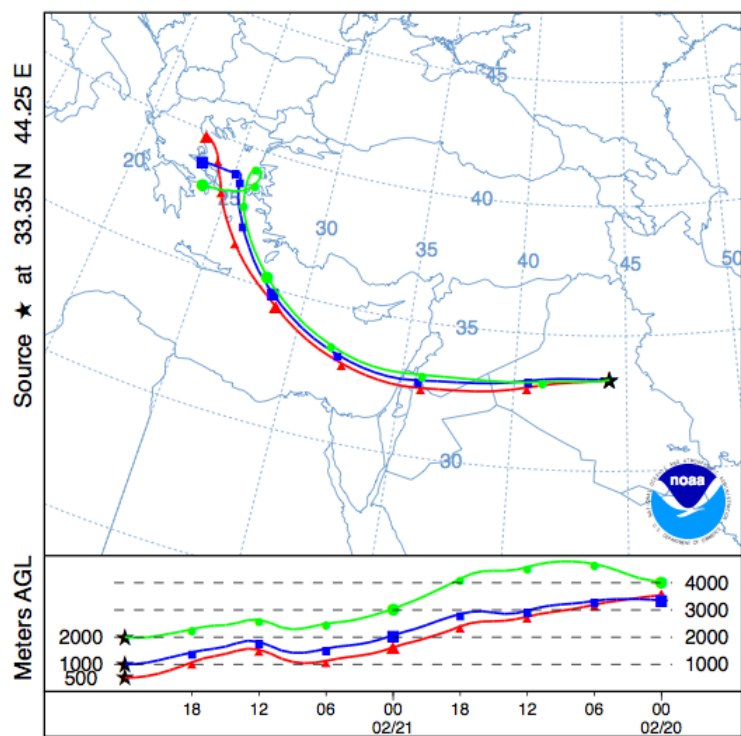
Figure 2-14. HYSPLIT backward meteorological trajectories for a period possessing signatures characteristic of the Mediterranean Sea. This trajectory is a 48-hour backward trajectory starting on February 22, 2009.

Shamal

Kous

Wind Speed m/s

	Wind Speed m/s
(cyan)	>= 11.0
(green)	8.8-11.0
(blue)	5.7-8.8
(red)	3.6-5.7
(yellow)	2.1-3.6
(pink)	0.5-2.1
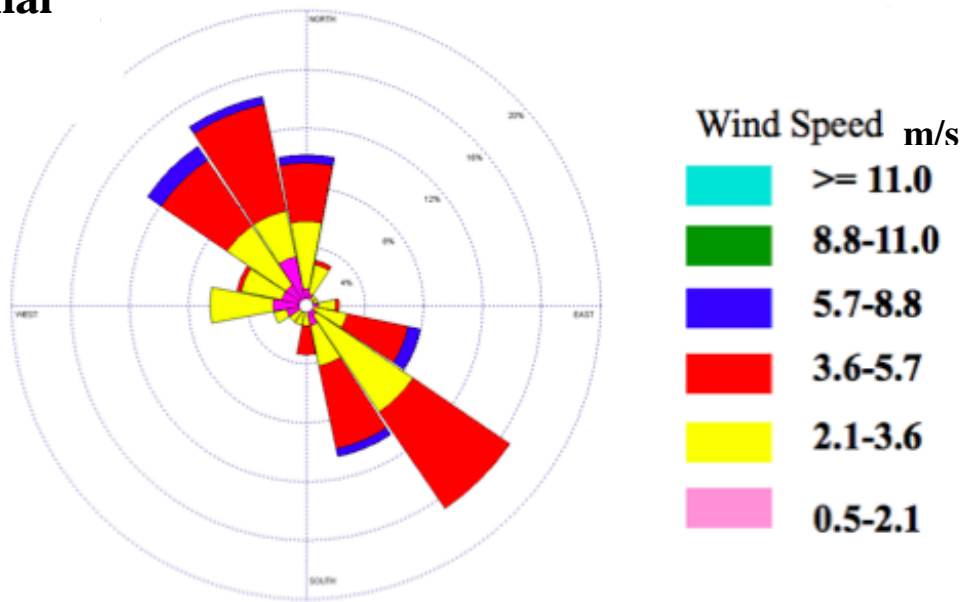
Figure 2-15. Wind rose for Baghdad, Iraq. Data collected during this three-week sampling campaign began March 10, 2010. It can be noted from this figure that Shamal and Kous winds are the prevailing winds during this time. It can also be seen that 41% of the time wind speeds were between 2.1-3.6 m/s during both Shamal and Kous winds. Wind directions and wind velocities were compiled from data retrieved on September 21, 2013 from Weather Underground METAR KTZR at Baghdad International Airport in Baghdad, Iraq. The wind rose was compiled using WRPlot from Lakes Environmental.
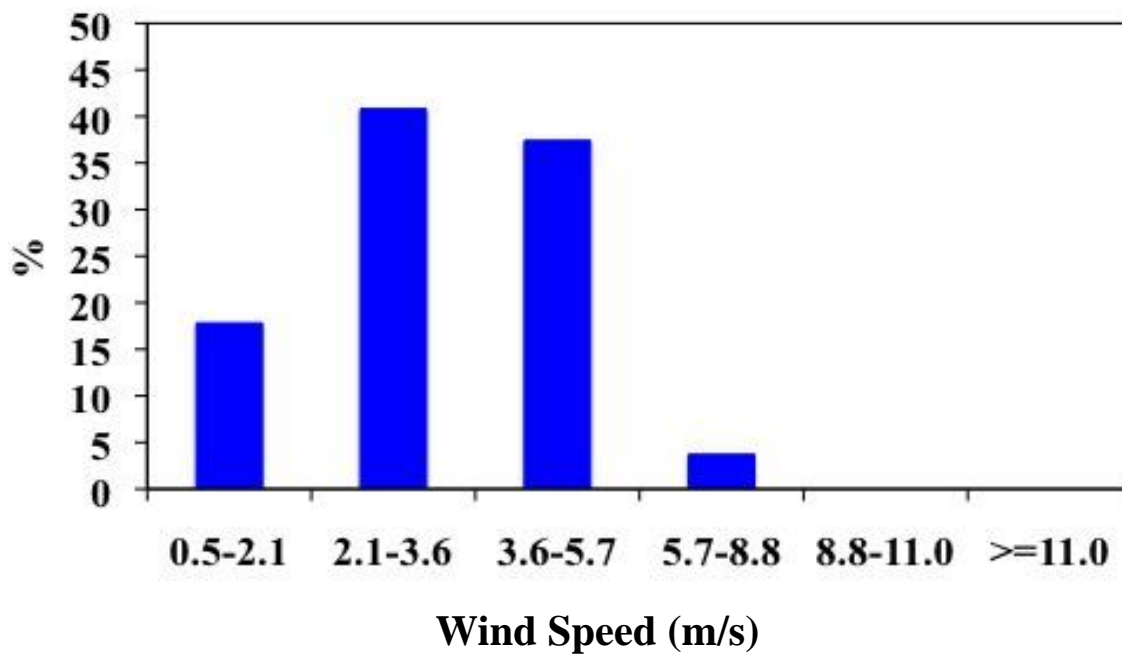
Figure 2-16. Wind speed ranges for the March 2010 sampling campaign. During this campaign typical winds ranged from 2.1 to 3.6 m/s (41%) and 3.6-5.7 m/s (37.4%) between Shamal and Kous winds.
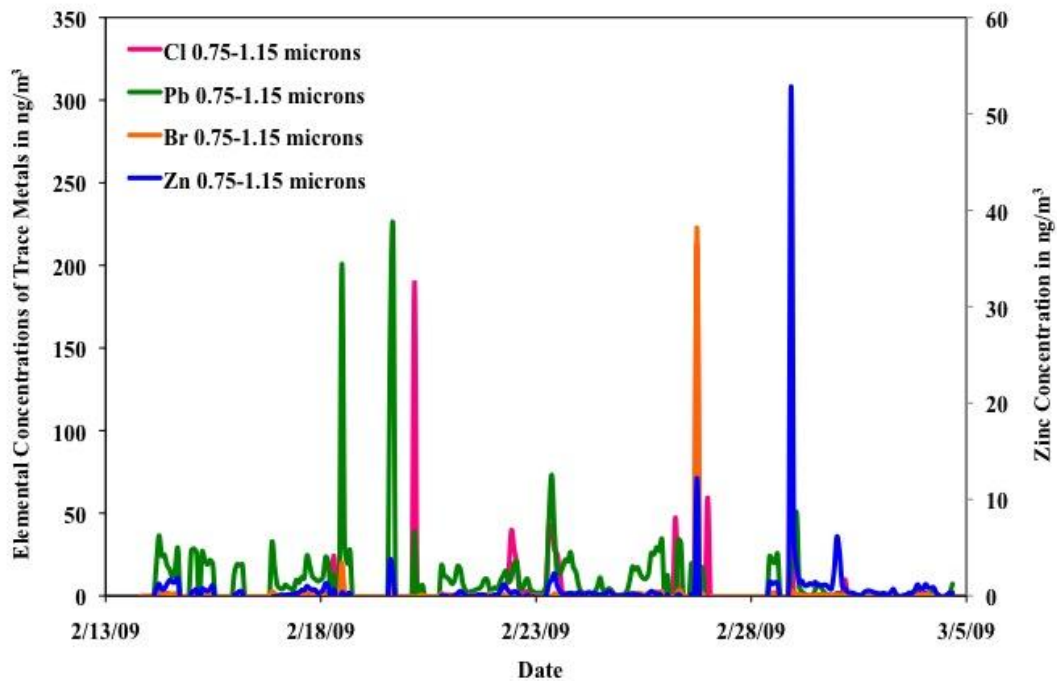
Figure 2-17. Time series of trace metals aerosols (Pb, Cl, Br, and Zn) in the 0.75-1.15 microns size fraction. The concentration of Zn is on the secondary axis. Aerosols were collected during the three-week sampling campaign beginning February 13, 2009.
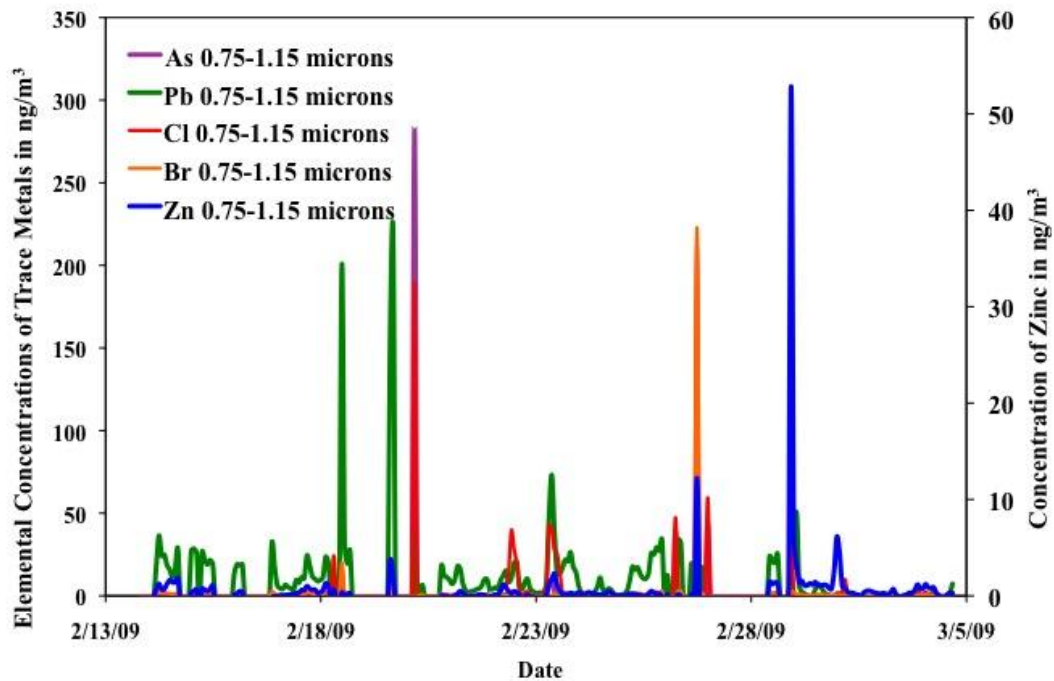
Figure 2-18. Time series of trace metals aerosols (As, Pb, Cl, Br, and Zn) in the 0.75-1.15 microns size fraction. The concentration of Zn is on the secondary axis. Aerosols were collected during the three-week sampling campaign beginning February 13, 2009.
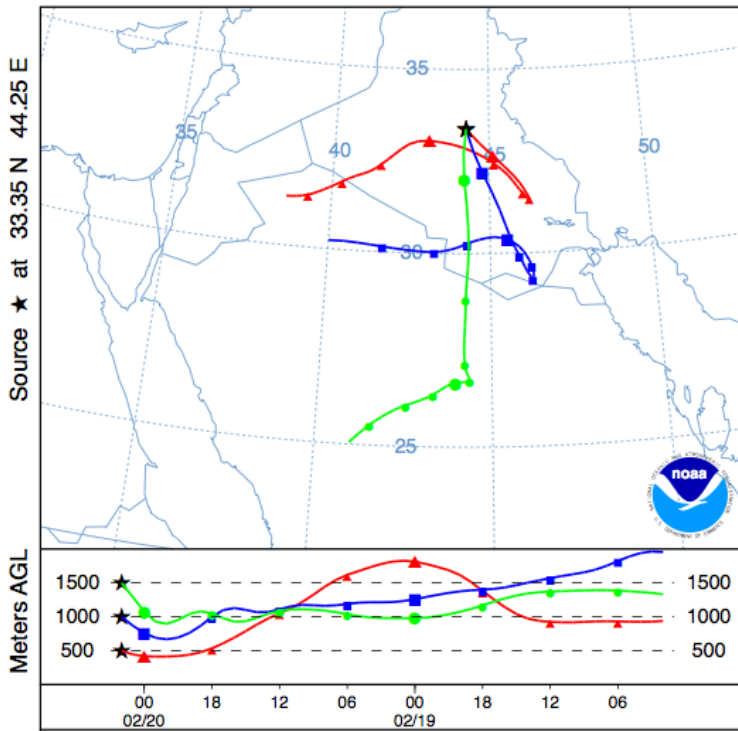
Figure 2-19. NOAA HYSPLIT Model backward meteorological trajectory ending on February 19, 2010 shows air parcels originating predominately around Baghdad and Saudi Arabia and is consistent with Kous winds.   This backward trajectory was calculated for 48-hour period and is representative of the trace metal peak seen in Figures 2-17 and 2-18.
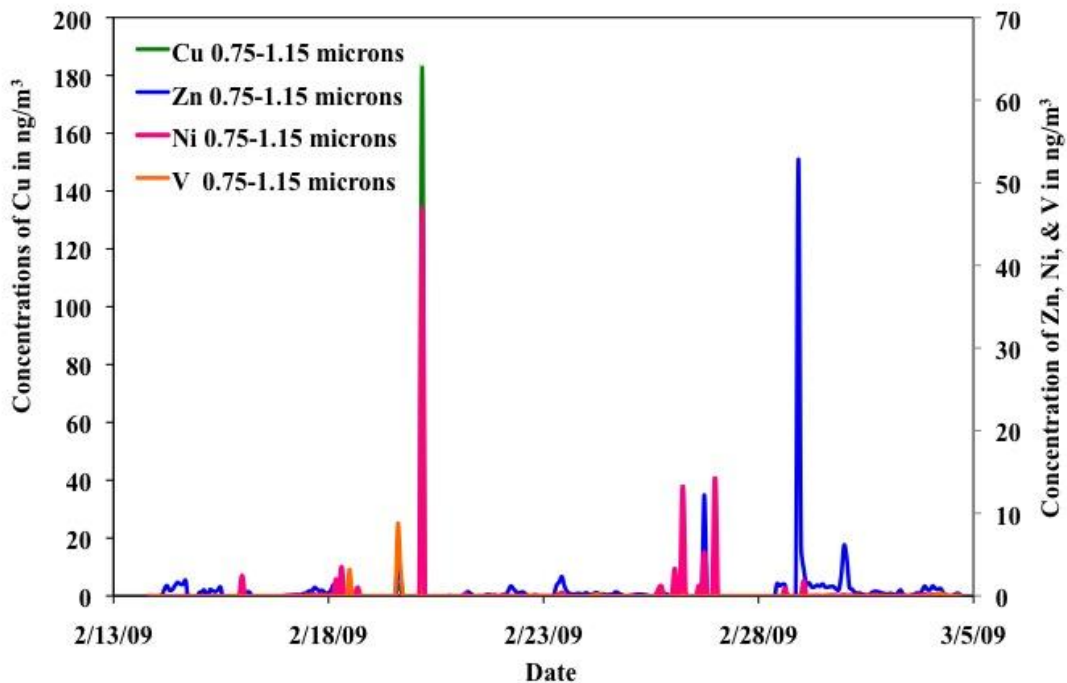
Figure 2-20. Time series of trace metal aerosols (Zn, Ni, V, and Cu) in the 0.75-1.15 micron size fraction. The concentration of Zn, Ni, and V are on the secondary axis. Aerosols were collected during the three-week sampling campaign beginning February 13, 2009.
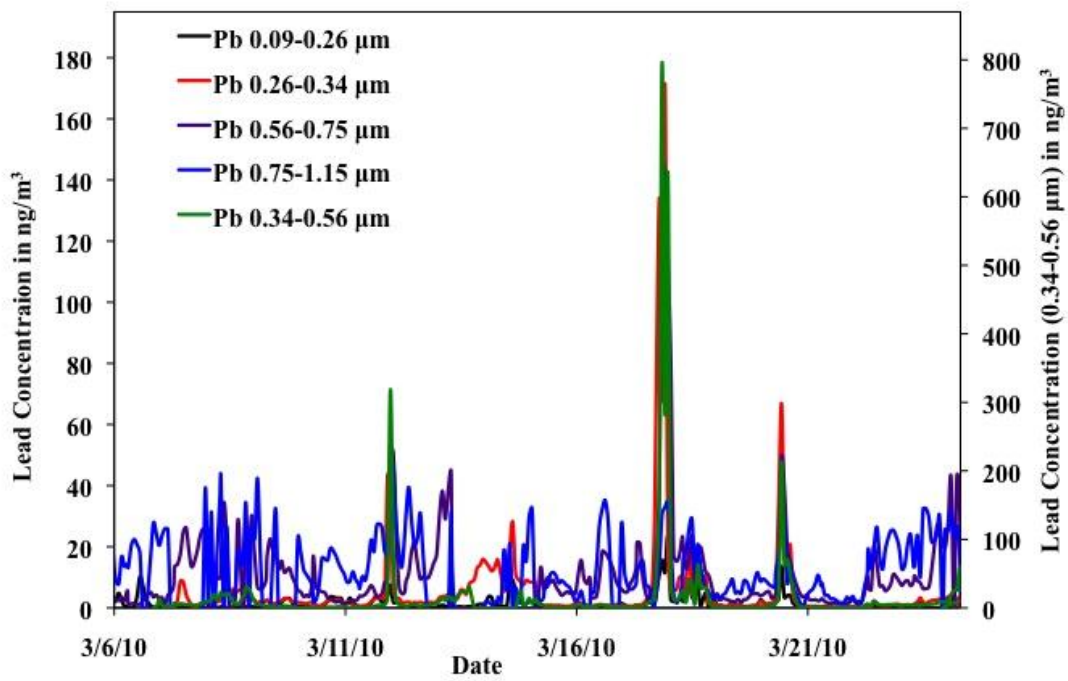
Figure 2-21. Times series of Pb in aerosols ranging in size from 0.09-1.15 microns. The concentration of Pb (0.34-0.56) is on the secondary axis.
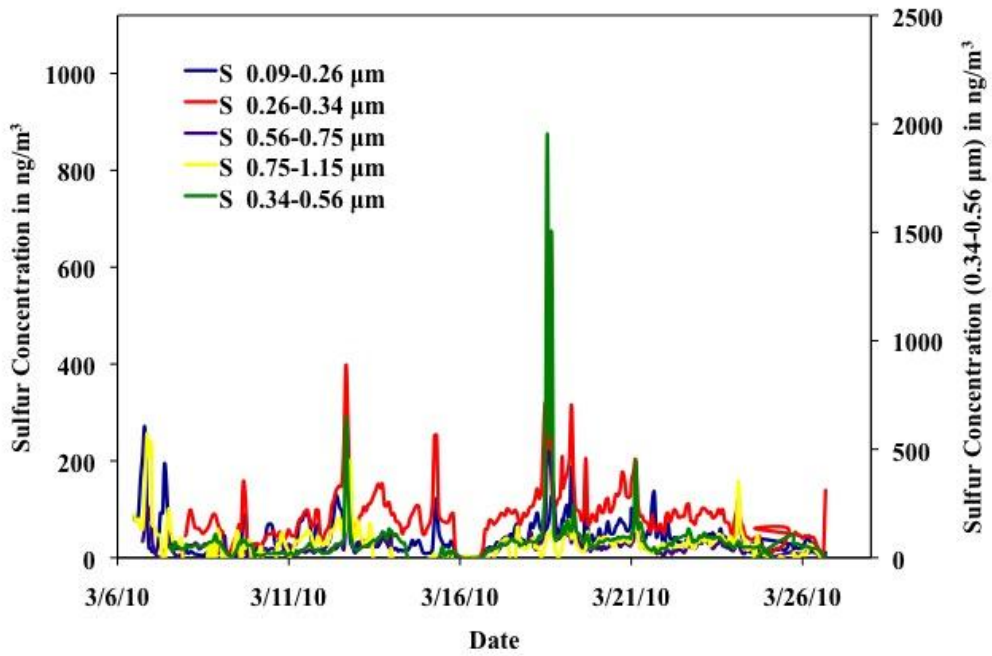
Figure 2-22. Time series of S in aerosols ranging in size from 0.09-1.15 microns. The concentration of S (0.34-0.56 microns) is on the secondary axis.
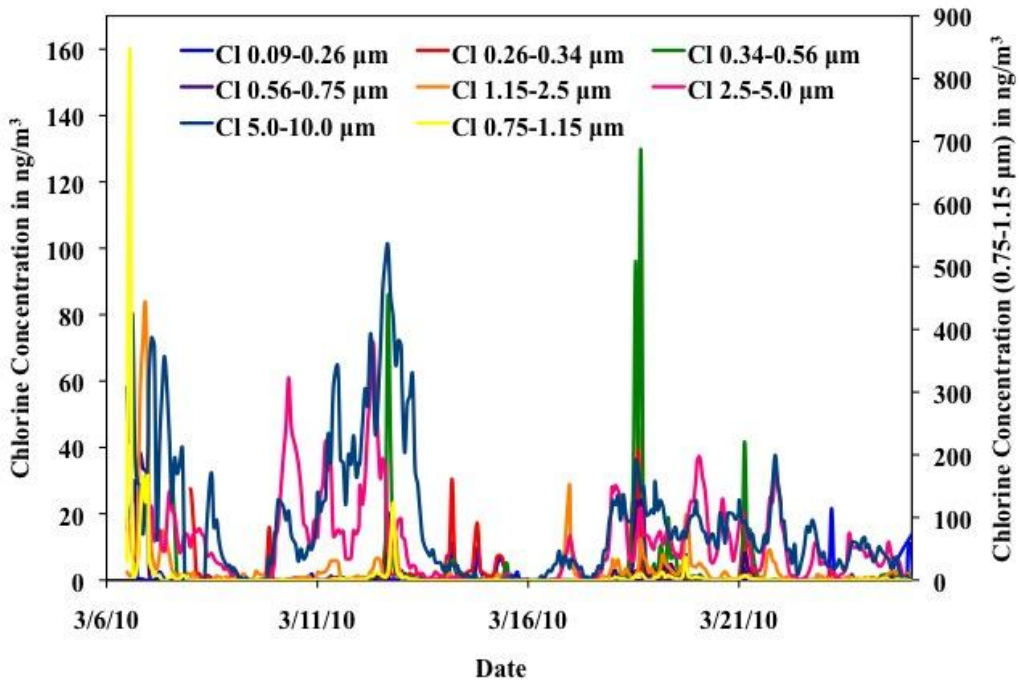
Figure 2-23. Time series of Cl in aerosols ranging in size from 0.09-10.0 microns. The concentration of Cl (0.75-1.15 microns) is on the secondary axis.
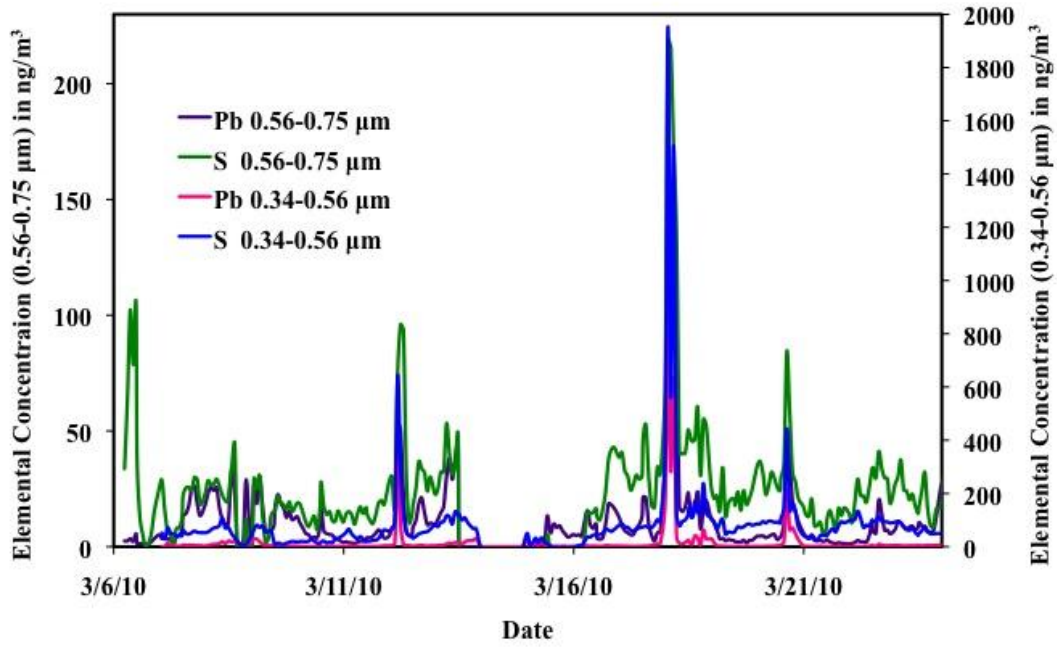
Figure 2-24. Time series of Pb and S in two size fractions ranging from 0.34 to 0.75 microns. Stage 6 (0.34-0.56 microns) was plotted on the secondary axis.
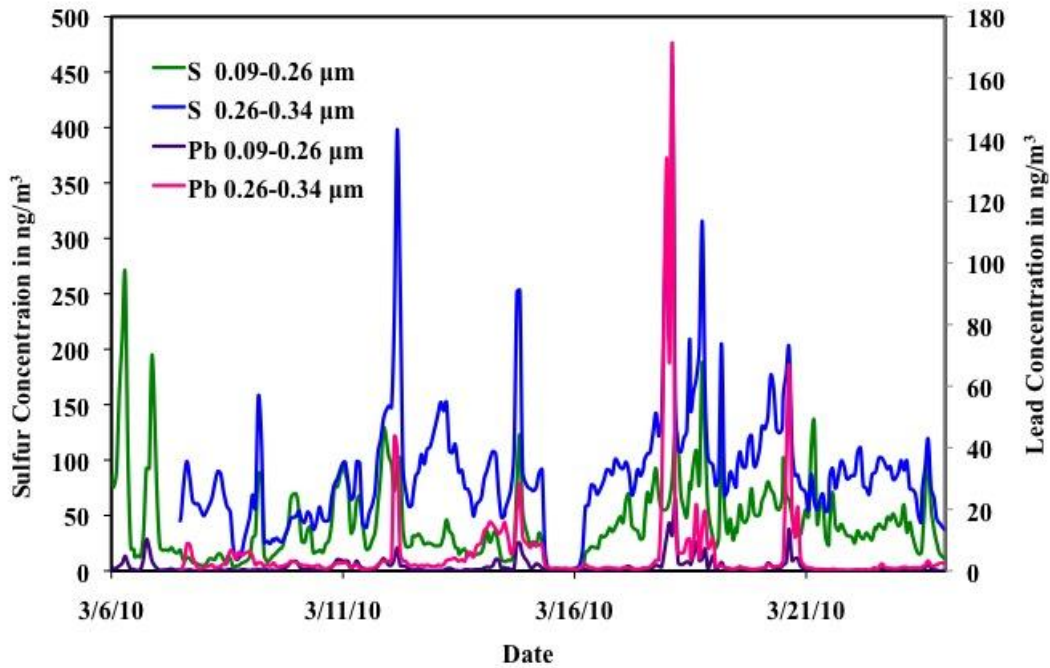
Figure 2-25. Time series of Pb and S in two size fractions ranging from 0.09 to 0.34 microns. The concentration of Pb (stages 6 and 8) were plotted on the secondary axis.
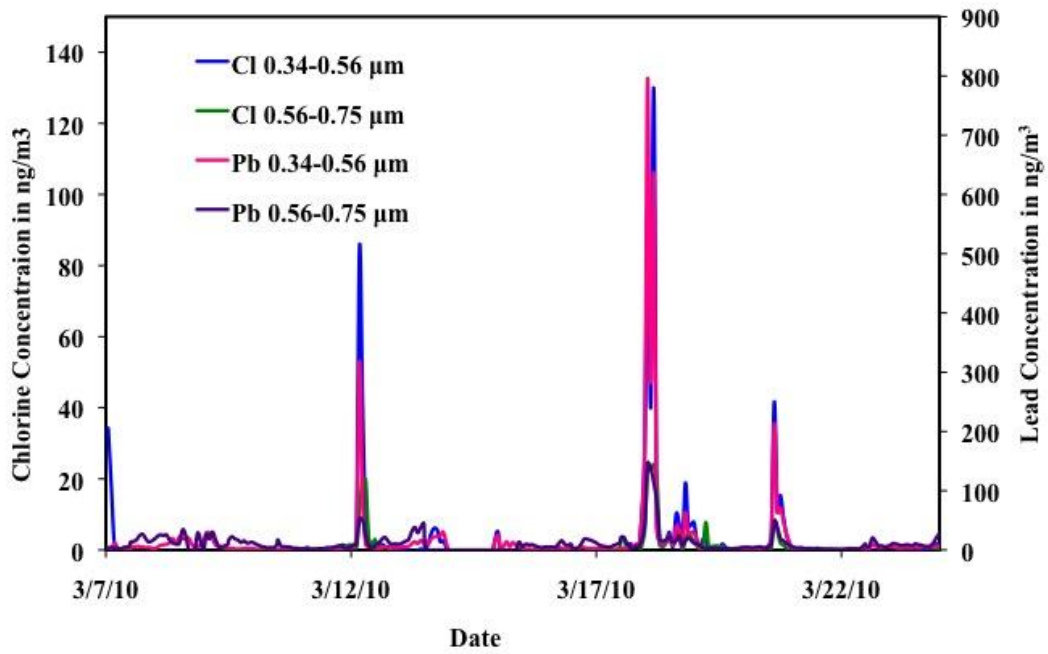
Figure 2-26. Time series of Cl and Pb in two size fractions ranging from 0.34 to 0.75 microns. The concentration of Pb (stages 6 and 8) were plotted on the secondary axis.
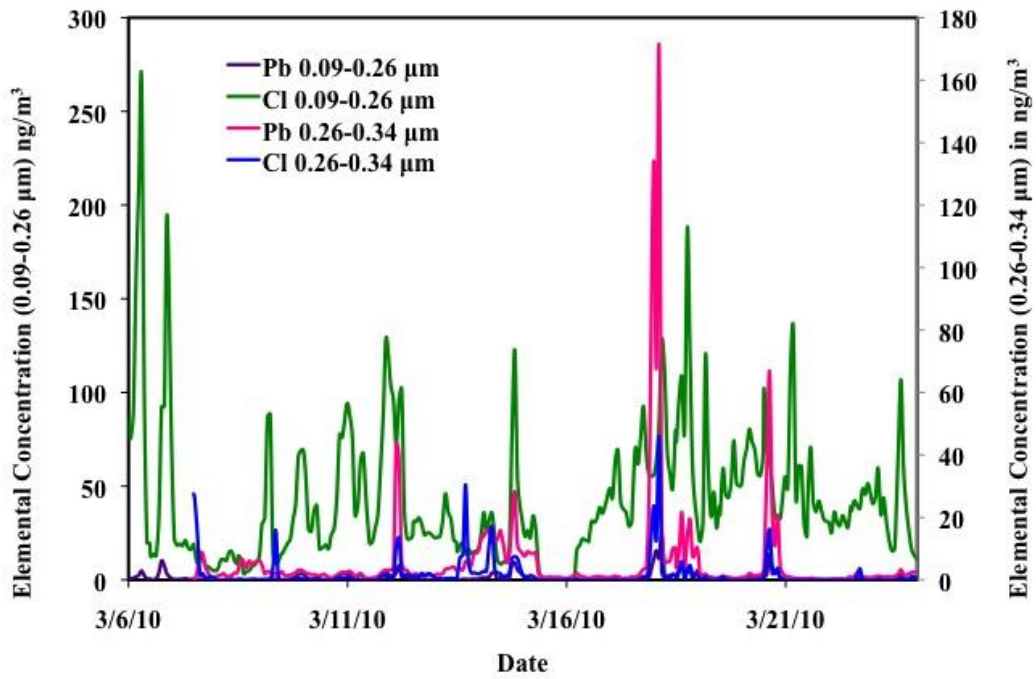
Figure 2-27. Time series of Cl and Pb in two size fractions ranging from 0.09 to 0.34 microns. Stage 7 (0.26-0.34 microns) were plotted on the secondary axis.
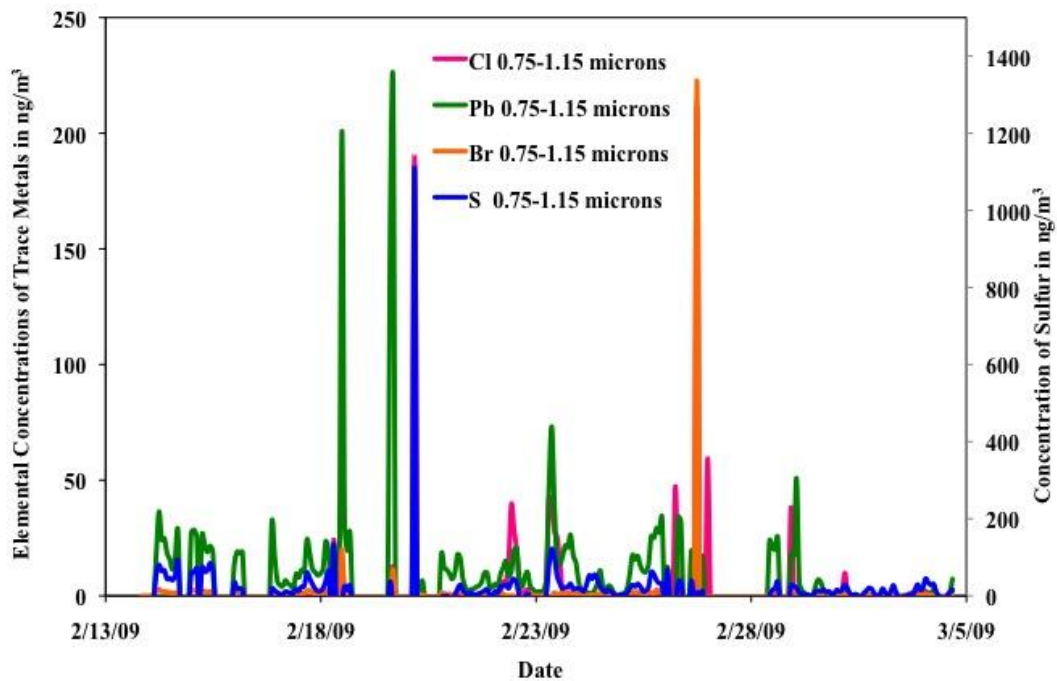
Figure 2-28. Time series of Pb, Cl, Br, and S aerosols in the 0.75-1.15 micron size fraction. The concentration of S was plotted on the secondary axis.
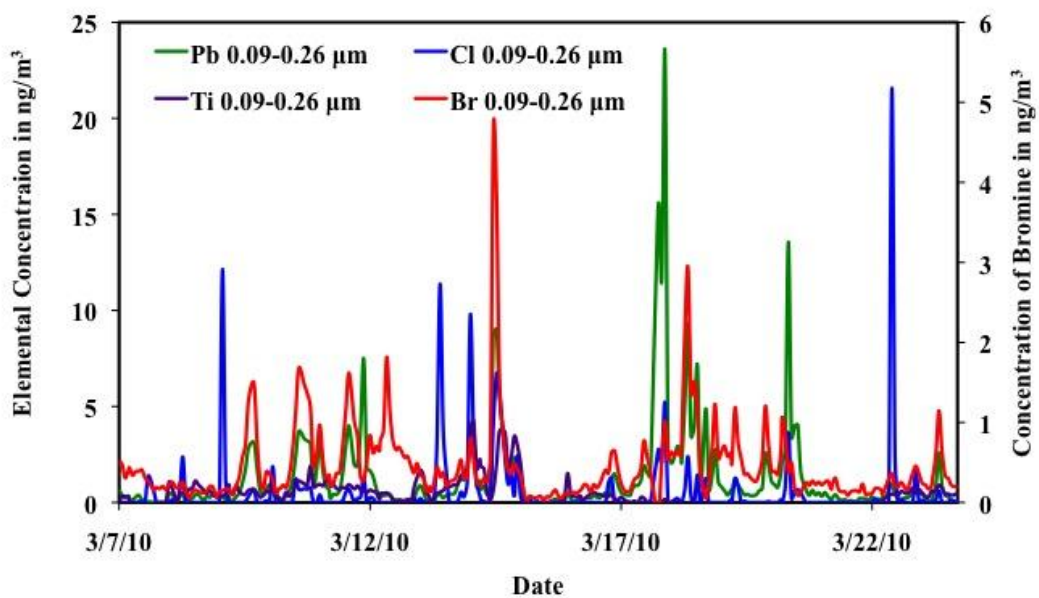
Figure 2-29. Time series of Pb, Cl, Ti, and Br in the 0.09-0.26 microns size fraction. The concentration of Br was plotted on the secondary axis. It can be noted when Br and Pb are not a signature for leaded gasoline, Pb correlates well to titanium and is likely a soil signature.
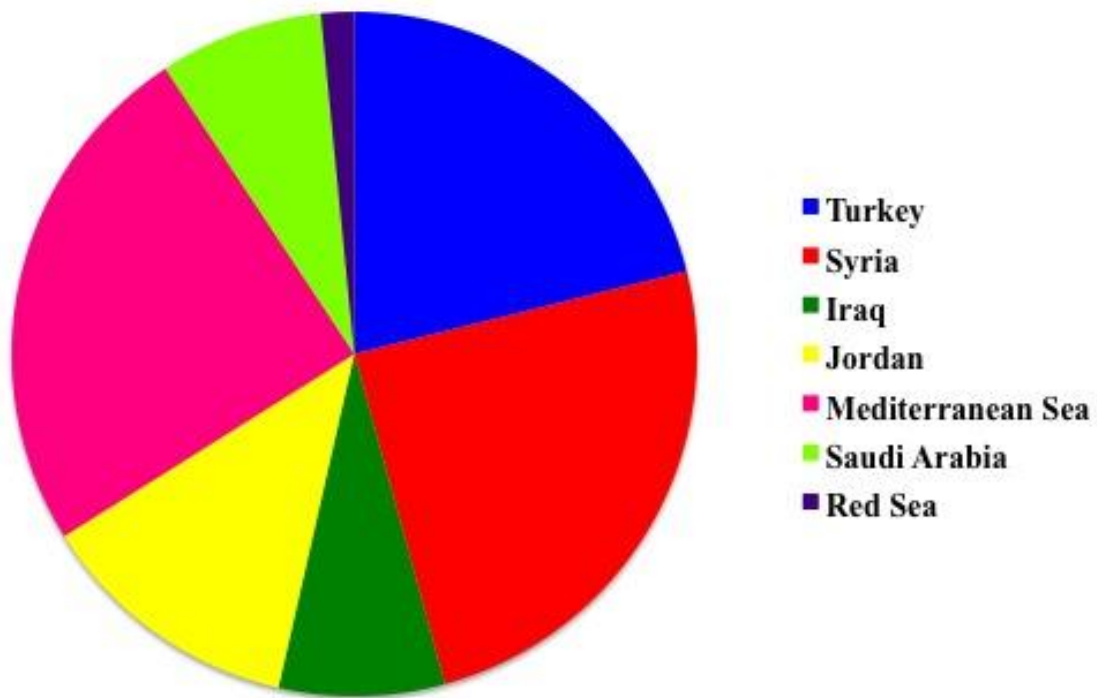
Figure 2-30. Wind sector graph for the May to June 2010 sampling campaign. It can be seen from this graph that predominate winds during this period were from a northwesterly direction consistent with Shamal Winds. Data was compiled from Weather Underground.

Shamal
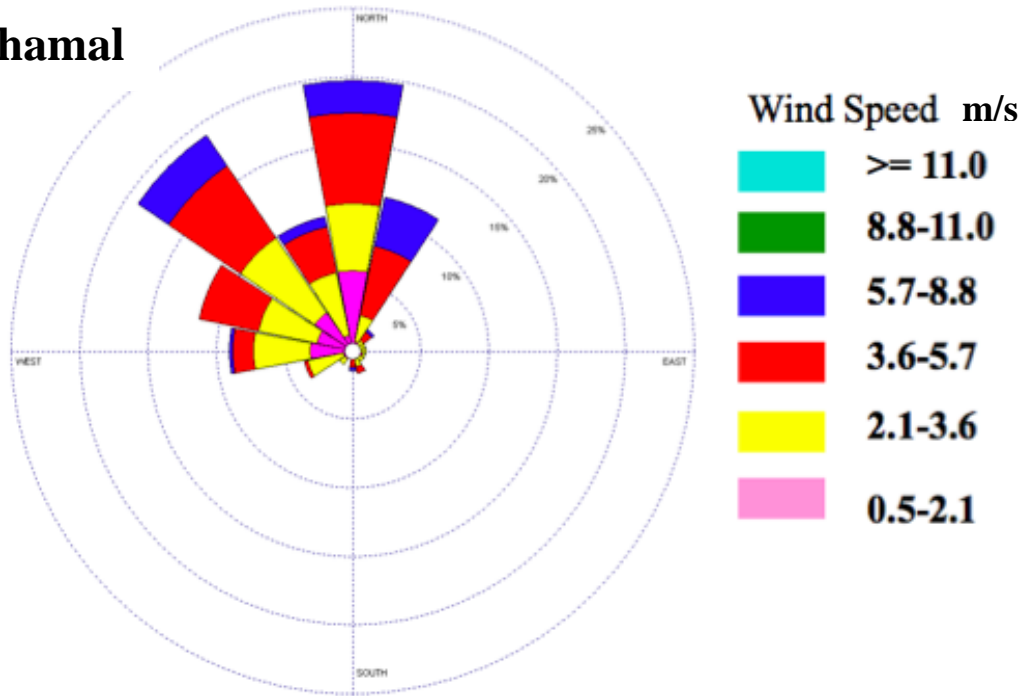
Figure 2-31. Wind rose for Baghdad, Iraq for the May to June 2010 sampling campaign. It can be noted from this figure that Shamal winds were the prevailing winds during time. Wind directions and wind velocity were compiled from Weather Underground. The wind rose was compiled using WRPlot from Lakes Environmental.
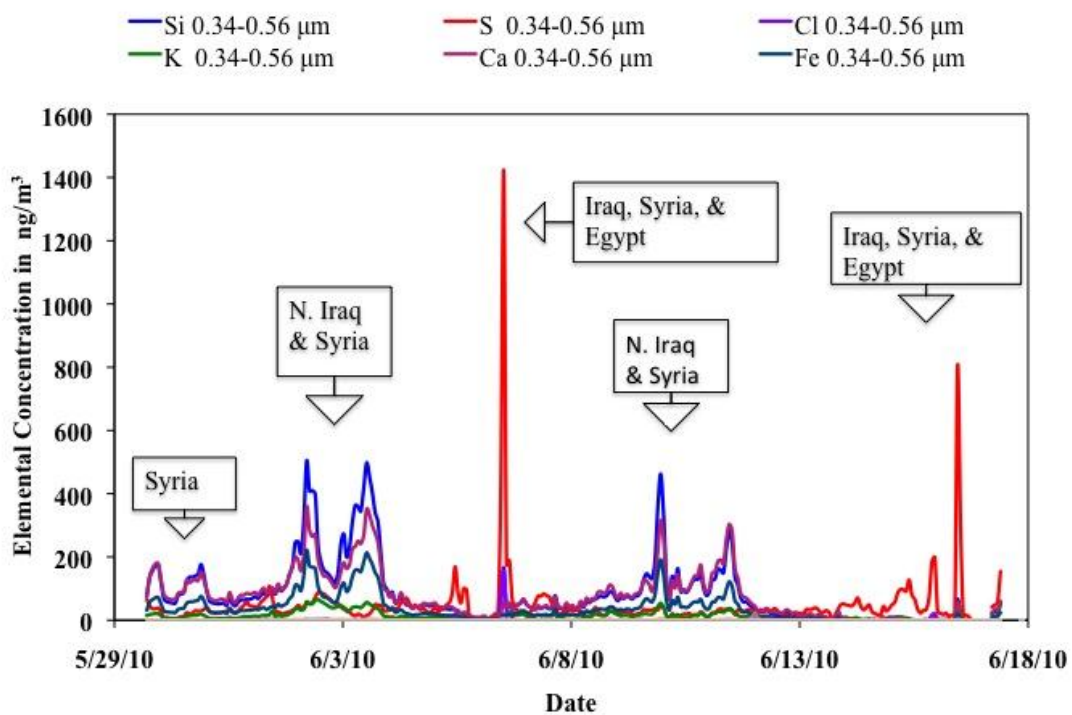
Figure 2-32. Elemental analysis of aerosols in the 0.34-0.56 micron size fraction. This period was influenced strongly by winds from Northern Iraq, Syria, and the Mediterranean Sea.
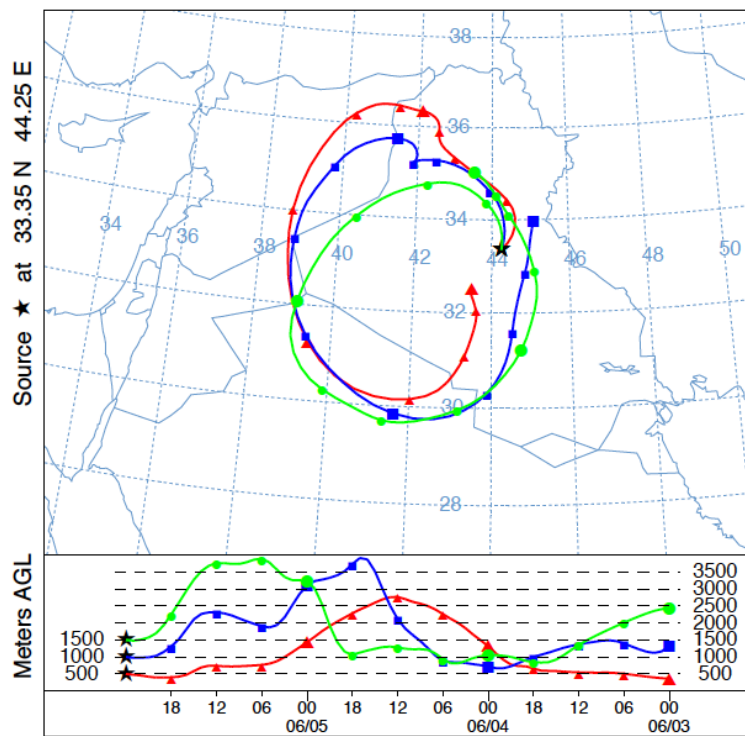
Figure 2-33. NOAA HYSPLIT Model backward meteorological trajectory beginning on June 6, 2010. This period possesses signatures characteristic of anthropogenic emissions from Iraq, Syria, and Saudi Arabia. This backward trajectory was calculated for 72-hour period.
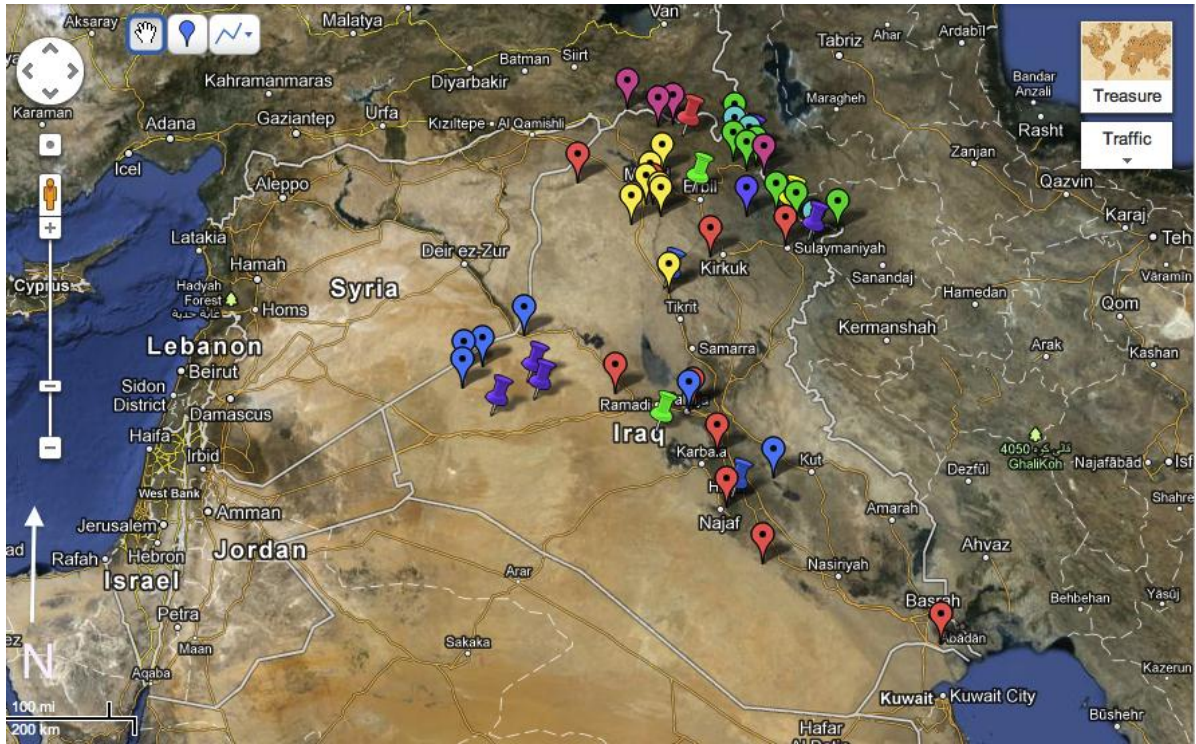
Figure 2-34. General vicinity of Iraqi mining resources. The markers depict active mines within Iraq, the Taurus and Zagros Mountains Ranges of Turkey and Iran, respectively. Image created from Google Maps. Data was compiled from Find the Data.

2.9   Tables

Table 2-1. Elements analyzed by Synchrotron X-Ray Fluorescence.

Magnesium (Mg)	Aluminum (Al)	Silicon (Si)	Phosphorus (P)
Sulfur (S)	Chlorine (Cl)	Potassium (K)	Calcium (Ca)
Titanium (Ti)	Vanadium (V)	Chromium (Cr)	Manganese (Mn)
Iron (Fe)	Cobalt (Co)	Nickel (Ni)	Copper (Cu)
Zinc (Zn)	Gallium (Ga)	Arsenic (As)	Selenium (Se)
Bromine (Br)	Rubidium (Rb)	Strontium (Sr)	Yttrium (Y)
Zirconium (Zr)	Molybdenum (Mo)	Lead (Pb)	

2.10   References

Adachi, K.; Tainosho, Y. Characterization of heavy metal particles embedded in tire dust. Environment International. **2004**, 30, 1009-1017.

Agency for Toxic Substances and Disease Registry (ATSDR). Toxicological profile for lead. (Draft for Public Comment). Atlanta, GA: U.S. Department of Health and Human Services, Public Health Service. **2005**, 194.

Al-Bassam, K.S.; Huk, J. Metallic and industrial rocks and minerals. *In Geology of Iraq.* Jassim, S.Z.; Goff, J., Ed.; Dolin, Prague and Moravian Museum, Brno: Czech Republic. **2006**, 288-302.

Al-Dabbas, M.A.; Abbas, M.A.; Al-Khafaji, R.M. Dust storm loads analysis Iraq. Arabian Journal of Geosciences. **2012,** 5, 121-131. doi: 10. 1007/s12517-010-0181-7.

Al-Dawachi, B.M. Origin of some limestone and gypsum natural bridges at N. Iraq. Raf. Journal of Sciences. **2005**, 16(2), 26-34.

Al-Farrajii, A.; Harvey, A. Desert pavement characteristics on wadi terrace and alluvial fan surfaces, Wadi Al-Bih, U.A.E. and Oman. Geomorphology. **2000**, 35(3-4), 279-97. doi:10.1016/S0169-555X(00)00049-0

Al-Frayh, A.R.; Shakoor, Z.; Gad El Rab, M.O., Hasnain, S.M. Increased prevalence of asthma in Saudi Arabia. Annals of Allergy, Asthma, and Immunology. **2001**, 86, 292-296.

Al-Hurban, A.E.; Al-Ostad, A.N. Textural characteristics of dust fallout and potential effect on public health in Kuwait City and suburbs. Environmental Earth Sciences. **2010**, 60(1), 169-181.

Al-Jebouri, M.M.; Younis, A.Y. Incidence of aminoglycosides-resistant rothia mucliagenosa causing respiratory infections in workers of Al-Baiji oil refineries, Iraq. Journal of Pharmaceutical and Scientific Innovation. **2012**, Nov-Dec, 1(6), 54-56.

Al-Khafaji, R.M.N. Effects of dust storms on some Iraqi territories. Ph.D. Thesis, College of Science, University of Baghdad, **2009**.

Al-Quzweny, B.B. Measurement of air pollutant in Baghdad city: Nitrogen oxide and Ozone. M.S. Thesis, University of Baghdad, **1999**.

Al-Rawi, A.H.; Jackson, M.L.; Hole, F.D. Mineralogy of some arid and semiarid soils of Iraq. Soil Science. **1969,** 6, 480–486.

Ali, A.H. Wind regime of the Arabian Gulf. *In: The Gulf War and the Environment*. El-Baz, F., Makharita, R.M., Eds.; Amsterdam, B.V. **1994**, 31-48.

Awadh, S.M. Geochemistry and mineralogical composition of the airborne particles of sand dunes and dust storms settled in Iraq and their environmental impacts. Environmental Earth Sciences. **2012**, 66(8), 2247-2256. doi:10.1007/s/12665-011-1445-6.

Ayhan, A.; Ersayer, M. Geochemical Prospecting for Carbonate Bearing Lead-Zinc Deposits in the Western Zamanti Aladaglar-Yahyai Region. Bulletin of the Mineral Research and Exploration Institute of Turkey. **1985**. 105-106, 45-56. http://www.mta.gov.tr/v2.0/eng/dergi_pdf/105-106/3.pdf (accessed Jan 10, 2014).

Bardoukia, H.; Liakakou, H.; Economou, C.; Sciare, J.; Smolíkc, J.; Zdímalc, V.; Eleftheriadis, K,; Lazaridise, M.; Dye, C.; Mihalopoulosa, N. Chemical composition of size-resolved atmospheric aerosols in the eastern Mediterranean during summer and winter. Atmospheric Environment. **2003**, 37, 195–208.

Bell, M.L.; Davis, D.L. Reassessments of the Lethal London Fog of 1952: Novel indicators of acute and chronic consequences of acute exposure to air pollution. Environmental Health Perspectives. **2001**, 109(3), 389-394.

Böckelmann, I.; Pfister, E.A.; McGauran, N.; Robra, B.P. Assessing the suitability of cross-sectional and longitudinal cardiac rhythm tests with regard to identifying effects of occupational chronic lead exposure. Journal of Occupational and Environmental Medicine. **2002**, 44, 59–65.

Cahill, C.F.; Rinkleff, P.G.; Dehn, J.; Webley, P.W.; Cahill, T.A.; Barnes, D.E. Aerosol measurements from a recent Alaskan volcanic eruption: Implication for volcanic ash transport predictions. Journal of Volcanology and Geothermal Research. **2010**, 76-80.

Cahill, T.A.; Goodart, C.; Nelson, J.W.; Eldred, R.A.; Nasstrom, J.S.; Feeney, F.J. Design and evaluation of the DRUM impactor. In: *Proceedings of the International Symposium on Particulate and Multiphase Processes*. Ariman, T.; Veziroglu, T., Eds.; Hemisphere Publishing Corporation. **1985**, 2, 319-325.

Cahill, T.A.; Wakabayashi, P. Compositional analysis of size-segregated aerosol samples. *In: Measurement Challenges in Atmospheric Chemistry.* Newman, L., Ed.; American Chemical Society. **1993**, 211-228.

Campbell, J.R.; Moss, M.E.; Raubertas, R.F. The association between caries and childhood lead exposure. Environmental Health Perspectives. **2000**, 108, 1099-1102.

Carroll, C.; Essik, P. High-tech trash. National Geographic. **2008**, 213, 64–81.

Central Intelligence Agency. World Factbook. https://www.cia.gov/library/publications/the-world-factbook/geos/iz.html (accessed Jan 29, 2014).

Cheng, Y.; Schwartz, J.; Vokonas, P.S.; Weiss, S.T.; Aro, A.; Hu, H. Electrocardiographic conduction disturbances in association with low-level lead exposure (the Normative Aging Study). American Journal of Cardiology. **1988**, 82, 594-599..

Derbyshire, E. Natural minerogenic dust and human health. Ambio: A Journal of the Human Environment. **2007**, 36(1), 73–77.

Dominici. F.; McDermott, A.; Zeger, S.L.; Samet, J.M. On the use of generalized additive models in time-series studies of air pollution and health. American Journal of Epidemiology. **2002**, 156, 193-203.

Dowdell, D.C.; Matthews, G.P.; Wells, I. An investigation into the sensitivity of the atmospheric chlorine and bromine loading using a globally averaged mass balance model. Atmospheric Environment. **1994**, 28, 1989-1999.

Draxler, R.R.; Rolph, G.D. HYSPLIT (Hybrid Single-Particle Lagrangian Integrated Trajectory) Model. **2013.** http://ready.arl.noaa.gov/HYSPLIT.php (accessed January 29, 2014).

Draxler, R.R.; Gillette, D.A.; Kirkpatrick, J.S.; Heller, J. Estimating PM10 air concentrations from dust storms in Iraq, Kuwait and Saudi Arabia. Atmospheric Environment. **2001**, 35, 4315-4330.

Duce, R.A.; Tindale, N.W. Atmospheric transport of iron and its deposition in the ocean. Limnology and Oceanography. **1991**, 36(8), 1715-1726.

Engelbrecht, J.P.; Jayanty, R.K.M. Assessing sources of airborne mineral dust and other aerosols. Aeolian Research. **2013**, 9, 153-160.

Engelbrecht, J.P.; McDonald, E.V.; Gilles, J.A.; Jayanty, R.K.M.; Casuccio, G.; Gertler, A.W. Characterizing mineral dusts and other aerosols from the Middle East – Part 1: Ambient sampling. Inhalation Toxicology. **2009**, 21, 297-326. dOI:10.1080/08958370802464273.

Fanning, D. A mortality study of lead workers, 1926-1985. Archives of Environmental Health An International Journal. **1988**, 43, 247-251.

Faure, G. Principles and Applications in Geochemistry, 2nd ed., Prentice Hall: New Jersey, **1998**, 46-51.

Find the Data. http://mineral-resources.findthedata.org/d/d/Iraq (accessed on April 1, 2013).

Foda, M.S.; Salama, H.S.; Selim, M. Factors affecting growth physiology of Bacillus thuringiensis. Applied Microbiology and Biotechnology. **1985**, 22, 50-52.

Fulton, M.; Raab, G.; Thomson, G.; Hunter, R.; Hepburn, W. Influence of blood lead on the ability and attainment of children in Edinburgh. Lancet. **1987**, 1,1221-1226.

Ghio, A.J.; Kim, C.; Devlin, R.B. Concentrated ambient air particles induce mild pulmonary inflammation in healthy human volunteers. American Journal of Respiratory and Critical Care Medicine. **2000**, 162 (3 Pt 1), 981-988.

Gribble, G.J. The natural production of organochlorine compounds. Environmental Science and Pollution Research. **2000**, 7, 37-49.

Griffin, D.W. Atmospheric movement of microorganisms in clouds of desert dust and implications for human health. Clinical Microbiology Reviews. **2007**, 13,450–477.

Hammond, G.W.; Raddatz, R.L.; Gleskey, D.E. Impact of atmospheric dispersion and transport of viral aerosols on the epidemiology of influenza. Reviews of Infectious Diseases. **1989**, 11, 494–497.

Harrison, R.M.; Sturges, W.T. The measurement and interpretation of Br/Pb ratios in airborne particles. Atmospheric Environment. **1983**, 17, 311-328.

Hursh, J.B.; Schraub, A.; Sattler, E.L.; Hoffmann, H.P. Fate of ^{203}Pb inhaled by human subjects. Health Physics. **1969**, 16, 257-267.

Jassim, S.Z.; Buday, T. Tectonic framework. In: Geology of Iraq. Jassim, S.Z.; Goff, J.C., Eds.; Dolin, Prague and Moravian Museum, Brno. **2006**, 45-56.

Kanbour, F.I.; Faiq, S.Y.; Al-Taie, F.A.; Bader, K.N. Variation of ozone concentrations in the ambient air of Baghdad. Atmospheric Environment. **1987**, 21, 2673-2679.

King, M.S.; Eisenberg, R.; Newman, J.H.; Tolle, J.J.; Harrell Jr, F.E.; Nain, H.; Nian, M.; Lambright, E.S.; Sheller, J.R.; Johnson, J.E.; Miller, R.F. Constrictive bronchiolitis in soldiers returning from Iraq and Afghanistan. North England Journal of Medicine. **2011**, 365(3), 222–230.

Kirkby, H.; Gyntelberg, F. Blood pressure and other cardiovascular risk factors of long-term exposure to lead. Scandinavian Journal of Work, Environment, and Health. **1985**, 11, 15–19.

Koh, G.; Wakeley, L.D. Impact of gypsum on electromagnetic properties of soils. IEEE Geosciences and Remote Sensing Letters. **2011**, 8(6), 1051-1054.

Koptagel, O.; Ulusoy, U.; Fallick A.E. Sulfur and Lead Isotope Investigations of the Carbonate Hosted Pb-Zn Deposits in the Yahyali Region Kayseri, Southern Turkey. Turkish Journal of Earth Sciences. **2006**, 16(1), 57-76.

Kosmider, S.; Petelenz, T. Electrocardiographic changes in older subjects with chronic occupational lead poisoning. Polish Archives of Internal Medicine. **1962**, 32, 437–442.

Lakes Environmental. http://www.weblakes.com/products/wrplot/index.html (accessed Jan 29, 2014).

Lammel, G.; Röhrl, A.; Schreiber, H. Atmospheric Lead and Bromine in Germany. Environmental Science and Pollution Research. **2002**, 9 (6) 397-404.

Liao, H.; Yung, Y.L.; Seinfeld, J.H. Effect of aerosols on troposphere photolysis rates in clear and cloudy atmospheres. Journal of Geophysical Research. **1999**, 104, 23697-23707.

MacNee, W.; Donaldson, K. Mechanism of lung injury caused by PM_{10} and ultrafine particles with special reference to COPD. European Respiratory Journal. **2003**, 21(40), 47a –51a.

McClellan, R.O. Particle interactions with the respiratory tract. *In: Gehr, Peter, Heyder*; *Joachim*, Eds.; Particle–Lung Interactions. Lung Biology in Health and Disease. Marcel Dekker, Inc.: New York, **2000**, 143, 3–56.

McDonald, J.A.; Potter, N.U. Lead legacy? Early and late mortality of 454 lead-poisoned children. Archives of Environmental Health. **1996**, 51, 116–121.

Measures, C.I.; Brown, E.T. Estimating dust input to the Atlantic Ocean using surface water aluminium concentrations. In: *The impact of desert dust across the Mediterranean, October 1995.* Guerzoni, S.; Chester, R. Eds Environmental Science and Technology Library 11, Dordrecht and London: Kluwer. **1996**, 301-312.

MEPA. An assessment of biotypes and coastal zone management requirements for the Araian Gulf. Meteorology and Environmental Protection Administration. Coastal and Marine Management Service and Technology Report. **1989**, 5.

Membery, D.A. Low level wind profiles during the Gulf Shamal. Weather. **1983**, 38, 18-24.

Middleton, N.J. Dust storms in the Middle East. Journal of Arid Environments. **2001**, 10, 83–96.

Miller, M.S.; Friedlander, S.K.; and Hidy, G.M. A chemical element balance for the Pasadena aerosol. *In: Aerosols and atmospheric chemistry, Part III: The 1969 Pasadena Smog Aerosol Experiment.* Hidy, G.M., Ed.; New York, Academic Press. **1972**, 301-331.

Misconi, H.; Navi, M. Medical geology in the Middle East. International Year of the Planet Earth. **2010**, 135-174. doi: 101007/978-90-481-3430-4_6.

Mohammed, B.A.R. Vertical tropospheric characteristics over Baghdad. International Journal of Application or Innovation in Engineering and Management (IJAIEM). **2013**, 2(9), 7-11.

Morman, S.A; Plumlee, G.S. The role of airborne mineral dusts in human disease. Aeolian Research. **2013**, 9, 203-212.

Mustafa, Y.A.; Mohammed, S.J. Measurement of ground level ozone at different locations. American Journal of Environmental Sciences. **2012**, 8(3), 311-321.

National Oceanic and Atmospheric Administration. www.ncdc.noaa.gov/oa/climate/afghan/iraq-narrative.html (accessed Jan 29, 2014).

National Oceanic and Atmospheric Administration. http://www.ready.noaa.gov (accessed Jan 29, 2014).

Nawrot, T.S.; Thijs L.; Den Hond E.M.; Roels, H.A.; Staessen, J.A. An epidemiological re-appraisal of the association between blood pressure and blood lead: a metaanalysis. Journal of Human Hypertension. **2002**, 16 (2), 123-131.

Needleman, H. Lead poisoning. Annual Review of Medicine. **2004**, 55, 209-222.

Novakov, T.; Mueller, P.K.; Alcocer, A.E.; Otvos, J.W. Chemical composition of Pasadena aerosol by particle size and time of day. III. Chemical states of nitrogen and sulfur by photoelectron spectroscopy. *In: Aerosols and atmospheric chemistry, Part III: The 1969 Pasadena Smog Aerosol Experiment*. Hidy, G.M., Ed.*;* New York, Academic Press: **1972**, 285-294.

Papanikolaou, N.C.; Hatzidaki, E.G.; Belivanis, S.; Tzarakakis, G.N.; Tsatsakis, A.M. Lead toxicity update. A brief review. Medical Science Monitor. **2005**, 11, RA329-RA336.

Phillip, A.T.; Gerson, B. Lead poisoning – Part I. Incidence, etiology, and toxicokinetics. Clinics in Laboratory Medicine. **1994**, 14, 423-444.

Pope III, C.A.; Bates, D.V.; Raizenne, M.E. Health Effects of Particulate Air Pollution: Time for Reassessments. Environmental Health Perspectives. **1995**, 103(5), 472-480.

Pope III, C.A.; Dockery, D.W. Health effects of fine particulate air pollution: Lines that connect. Journal of Air and Waste Management. **2005**, 56, 709-742.

Prospero, J.M. Long-term measurements of the transport of African mineral dust to the Southeastern United States: Implications for regional air quality. Journal of Geophysical Research. **1999**, 104(D13), 15,917–15,927.

Qatar Department of Meterology. Long period means and extremes of climatological elements for Doha International Airport, (Period 1960-1990). Climate Section Publications. Doha. Qatar. **1990.**

Raabe, O.G.; Braaten, D.A.; Axelbaum, R.L.; Teague, S.V.; Cahill, T.A. Calibration studies of the DRUM impactor. Journal of Aerosol Science. **1988**, 19(2), 183-195.

Rabinowitz, M.B. Toxicokinetics of bone lead. Environmental Health Perspectives. **1991**, 91, 33-37.

Radi, A.; Al-Katheri, A.A; Dhanhanj, A. Implementation and preliminary test of an air quality forecasting systems based on WRF-Chem over Middle-East, Arabian Peninsula and United Arab Emirates. United Nations Development Programme, Abu-Dhabi, UAE. **2007**.

Rolph, G.D. Real-time Environmental Applications and Display sYstem (READY) [Online] **2013**. (http://ready.arl.noaa.gov). NOAA Air Resources Laboratory, Silver Spring, MD.

Saeed, T.M.; Hassam, A. Optical and physical characterization of "Iraqi Freedom" dust storm, a case study. Theoretical and Applied Climatology. **2010**, 104, 123-137.

Sanders, J.W.; Putnam, S.D.; Riddle, M.S.; Tribble, D.R. Military importance of diarrhea: lessons from the Middle East. Current Opinion in Gastroenterology. **2005**, 21, 9–14.

Schmaltz, J. Visible earth dust storm in Iraq, June 08, NASA Image, **2008**. Online at http://visibleearth.nasa.gov/view.php?id=20029

Schober, S.E.; Mirel, L.B.; Graubard, B.I.; Brody, D.J.; Flegal, K.M. Blood lead levels and death from all causes, cardiovascular disease, and cancer: results from the NHANES III mortality study. Environmental Health Perspectives. **2006**, 114, 1538–1541.

Schwartz, J. Lead, blood pressure, and cardiovascular disease in men. Archives of Environmental Health. **1995**, 50, 31-37.

Seaton, A.; MacNee, W.; Donaldson, K.; Godden, D. Particulate air pollution and acute health effects. Lancet. **1995**, 345, 176–178. doi:10.1016/S0140-6736(95)90173-6.

Seinfeld, J.H.; Pandis, S.N. *Atmospheric Chemistry and Physics: From Air Pollution to Climate Change*, 2nd ed.; J. Wiley, New York. **1998**.

Shahsavani, A.; Naddafi, K.; Haghighifard, N.J.; Mesdaghinia, A.; Yunesian, M.; Nabizadeh, R.; Arhami, M.; Yarahmadi, M.; Sowlat, M.H.; Ghani, M.; Jarahi, A.J.; Alimohamadi, M.; Motevalian, S.A.; Soleimani, Z. Characterization of ionic composition of TSP and PM10 during the Middle Eastern Dust (MED) storms in Ahvaz, Iran. Environmental Monitoring and Assessment. **2012**, 184:6683-6692. doi: 10.1007/s10661-011-2451-6.

Staessen, J.A.; Bulpitt, C.J.; Fagard, R.; Lauwerys, R.R.; Roeis, H.; Thijis, L.; Amery, A. Hypertension caused by low-level lead exposure: myth or fact? Journal of Cardiovascular Risk. **1994**, 1, 87-97.

Sturges, W.T.; Harrison, R.M. Bromine to lead ratios in airborne particles from urban and rural sites. Atmospheric Environment. **1986**, 20, 577-588.

Szema, A.M.; Peters, A.; Weissinger, K.M.; Gagliano, C.A.; Chen, J.J. New-onset asthma among soldiers serving in Iraq and Afghanistan. Allergy and Asthma Proceedings. **2010**, 31(5), e67–e71.

Taylor, S.R.; McLennan, S.M. The Continental Crust: its composition and evolution. London: Blackwell Scientific Publications. **1985**, 312.

Thalib, L.; Al-Taiar, A. Dust storms and the risk of asthma admissions to hospitals in Kuwait. Science of the Total Environment. **2012**, 433, 347-351. doi:10.1016/j.scitotenv.2012.06.082.

Thoppil, P.; Hogan, P. Persian Gulf response to winter Shamal event. Deep Sea Research I. **2010**, 57, 947-955.

Uematsu, M.; Duce, R.A.; Prospero, J.M.; Chen, L.; Merrill, J.T.; McDonald, R.L. Transport of mineral aerosol from Asia over the North Pacific Ocean. Journal of Geophysical Research. **1983**, 88, C9, 5343–5352. doi: 10.1029/0JGREA0000880000C9005343000001.

UNEP, 2003. Desk Study on the Environment in Iraq. United Nations Environment Programme, Switzerland.

U.S. Environmental Protection Agency. www.epa.gov/air/criteria.html (accessed January 29, 2014).

USACHPPM RD 230. Environmental health risk assessment and chemical exposure guidelines for deployed military personnel. Technical Guide 230 [Online] **2013**. http://phc.amedd.army.mil/PHC%20Resource%20Library/TG230.pdf (accessed Jan. 10, 2014)

Van Der Eeden, S.K.; Quesenberry, C.P.; Shan Jr., J.; Lurmann, F. Particulate air pollution and morbidity in the California Central Valley: a high particulate pollution region. Final Report to the California Air Resources Board, **2002**.

Weather Underground. http://www.wunderground.com/history/airport/KQTZ/2009/2/13/DailyHistory.html? (accessed Jan 29, 2014).

Weese, C.; Abraham, J. Potential Health Implications Associated with Particulate Matter Exposure in Deployed Settings in Southwest Asia. Inhalation Technology. **2009**, 21, 291-296.

Whitby, K.T.; Cantrell, B.K. Proceedings of the International Conference on Environmental Sensing and Assessment (ICESA), Institute of Electrical and Electronic Engineers (IEEE) 1976. Atmospheric aerosols: characteristics and measurement. **1976**, IEEE #75-CH 1004-1, ICESA paper 29-1, Washington, DC: IEEE. p. 6.

World Health Organization. [Online] **2012**a. http://www.who.int/ mediacentre/factssheete/fs313/en/. (accessed Oct. 20, 2013).

Chapter 3 High Velocity Shamal and Kous Winds Influence Brittle Fragmentation's Particle

   Size Distributions: A Case Study of Iraqi Aerosols[1.]

3.1   Abstract

High concentrations of dust particles are lofted into the atmosphere by the strong winds that frequently blow across the Middle East. A study was initiated in 2008 to determine the concentrations and compositions of fine particulate matter in the atmosphere over Baghdad, Iraq. This study used a DRUM aerosol impactor to continuously collect size (eight stages between 0.09 and 10.0 microns in aerodynamic diameter) and time (hour and a half resolution) resolved aerosol samples for analysis for mass concentration and elemental composition. The samples collected during this study contained high concentrations of dust aerosols across the measured size distribution. The brittle fragmentation model successfully explained particle breakdown in no wind/low wind situations. However, a peak in mass concentration was observed within the ultrafine (0.09-0.26 microns) size fraction during high wind scenarios that is not consistent with the brittle fragmentation model and current hypotheses about the sizes of mechanically produced soil particles; therefore, another mechanism apparently exists for the production of geogenic Aitken size particles.

3.2   Introduction

High concentrations of aerosols exist throughout the Middle East, including Iraq (Al-Hurban and Al-Ostad, 2010; Engelbrecht et al., 2009; Misconi and Navi, 2010; Awadh, 2012). A predominant source of aerosols in the region is high velocity winds lofting, transporting, and depositing large quantities of sand and silt during desert dust storms (Figure 3-1). However, significant portions of Iraq's crustal surfaces have been disturbed, increasing the opportunity for

---

[1.] Bell, J.M.; Cahill, C.F.; Egan, S.D.; Gill, T.E. University of Alaska Fairbanks, Fairbanks, Alaska. In preparation for submission to the American Chemical Society, 2014.

finer soil particles to loft. Local geologists suspect the break-up of desert surfaces to be partially attributed to excavations from increased urbanization, oil field drilling, and military operations (El-Baz, 1994; Wilkerson, 1991; Shahsavani et al., 2012). Additionally, historical wind events have weakened desert surfaces, enhancing erosion processes along the path of prevailing winds (Al-Dabi et al., 1977). The enhancement of erosion processes allows for increased opportunities for soil to loft with each successive wind event. The lack of rainfall (50-100 mm per year), few desert plants, and dry climate worsen and magnify the occurrences, effects, duration, and severity of dust storms (Jassim and Buday, 2006).

Aerosols lofted from desert environments account for a large fraction of the mineral dust found in the troposphere (Andreae, 1995; Krueger et al., 2004). Mineral dust contains trace amounts of heavy metals and other elements that can be used to characterize the sources of soil in the region. Iraq has significant heavy metal resources within its local deposits (Liaghat et al., 1999; Al-Juboury et al., 2008; Ismail et al., 2009; Awadh, 2012) as well as materials deposited by anthropogenic pollution, both which could provide potential geochemical signatures to identify some regions; however, it also means there are potentially multiple locations with similar signatures.

Soils deposited during wind events are sorted and fall-out based on grain size: fine particles (clay and silts) remain suspended in the atmosphere as dust, fine to medium sands undergo sandblasting and bombardment from saltation, and coarse particles creep or roll just above the soil surface during strong desert winds (El-Baz, 1994; Breed and Grow, 1979). Given the natural sorting that occurs in desert environments, this paper only focuses on soil that remains suspended in the atmosphere as dust transported by winds. Safar (1985) established

three conditions existing in desert environments that optimize the lofting of dust particles: 1) land surfaces are dry and dusty; 2) the lack of vegetation and uninterrupted surfaces allow winds to reach speeds necessary to emit soils as aerosols; and 3) unstable atmospheric conditions result from extensive vertical motions of the near-surface atmosphere and strong insolation.

Iraq is located in the Arabian Desert in the northeast corner of the Arabian Peninsula, in the valley of the Tigris and Euphrates Rivers of the Fertile Crescent (Figure 3-2). Iraq is bordered to the north and northeast by the Taurus and Zagros mountains (Sibrava, 2006), to the east by the Makhul-Hemrin-Pesh-i-Kuh Range, and to the west by Saudi Arabia and Jordan (Jassim and Buday, 2006). Iraq has an arid climate, known for its hot dry summers, cold wet winters, and strong Shamal and Kous winds (Al-Farrajii, 1998; Awadh, 2012). Iraq's hot lowland surfaces and lack of vegetation provide conditions that allow the strong northwesterly Shamal winds and southeasterly Kous winds to reach high velocities. The terms Shamal (north to northwest) and Kous (south to southeast) describe specific wind patterns, regardless of the season (Ali, 1994). These winds are generally a result of gradients in surface pressures over Saudi Arabia, the Gulf of Oman, and/or Pakistan (Ali, 1994). Chapter 2 provides a more detailed description of Shamal and Kous winds. Figure 3-3 shows the strong Shamal winds carrying large plumes of dust from the direction of the Zagros Mountains and the Taurus mountains in Turkey through the Baghdad area, while Figure 3-4 provides a vicinity map of this location.

The Shamal and Kous winds are of interest as they are responsible for: 1) the large quantities of aerosols lofted during Iraqi dust storms; 2) long-range transport of mineral dust (Clarke et al., 2001; Moore et al., 2003; Awadh, 2012); 3) the increased erosion of surface areas along predominant wind paths; and 4) significant reductions in visibility (Ali, 1994) (Figure 3-1).

The Shamal winds have been documented to reach 100 km/hr so regional winds of this magnitude have resulted in conditions of zero visibility in dust (Membery, 1983; Foda et al., 1985; de Villiers and van Heerden, 2007).

This paper describes the results from a sampling campaign in Baghdad, Iraq, designed to collect continuous, high temporal resolution, aerosol size and composition data. During the course of this study, high concentrations of ultra-fine soil particles were repeatedly sampled suggesting an ultra-fine soil particle generation mechanism exists in Iraq.

3.3   Experimental Methods

3.3.1   Sampling Site

The site used in this study was Camp Victory, Iraq, a part of the Victory Base Complex, a U.S. military base used during the Iraq War that commenced in 2003 (Figure 3-2). Camp Victory is located to the west of downtown Baghdad. The sampler was placed outside the living quarters of the personnel responsible for sampler operation and the sampler was checked regularly.

3.3.2   Aerosol Sampling and Analysis

Size and time-resolved measurements of aerosol size and composition were collected at the site starting on February 14, 2008. The study used an 8-stage DRUM aerosol impactor shown in Figure 3-5 (Raabe et al., 1988; Cahill and Wakabayashi, 1993). The eight aerosol size fractions collected by the sampler were: 5.0-10.0, 2.5-5.0, 1.15-2.5, 0.75-1.15, 0.56-0.75, 0.34-0.56, 0.26-0.34, and 0.09-0.26 μm in aerodynamic diameter. The samples were collected on 16.8-cm, Apiezon L^{TM} coated Mylar^{TM} strips wrapped around metal sampling drums. Each size fraction was collected on an individual drum stage that rotated 8-mm per day underneath an

aerosol nozzle that separated the particles into the correct aerodynamic size for that sampling stage using a momentum separation. Each set of samples was collected over the course of a three-week period.

The DRUM was programmed to concentrate the initial aerosol peak by collecting aerosols for six hours before beginning its normal 8-mm per day rotation. A blank of 6-mm was collected in the middle of the sample run by advancing the sample strip. This blank is represented as a gap in the data set. The gap allows a more efficient matching of peaks on different size fractions. At the conclusion of the three-week sampling event the sampler again concentrates the sample. The 6-12-6 hour programming improves the identification of the sample start and stop times on the Mylar^{TM} strip.

The aerosol samples were removed from the metal drums and placed on slide frames in the laboratory. Then they were analyzed for mass using beta-attenuation and elemental composition (28 selected elements between Na and Pb) using synchrotron x-ray fluorescence (Cahill et al., 2010) with 1.5-hour resolution. The synchrotron x-ray fluorescence was performed at Lawrence Berkeley National Laboratory's Advanced Light Source. Synchrotron x-ray fluorescence is advantageous in that it is a non-destructive technique, which allowed each unique sampling event to be further studied via Scanning Electron Microscopy (SEM).

The SEM was chosen for further analysis following the synchrotron x-ray fluorescence as it provides the ability to visually inspect the particles on the sample and determine their chemical composition. Samples were prepared by cutting each time-resolved sample from the Mylar™ strip, adhering the sample to a micro petri dish; carbon coating the sample using a Hummer VI Sputter Coater, and placing the sample at a 45-degree angle in the sample holder. The SEM

analysis was performed on a Hitachi S-2700 equipped with an EDAX elemental analysis system at California State University San Bernardino's Stable Isotope Laboratory.

3.3.3 Meteorological Modeling

The National Oceanic and Atmospheric Administration Air Resources Laboratory's Hybrid Single Particle Lagrangian Integrated Trajectory Model (HYSPLIT) was used to calculate backwards meteorological trajectories from the global data assimilation system (GDAS, 2006-present) to help determine the source of aerosols and atmospheric contaminants (Draxler and Hess, 1997; Draxler and Hess, 1998; Draxler, 1999; Draxler and Rolph, 2013; Rolph, 2013). The GDAS was used because trajectories were calculated outside of the United States and it provides gridded meteorological data for the Middle East and other non-U.S. locations. Parameters used in the vertical velocity trajectory calculations were starting heights of 500, 1000, and 1500 meters above ground level with backwards running times of 24 to 76 hours. These vertical heights and times were chosen to: 1) identify winds likely to touch ground and loft dust and 2) separate individual storm events. Such a combination of trajectories shows where the aerosols collected at the site at a specific time may have been emitted into the atmosphere and the likely path taken while being transported to the site (Engelstaedter et al., 2009).

3.4   Results and Discussion

Engelbrecht et al. (2009) noted higher concentrations of calcium (Ca) and magnesium (Mg) in Iraq than most desert soils. Much of the Ca is found as calcite ($CaCO_3$) and gypsum ($CaSO_4$) (Al-Dawachi, 2005; Al-Bassam and Huk, 2006; Awadh, 2012; Koh and Wakely, 2011; Al-Dabbas et al., 2012). High concentrations of Ca and Mg are also found within the data collected during this study. The elemental concentration time series depicted in Figure 3-6

shows the DRUM's eight size fractions for Ca and how each stage varied according to time during a sampling period. Although the coarsest fraction (5.0-10.0 microns in aerodynamic diameter) is expected to provide most of the mass of the Ca collected during sampling, this is not the case for this time series due to sample loss in the laboratory. Significant mass loading during dust storms led to solid, curved particulate deposits that flake off the sample substrate when straightening the aerosol-laden Mylar[TM] strips for mounting on an analysis slide frame. As a result, the 2.5 to 5.0 microns size fraction (stage 2) tends to show the highest mass concentrations because it has less mass deposited on the strip and the problems associated with flaking occur less often. As a result of the flaking potential of the two coarsest stages, this study focused on size fractions less than 2.5 microns in aerodynamic diameter as these particles stick well to the Mylar[TM] strips and are of the size capable of becoming embedded in the deepest part of the lungs (Weese and Abraham, 2009).

The time series of aluminum (Al), calcium (Ca), silicon (Si), magnesium (Mg), titanium (Ti), and iron (Fe) in Figure 3-7 depict the elemental mass concentrations for size fraction six (0.34-0.56 microns). Figure 3-7 is noteworthy in that the peaks are overlying one another in a "fingerprint" pattern and this relationship was explored further by comparing them to Si (Figure 3-8). The fingerprint includes the key soil components of Si (26.8%), Al (8.40%), Fe (7.06%), and Ca (5.3%) found within the earth's crust (Faure, 1998). The results from stage 6 are interesting in that particles of this size fraction (0.34-0.56 microns) are unusually fine for dust aerosols (Seinfeld and Pandis, 1998) but the particles captured on this stage clearly contain crustal soils.

Figures 3-9 and 3-10 are of interest because they show no particles in the finest size fraction (0.09-0.26 microns) during low/no wind conditions, but they do show increasing concentrations of soil in this size fraction as wind speed increases. The presence of particles in the 0.09-0.26 micron range during high wind conditions that do not appear during local wind events would suggest that sources are less likely anthropogenic and that some aerosol production or transport mechanism exists that favors windy conditions. Comparing the wind data shown in Figures 3-9 and 3-10, with the soil correlation data in Figure 3-11 (0.09 – 0.26 microns) shows the aerosols in the finest size fraction are consistent with typical desert soils being lofted by high winds. This finding is noteworthy as it suggests that particles consistent with crustal surfaces are fragmenting into small sizes not expected to be formed from the brittle fracture of larger mineral grains.

Seinfeld and Pandis (1998) summarized Whitby and Cantrell's (1976) explanation of typical aerosol growth patterns in a diagram outlining a tri-modal distribution. This diagram remains the basis for our current understanding of aerosol size distributions. In this diagram the very fine particles in the Aitken mode, that includes the particle sizes collected on stage 8 of the DRUM sampler, are the primary particles associated with anthropogenic processes and result from gas-to-particle conversions (Whitby and Cantrell, 1976; Jaenicke, 1993; Seinfeld and Pandis, 1998). The particles collected on stage 8 are Aitken mode in size; however, their composition is consistent with soil and they only appear during Shamal and Kous wind events (Figures 3-9 and 3-10). This behavior suggests that a mechanism exists for the production of Aitken mode geogenic particles and that this mechanism is occurring on desert surfaces or as aerosols undergo transport after emission. The higher concentrations of lofted fine soils at

higher wind velocities could result from: 1) sandblasting/disruption of surface coatings (clay minerals, chemical precipitates, weathering rinds, surface ion oxides) on sediments; 2) fine soil aerosols being produced by gouging/chipping of mineral grains during saltation and collisions; 3) very fine soil particles transporting long distances to the site; and 4) anthropogenic industrial, urban, and military activities creating very fine soil particulates that do not occur naturally.

The linear regression lines obtained from plotting the major soil elements against silicon show that crustal elements correlate well with each other (Figure 3-11). Deviations from the regression line between a given element and silicon may be attributed to soils mixing with anthropogenic aerosols and/or coming from another source region or production mechanism. Lead, on the other hand can be associated with geogenic emissions of contaminated soil transported into Iraq and anthropogenic source emissions of local pollution episodes such as leaded gasolines, road dusts contaminated with lead emitted from vehicles, and industrial emissions.

The overlapping peaks of Ti and Pb (Figures 3-12 and 3-13) demonstrate a common source for these two metals. Figure 3-12 is noteworthy because Pb is correlated to Ti in the 2.5 to 5.0 micron range. This is a larger size fraction than would be expected with particles associated with combustion products. However, the correlation between Pb and Ti in Figure 3-13 is almost certainly urban and likely associated with re-suspended industrial/urban/military dusts. It is likely that many of the minerals native to the desert soils of Iraq have been spread across the region due to successive wind events, and elements derived from anthropogenic contamination are likewise spread across the region. As a result it is very probable the surface of every single road in Baghdad and Camp Victory and of every tire of every vehicle are well

coated with Pb (from gasoline, urban, and industrial sources) and Zn (from urban and industrial sources and the tires themselves). Figure 3-14 is a time series plot of Pb, Zn, and Ti in the 0.09-0.26 micron size fraction. Figure 3-14 is significant because Zn and Ti, which as oxides are significant tire components, can be correlated to Pb, thus further relating these compounds to urban aerosols. HYSPLIT backward trajectories were used to confirm the source regions for Zn, Ti, Pb, and all trace element signatures (Figure 3-15).

It should be noted that significant Pb is found during local wind events. High concentrations of Pb in no wind or local windy conditions are likely the result of the accumulation of Pb from the continued use of leaded fuels, local smelting and industrial operations, re-suspended urban/fugitive dusts, tire wear, and combustion related activities (Engelbrecht, et al., 2009; Schmaltz, 2008; Al-Khafaji, 2009; Al-Dabbas, et al., 2012).

Since the combustion products of mining activities and some industrial activities (cement manufacture) can resemble soil, the aerosol samples were visually and elementally inspected using an SEM (Figure 3-16). The purpose of the SEM analysis was to validate that samples were indeed soil and not products of high temperature combustion. If the particles are the product of high temperature combustion and gas-to-particle conversion they would be more spherical and uniform in appearance than fragmented soil particles. From a visual analysis of the SEM images, all samples appeared to be jagged and not spherical, consistent with eroded soils (Miller and Gosar, 2009). The particle shown in Figure 3-16 is jagged and comprised of Si (51.8%), Al (23.13%), Ca (0.76%), Fe (4.8%), Ti (1.76%), Pb (12.24%) and Mg (2.16%), consistent with a clay type material. Further, this particle is an ultra-fine aerosol (0.09 to 0.25 microns) that was

collected during a dust event in the February 13, 2009 sampling campaign. The presence of Pb at 12.24% by weight means the soil particle was probably contaminated.

Local geologists hypothesize that military operations and war efforts have contributed to the disturbance of desert surfaces, which would increase their erodibility by the wind (El-Baz, 1994; Shahsavani et al., 2012). The presence of soil elements within the collected aerosols is consistent with this fact. However, given that the aerosols are likely clay minerals, as suggested by the composition, a more reasonable explanation for the composition and generation of the aerosols would be a result of chemical weathering over past climates, the accumulation of pollutants with time onto the clay mineral surfaces, and the emission of extremely fine clay particles as aerosols in strong winds.

Kok (2011a) applied the theory of brittle fragmentation (Astrom, 2006; Oddershede et al., 1993; Gilvarry and Bergstrom, 1961; Astrom et al., 2004) to aerosols to determine if the theory could explain the particulate size distributions obtained from dust flux measurements made in desert environments. Kok applied the theory of brittle fragmentation to the surface of the primary larger mineral grain since the surface is considered the weakest point of the particle. The ability to weaken the surface of the mineral grain and produce fragments is dependent on impact energies and the cohesiveness of the particle. As a result, dust emissions correlate to the ability of a stressor to produce fragmenting impacts (Kok, 2011a). Kok's (2011b) theoretical model (Figure 3-17) concluded that particle size distributions follow a power law and that the process is scale-invariant. Kok (2011b) selected data from leading saltation theorists to draw correlations with his brittle fragmentation model and validate his theory that particle size distribution is independent of wind velocity. His model correlates nicely with previous wind

tunnel studies and field measurements conducted by Gillette et al. (1972), Gillette (1974), Sow et al. (2009), and Shao et al. (2011) (Figure 3-17). The theory of brittle fragmentation was used to determine if the data from this study also fits Kok's model. However, given that there are differences in particle fragmentation behavior under different wind regimes, specifically the large number of Si particles on size fraction six during large windstorms (Figures 3-9 and 3-10), the data collected in Iraq was separated into local, Shamal, and Kous wind bins before the model was applied to it.

The wind rose (Figure 3-18) provides a basis for separating the direction and velocity of wind events. The wind sector graph, Figure 3-19, overviews wind drainage patterns during the February 13, 2009 sampling campaign. Figures 3-18 and 3-19 are important as they demonstrate the direction and speed of wind events during the sampling campaign. It was noted that certain wind speeds would result in similar soil concentration ranges. As a result the average was calculated from grouping twenty-five 1.5-hour sampling events with similar concentrations and wind speed ranges. The greatest changes in soil concentrations occurred around 3.1 m/s. It was also noted that when local winds exceeded 3.1 m/s the wind was greatly influenced by an incoming dust storm. As such, 3.1 m/s was chosen as the break point between the higher speed Shamal and Kous winds and the slower local winds. This break point is consistent with the lofting of fugitive dust described by Countess et al. (2001) who suggested that winds of 2.5 m/s can loft dust 100 m in 40 seconds, and in the range of wind velocities reported for severe dust episodes advecting into Beijing, China (Shi et al., 2005).

Once the wind-bin ranges were chosen and data were separated into their respective wind event bins (local, Shamal, or Kous) by date and time of each sampling event, soil concentration

averages were calculated and plotted by size fraction (Figure 3-20). Three points of interest in this graph are: 1) there is not enough mass during the local wind events to detect any soil particles on stage 8, 2) mass concentration for all wind speed bins increase from non-detectable in the finest size fraction to a local maximum in the 0.34-0.56 microns size fraction followed by a decrease to a minimum in the 0.75-1.15 micron size fraction and then an increase as aerodynamic diameter increases, and 3) mass concentrations on the larger stages increase with increasing wind velocities. Although we see a systematic increase with wind speed, the data trends well with the brittle fragmentation model (Figure 3-21; Kok, 2011a, Kok, 2011b). This agreement with the Kok model suggests the brittle fragmentation model works for aerosol sampled close to the source.

The Shamal wind-bin graph (Figure 3-22) is of interest because there are significant mass concentrations recorded for stage 8 (0.09 to 0.26 microns) and soil concentrations continue to increase as wind velocity increases. The mass concentrations appear to decrease in the largest size fraction (5.0-10.0 microns), but this is probably due to the high concentrations of large particles collected during high wind events creating samples that flaked off the substrate during sample handling. It may also be due to larger particles settling out of the dust storm during long-range transport. Correlating this data to that of the Kok model (Figure 3-23) suggests that the model may not be apt for reacting, mixed, complex, and long transport distance dust clouds such as experienced with the Shamal. The mass concentrations noted on stage eight (Figure 3-22) are seen as an uptick in Figure 3-23 that clearly deviates from the Kok model of brittle fragmentation alone. The presence of ultra-fine particles and the uptick are also seen with the Kous wind events (Figures 3-24 and 3-25, respectively). Further, a similar uptick is also seen within the

107

Sow et al. (2009) data set used in Kok (2011b) (Figure 3-17). The uptick was not fully explored in Kok (2011b) because Sow et al. (2009) did not specify soil types with their dust flux studies and, according to Okin and Gillette (2002), the documentation of soil type in dust flux studies is required to understand wind erosion because it is a function of soil type. Although Kok's (2011b) brittle fragmentation model included only dust flux measurements, the non-dust flux aerosol data collected in Iraq, with the exception of the uptick in mass concentration in the smallest size fraction, trends well with the model. However, the uptick and the increases with wind speed suggest that brittle fragmentation is not the only explanation for the observed particle size distributions.

Desert aerosols sampled in and around Baghdad, appear to be different from "standard" desert dusts in that they have a peak in the smallest size fraction (0.09-0.26 microns; Figure 3-26) as opposed to the model summarized and discussed by Seinfeld and Pandis (1998). This distribution is more likely associated with particles that are reacting with other particles, mixed, complex in nature and formation, and/or transported long distances.

It was stated earlier in this paper that saltation would not be discussed. However, an exception is made for the few studies covered in Kok (2011b) that contained finer aerosols in their size distributions and looked at the effect of wind speed on the size distributions. If higher saltation impact energies produce more disaggregation of mineral grains, then dust storms would favor disaggregation and particle size distributions would always have high particle number concentrations within the finest size fractions. This is not usually observed. Also, brittle fracture theory predicts that primary particles would only break down to a minimum size. Alfaro and Gomes (2001) used wind tunnel studies to argue that increasing saltating impact energies

produced more disaggregation resulting in smaller particles (1.5-14.6 microns), but not the very fine particles observed in this study. This agrees well with the Kok model. Sow et al. (2009) and Shao et al. (2011) measured three dust storms with friction velocities between 0.4 and 0.6 m/s. Sow et al. (2009) reported aerosol particles ranging from 0.3 to 20 microns. Although most of the data highlighted from Sow et al. (2009) in Kok (2011b) agreed with the model, an uptick in mass concentration within their finest fraction was noted and then ignored due to the absence of soil types in dust flux measurements. Shao et al. (2011) reported similar friction velocity ranges (0.2 to 5.5 m/s) with particles ranging from 0.3 to 8.4 microns although they questioned the reliability of their finest size fraction (0.3-0.6 microns). Again, the data followed the Kok model.

It can be seen from Figures 3-21, 3-23, and 3-25, that the brittle fragmentation model predicts, with a reasonable level of confidence, the production of fine particles from the original fragmentation of primary mineral grains by purely mechanical means. As a result Kok (2011a) argues that saltator impact speed and impact energy are independent of wind velocities. Rather, Kok hypothesizes that saltation is a scale-invariant process caused by a succession of cracks and new cracks in primary mineral grains merging until the stress has been alleviated and no new cracks will form from the given impact (Kok, 2011a; Kok, 2011b). However, discounting wind velocity in particle fragmentation may be incorrect, as wind is known for its ability to impact and even enhance erosion processes (Tarbuck and Lutgens, 2013). This study routinely captures particles on stage 8 (0.09-0.26 microns) during higher wind speed events. The uptick in mass concentration on stage 8 shown in Figures 3-22 and 3-24 clearly deviates from Kok's model indicating that brittle fragmentation alone may not explain the presence of these particular

aerosols. This suggests that another mechanism, besides brittle fragmentation of primary mineral grains, is at work. Given that the uptick in mass concentration only appears during windy conditions, the role of wind velocity in generating and/or transporting aerosols produced by non-fragmentation processes, including aerosols resulting from chemical and anthropogenic pathways, cannot be discounted.

The theory of dust aerosols produced from saltation is built on the premise that the dust size distribution is dependent on wind velocity for dusts produced from purely mechanical breakage of larger crystal grains (i.e., fracture of pure SiO_2). If this were true, larger windstorms would produce, to a certain point, finer particles. Our elemental data and several new hypotheses and other data sets suggest that saltation is not the only explanation for fragmentation and dust production. Carneiro et al. (2013) hypothesize that the ability of saltons (particles ejected from the granular bed by impacts with faster moving particles) to remain suspended high in the dust cloud (by leaping off other particles creeping along the granular bed), where drag acceleration is not as strong, results in increased opportunities for midair collisions. They theorize that saltons may sustain the life of the storm (by acquiring additional momentum from the wind and using it to eject other particles through these collisions). Additionally, high-energy saltons continue to gain speed and interact with slower, more brittle particles through collisions and bounce, enough stress could be generated across the surface of the particle to result in fragmentation. This increase in fragmentation may explain the production of fine particles seen during large wind events.

Butler et al. (2012) suggest that the distance a plume travels should be considered when examining particle size distributions. Larger source areas are more likely to have finer dust

concentration profiles at downwind receptor sites, due to greater transport distances allowing time for larger particles to settle out while finer particles remain entrained in the plume. Considering the distance traveled by a dust plume may be a key factor in understanding Iraq's unique data set. Figure 3-26 depicts the average soil concentration as function of wind speed for both the Shamal and Kous wind events. It can be seen in Figure 3-26 that the highest average soil concentration for the 0.56-0.75 micron size fraction occurred during the Shamal winds, while the highest average soil concentration for the 1.15-2.5 micron size fraction occurred during the Kous winds. The shift in plume size distributions caused by aerosols settling out at different rates during different distances of transport may effectively explain why we routinely collect high concentrations of fine particles during the Shamal and Kous wind events.

Stokes's law, equation 3-1, describes the terminal settling velocity of a spherical particle as it settles in still air (Reist, 1993; Cahill et al., 2010).

$$v_t = \tau g\ _c C$$
$$\tau = \frac{d^2 \rho_p}{1\ \mu 8}$$
$$C_c = 1 + \frac{2\lambda}{d}[A + Qe\ \left(x - \frac{b}{2\lambda}\right)d]$$

3.1

where,

g = gravity
τ = particle relaxation time
C_c = Cunningham correction factor applied to particles smaller than 10 μm to correct for air resistance
d = aerodynamic diameter of particle
ρ_p = the density of the particle (1000Kg/m^3)
μ = the viscosity of air (1.82 x10^{-6}P)
λ = mean free path of the gas molecules
A, Q, b are the Cunningham correction constants (1.155, 0.471, and 0.596 respectively) (Allen and Raabe, 1982)

Table 3-1 provides estimates for the terminal settling velocities of the average particle diameter for each stage of the DRUM aerosol impactor assuming that the particles were initially at a height of 5500 m above the ground surface. Although Table 3-1 provides calculated settling velocities it should be noted that these are not truly representative of how quickly particles are removed from the atmosphere. If settling velocities were exact we would never experience a clear sky. Rather, particles undergo interactions with the environment, such as gases depositing on their surface or coagulation with other particles, that leads to particles large enough to settle out of the atmosphere more quickly or coagulation with or nucleation of rain droplets resulting in the particle being washed out of the atmosphere (Whitby and Cantrell, 1976).

Dust clouds vary in severity and storm length and some may last several days along a transport pathway (Wilkerson, 1991; Saeed and Hassam, 2010). Wilkerson (1991) suggests the likelihood of exposed soils in Iraq lofting during gentler wind events is increased fivefold due to weathering, breakdown, and inflow of new sediment. It is likely that larger particles will loft and then settle out quickly while smaller particles remain entrained in the cloud, eventually settling on the surface. As subsequent wind events occur, soil particles continue this cycle of lifting and settling thereby creating a favorable probability that each successive cycle would further reduce particle sizes downwind of a specific source region.

Several prior field and laboratory studies of dust production in other desert environments suggest an additional mode of sub-0.1µm desert aerosol generation. d'Almeida and Schütz (1983) first showed data that crustal-generated aerosols in the Aitken size range were present in Saharan dust, suggesting that they were formed by sandblasting disaggregation of compound particles of the parent soil, rather than by brittle fragmentation of mineral grains. Gomes et al.

(1990) studied the generation of Saharan dusts near their source at El Abiod in northern Algeria, an environment with topographic and meteorological similarities to the Iraq sampling site. Gomes et al. (1990) echoed the results of d'Almeida and Schütz (1983): aerosols collected with a cascade impactor showed particles as small as 0.1 μm with a similar composition to those in coarser modes, "implying that these particles have a common origin" consistent with clay minerals (weathering-derived coatings loosely attached to larger mineral grains) sandblasted off the surface of desert soils. Gomes et al. (1990) also pointed out that such fine particles are likely to stay preferentially suspended in desert winds and will be disproportionally represented in dust clouds advected into a sampling site.

More recently, data presented in Radhi et al. (2010) clearly showed the presence of crustal particles in aerosols 0.1 um and smaller collected with a MOUDI multistage impactor during dust storms in Australia's Lake Eyre desert basin. The chemistry of these particles was also generally consistent with calcium-bearing clay minerals of complex composition, which could have been removed from the surface of larger grains under strong winds and saltation. Finally, Baddock et al. (2013) abraded Australian dune sands in a laboratory chamber for ~1 hour, detecting the emission of aerosols with a mean size of 110-130 nm and as small as 18 nm. They stated, "… the number concentration of particles approximately trebled over the course of the experiment with results suggesting that collisions between mobile sand grains led to the production of new nanosized particles over time…. chemical composition suggests that nanoparticles are produced from the clay coatings surrounding the parent sand grains."

The Kok model (2011b) was specifically designed to exclude transport, deposition, and mixing. A single pathway such as this would not clearly explain all dust production mechanisms

and thus would not always explain observed aerosol particle size distributions; rather, it is more likely that transport, mixing, and mechanisms of dust and aerosol production other than brittle fragmentation of primary mineral grains combine to create conditions favorable for the production of the specific particle size distribution observed at Camp Victory. The combination of ultrafine aerosol production by sandblasting of clay-type mineral coatings on the surface of larger grains (d'Almeida and Schütz, 1983; Gomes et al., 1990; Radhi et al., 2010; Baddock et al., 2013), coupled with the apparent production and advection of ultrafine particles within dust plumes carried long distances by strong desert winds (Gomes et al., 1990; Butler et al., 2012; Carniero et al., 2013) and fine to coarse aerosols produced by brittle fragmentation particle generation as described by Kok (2011a, 2011b), together provides a logical explanation for the particle size distributions observed in the Camp Victory data during Shamal and Kous wind events.

3.5   Conclusions

Elemental signatures consistent with crustal materials have been found in the aerosols collected at Camp Victory, Iraq, using a DRUM aerosol impactor. The presence of high concentrations of soil aerosols in the finest size fraction (0.09-0.26 μm in aerodynamic diameter) collected by the DRUM sampler was surprising because most hypotheses about the generation of soil aerosols do not produce particles of this size. The very fine particles only occur under windy conditions implying that the source of these particles is not local anthropogenic activity. Wind roses, HYSPLIT meteorological backwards trajectories, and the aerosol composition show that although there are differences between the aerosols impacting the site during Shamal and Kous wind conditions, the finest size fraction of soil aerosols is produced under both Shamal and Kous

114

wind conditions. The conclusion from these results is that a mechanism exists for the production of Aitken mode geogenic particles from desert surfaces.

The soil data collected during this study agree with Kok's (2011a) model based on the brittle fragmentation hypothesis except for the particles in the finest size fraction. Therefore, brittle fragmentation, which is hypothesized to be independent of wind speed, may provide one mechanism for generating the small crustal particulates observed in the data, but it is not the only explanation. The data presented in this study show wind velocity plays a significant role in the fragmentation process and fine particle production. The combination of hypotheses put forward in recent papers by Carneiro et al. (2013) and Butler et al. (2012) could explain the deviation from the brittle fragmentation model via a fine particle production model in high wind, dust storm conditions that would lead to additional particle break down during particle transport in a dust plume. In addition, the hypotheses and data of d'Almeida and and Schütz (1983), Gomes (1990), Radhi et al. (2010) and Baddock et al. (2013) suggest an additional mechanism of ultrafine dust aerosol production via sandblasting of clay and weathering-related coatings on desert sands. These hypotheses are worthy of further testing to determine in they can explain the size distributions observed in the Camp Victory aerosol data.

3.6   Acknowledgments

3.7   Figures

Figure 3-1. Photograph of a dust storm in Baghdad (courtesy of Kevin Geisbert).

Figure 3-2. A general vicinity map of Iraq. The green and red place markers depict the Taurus and Zagros Mountains ranges of Turkey and Iran, respectively. Baghdad is represented with a blue thumbtack and Camp Victory is located in Baghdad. Image created from Google Maps: www.google.com.

Figure 3-3. Shamal dust storm passing through Iraq. This Envisat/ASAR image is of a dust storm over Iraq occurring from September 12 -15, 2008. The star marker indicates the approximate location of Baghdad with respect to the Storm. The image was taken by Envisat/ASAR passes on the 12th and 15th of September. ASAR images are generated from Level-0 (raw) and Level-1b products Envisat source Level-0 and Level-1b products are provided by ESA. Envisat/ASAR image courtesy of Earth Snapshot.
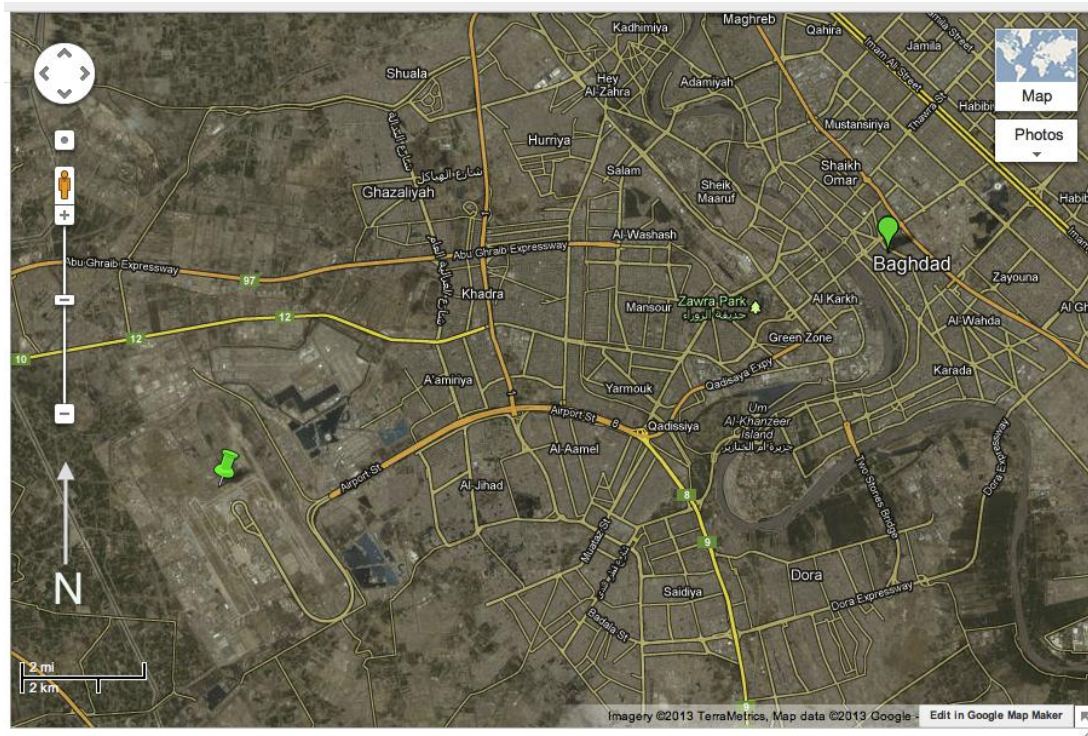
Figure 3-4. Camp Victory with respect to Baghdad. Camp Victory is indicated with a green thumbtack and Baghdad is represented with a place marker. Image created from Google Maps: http://www.google.com.

Figure 3-5. Photograph of a Davis rotating drum unit for monitoring (DRUM) aerosol impactor.
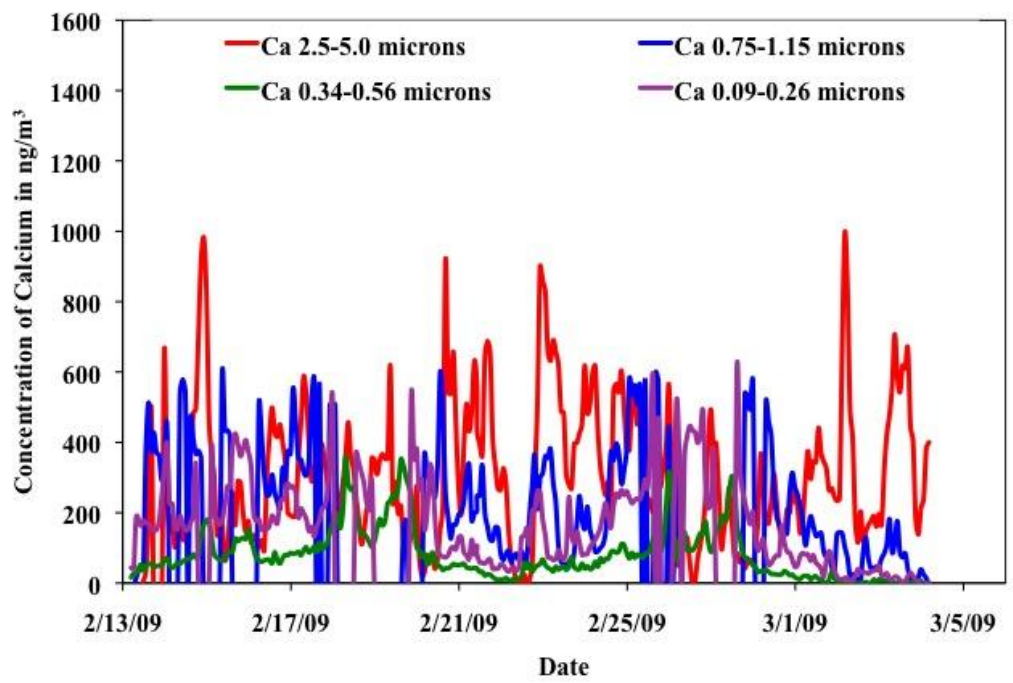
Figure 3-6. Time series of calcium showing the temporal variability of representative size fractions over a three-week period in February 2009.
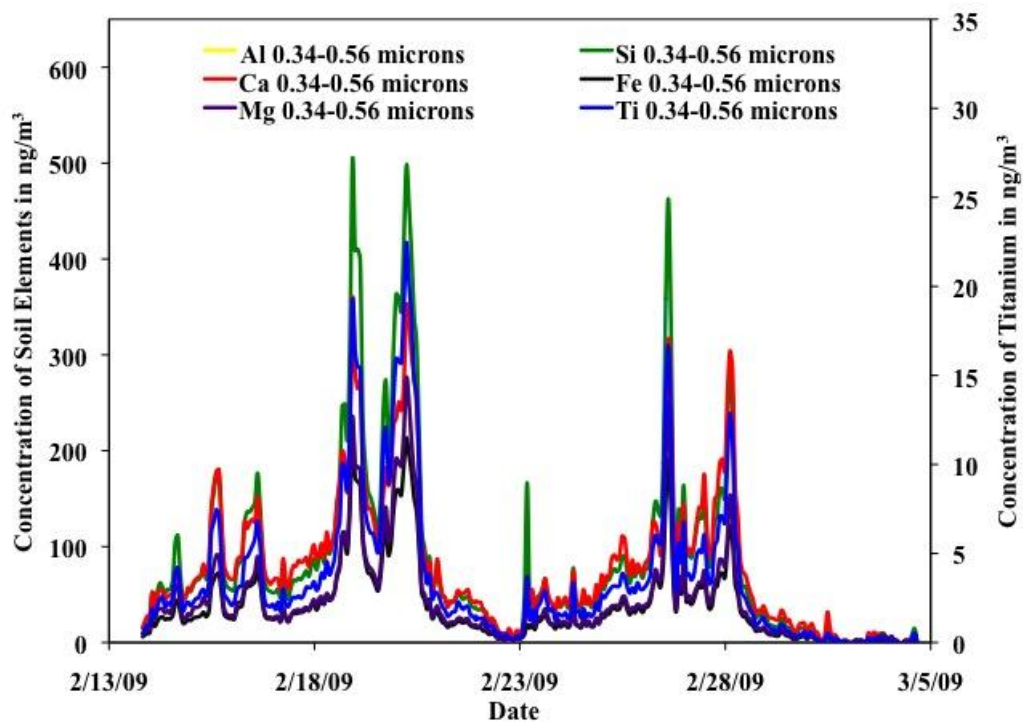
Figure 3-7. Time series of the soil elements Al, Si, Ca, Mg, Ti, and Fe in the 0.34-0.56 micron size fraction. The concentration of Ti is on the secondary axis. This figure shows the presence of soil within the fine aerosols.
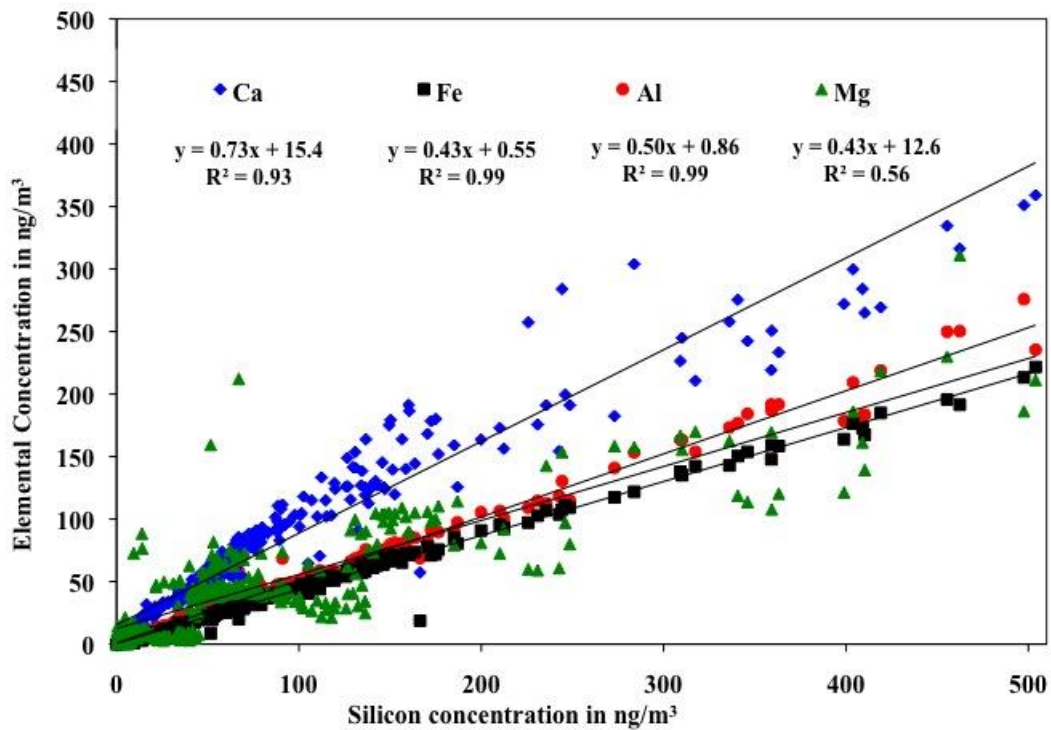
Figure 3-8. Variation of specific crustal elements as they correspond to Si in the 0.34-0.56 micron range during the February 13, 2009 sampling campaign. This figure demonstrates how well Ca, Fe, Mg, and Al correlate to Si. This indicates that these particles are from the same source and appear to be crustal soils within the 0.34 to 0.56 micron size fraction.
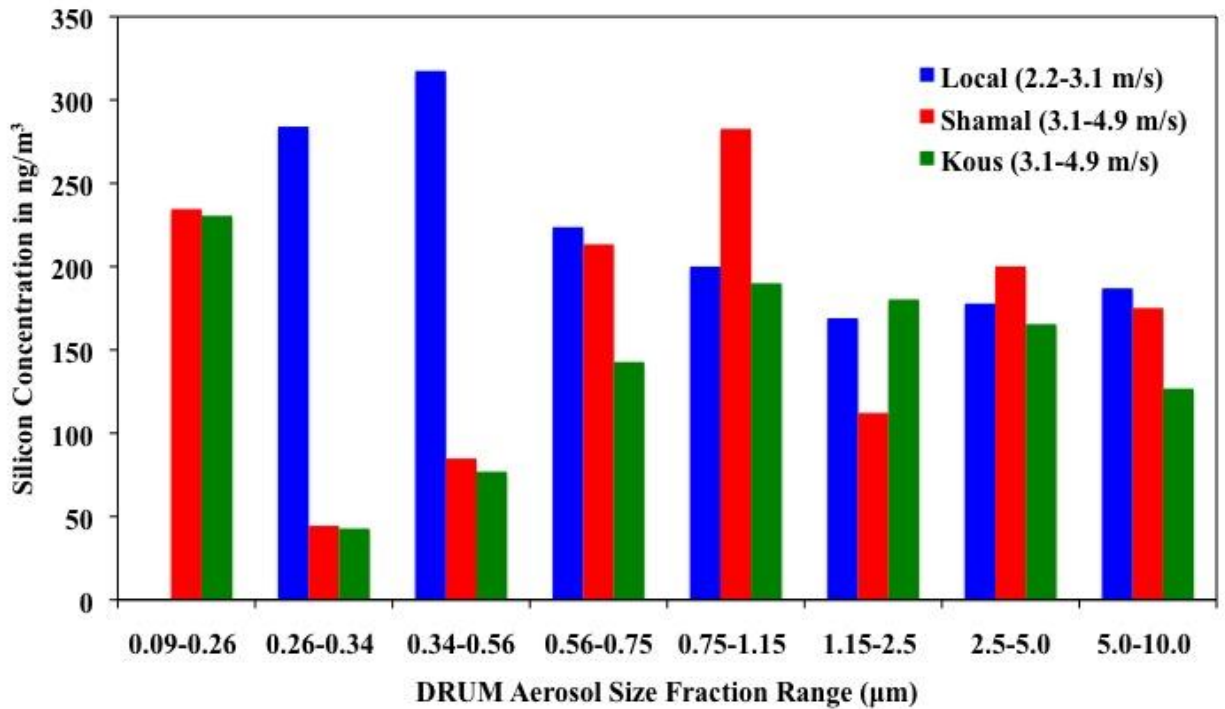
Figure 3-9. Histogram of elemental mass concentrations (ng/m^3) for silicon ranging from 0.09 to 10 microns under local, Shamal, and Kous wind conditions. It is apparent from this graph that there are greater concentrations of ultra-fine aerosols (0.09 to 0.26 microns) than in some of the larger stages as shown by the 0.34 to 0.56 micron stage. It is also noteworthy that a larger percentage of 0.34-0.56 silicon particles are present during local wind events.
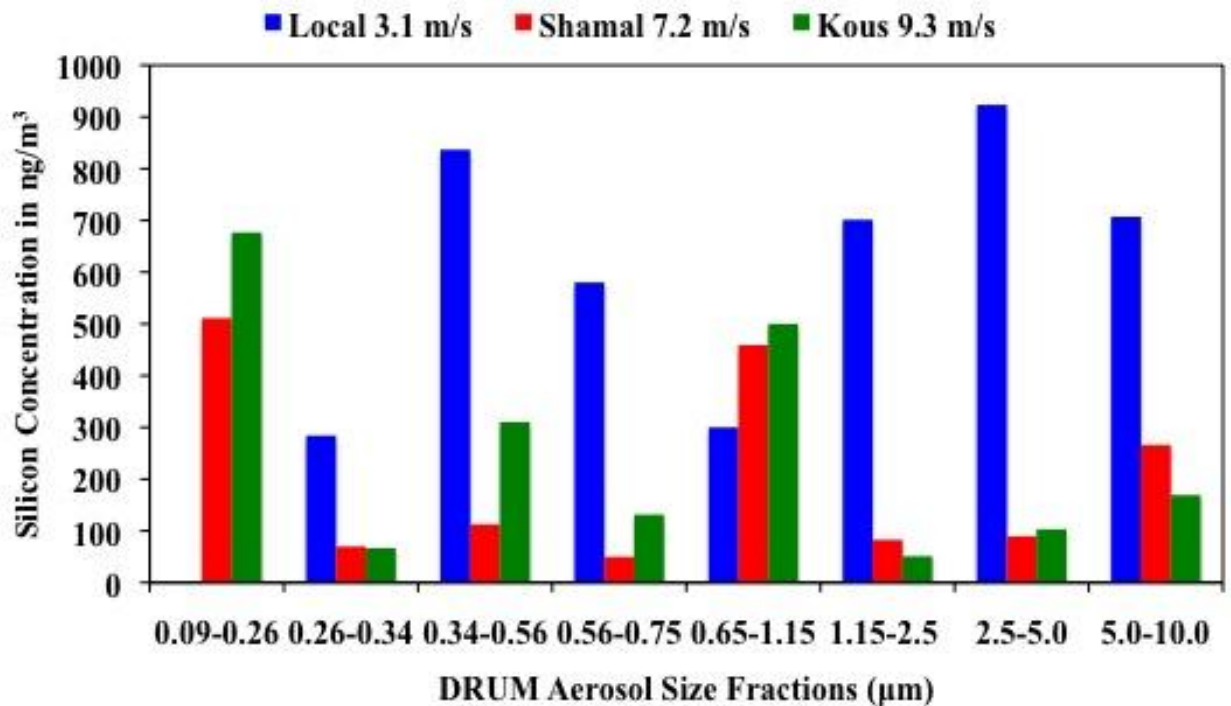
Figure 3-10. Histogram of elemental mass concentrations (ng/m^3) for silicon ranging from 0.09 to 10 microns under maximum wind speeds for local, Shamal, and Kous wind conditions. It is apparent from this graph that there are greater concentrations of ultra-fine aerosols (0.09 to 0.26 microns) during Kous and Shamal winds than in some of the larger stages as shown by the 0.34 to 0.56 micron stage. It is also noteworthy that a larger percentage of silicon particles are present during local wind events but not during the Shamal and Kous wind events. This may be due to flaking of the large sample deposits associated with the Shamal and Kous winds.
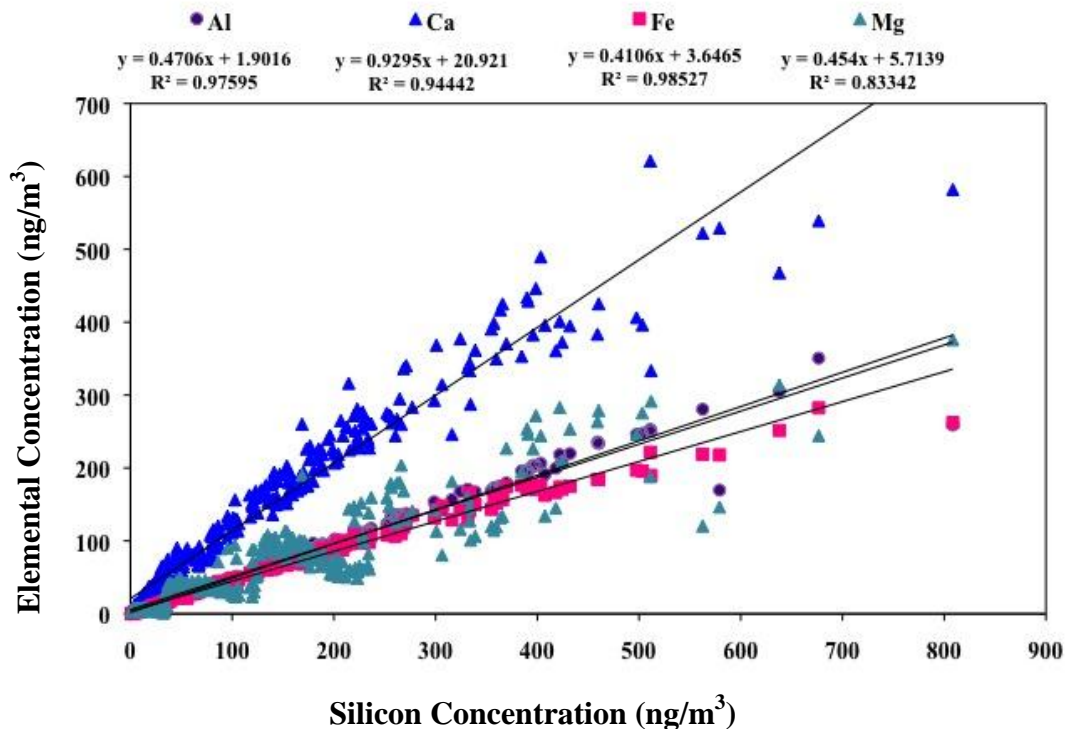
Figure 3-11. Variation of specific crustal elements as they correspond to silicon in the 0.09-0.26 micron size fraction.
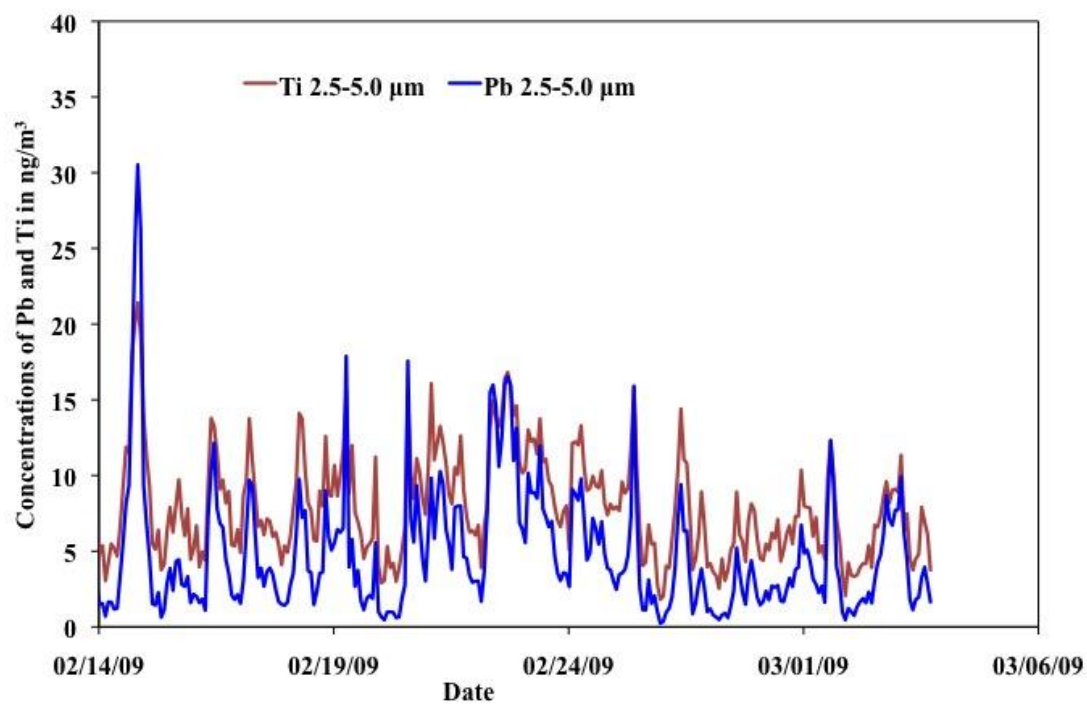
Figure 3-12. Time series of Ti and Pb in the 2.5-5.0 micron size fraction.
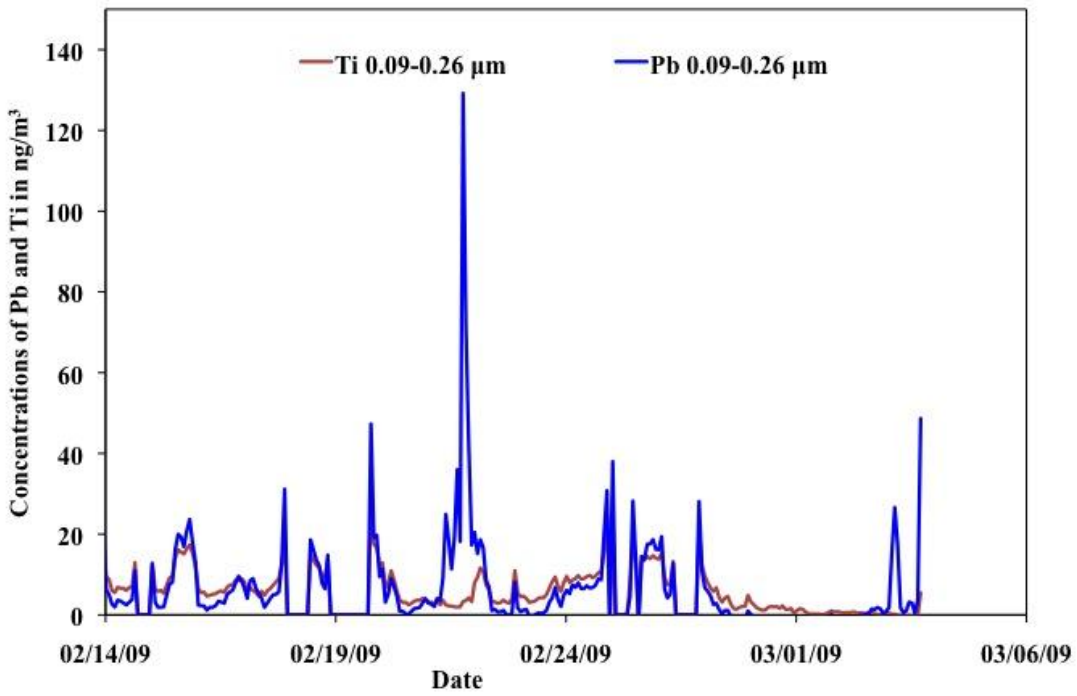
Figure 3-13. Time series of Ti and Pb in the 0.09-0.26 micron size fraction.
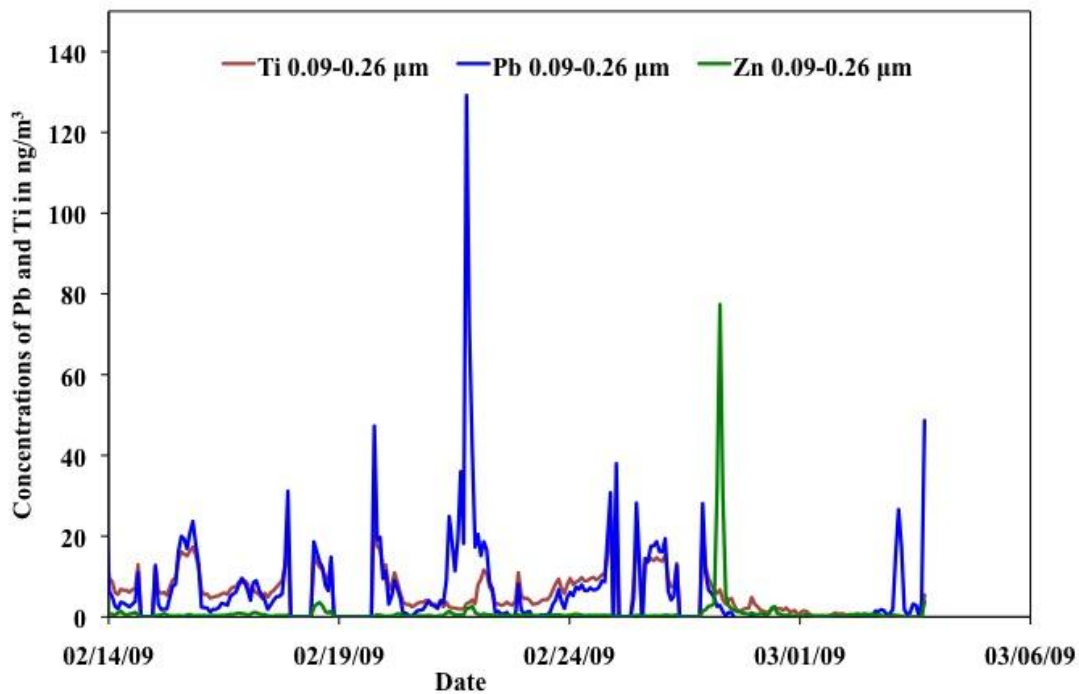
Figure 3-14. Time series of Ti, Pb, and Zn in the 0.09-0.26 micron size fraction. This figure is significant in that it can relate Ti, Pb, and Zn to anthropogenic emissions of leaded fuel and brake and tire dust.
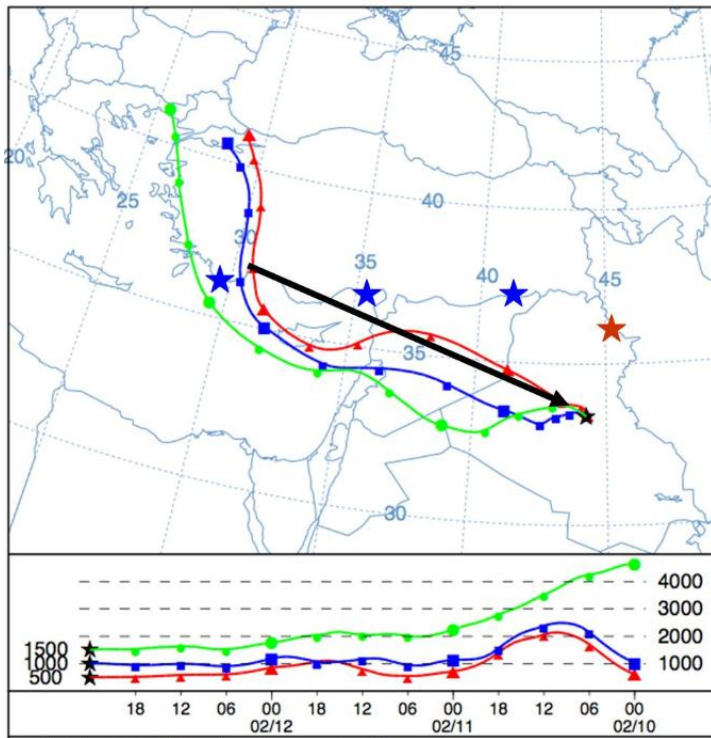
Figure 3-15. HYSPLIT backward meteorological trajectories showing air crossing the Taurus mountains (line of blue stars) on its way to the site. This period is based on a 72-hour backward trajectory beginning on February 13, 2009. The black line represents the predominant drainage path into Baghdad and the red star denotes the Zagros Mountains bordering Iraq and Iran.

131
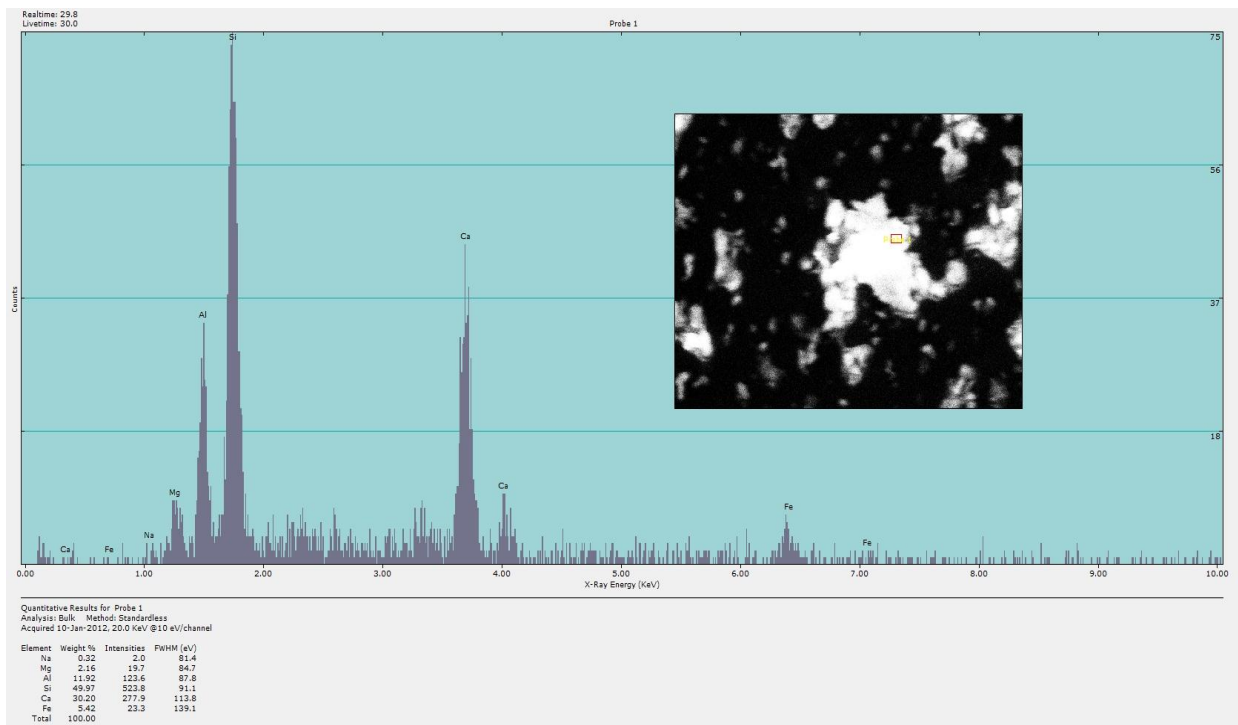
Figure 3-16. SEM analysis of an aerosol sample (0.26-0.09 microns size fraction) from the February 13, 2009 sampling campaign. The particle contains Si, Al, Ca, Fe, and Mg, consistent with being a particle of soil/clay mineral produced through chemical reactions in the soil.
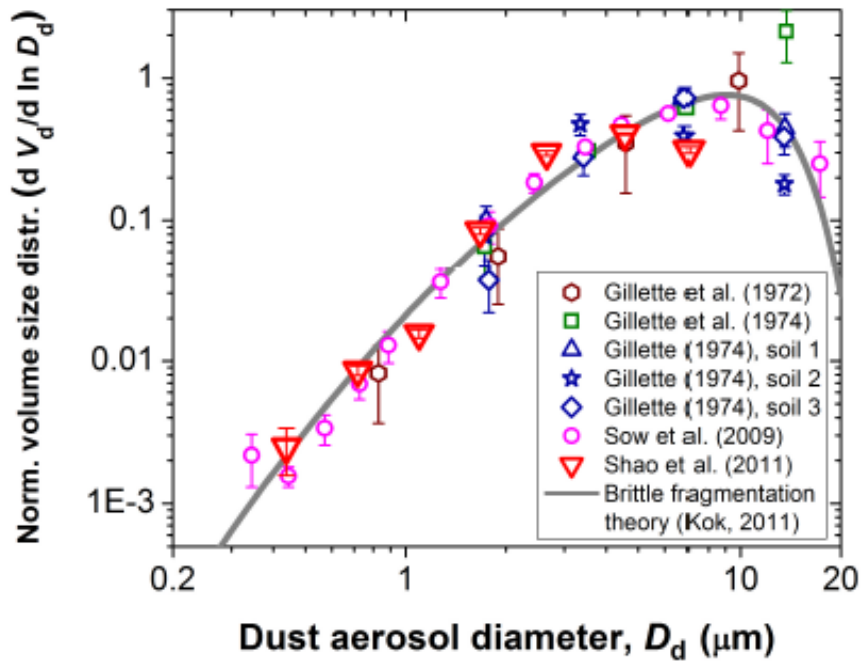
Figure 3-17. Kok Brittle Fragmentation Model. This figure depicts the correlation of Kok's Brittle Fragmentation Theoretical Model with that of laboratory and field data. It can be seen that the model has a good correlation with the laboratory and field. Figure from Jasper Kok, used by permission (Kok, J.F., 2011b.)
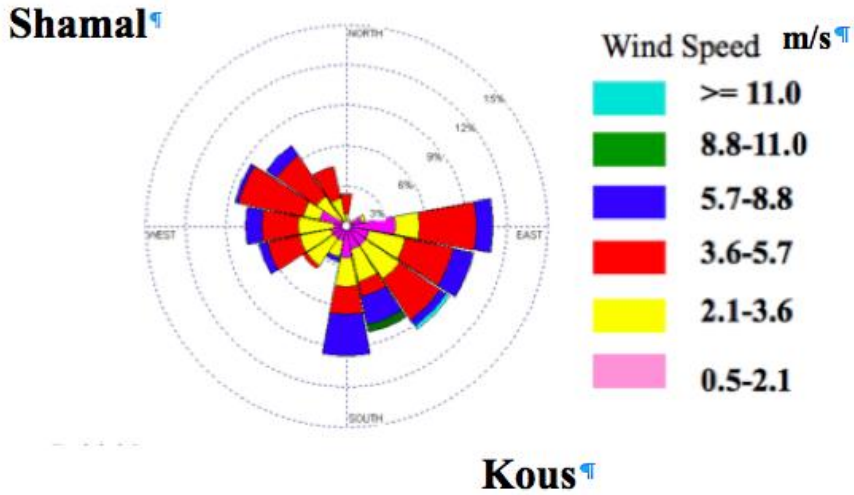
Figure 3-18. Wind rose for Baghdad, Iraq for the February 13, 2009 sampling campaign. It can be noted from this figure that Shamal and Kous winds are the prevailing winds during this period. It can also be seen that winds were recorded in excess of 11 m/s. Wind directions and wind velocity were compiled from Weather Underground. The WRPlot was compiled from Lakes Environmental.
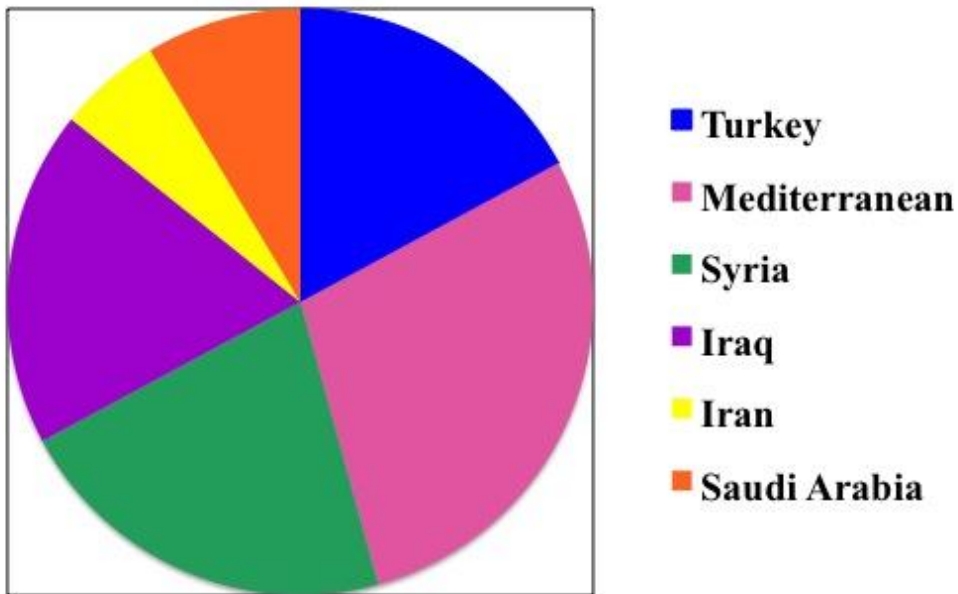
Figure 3-19. Pie chart of wind paths. The pie chart depicts predominate wind paths for the February 2009 sampling campaign. It can be seen that predominate drainage comes from the Mediterranean Sea, Turkey, and Syria areas consistent with the northwesterly Shamal winds.
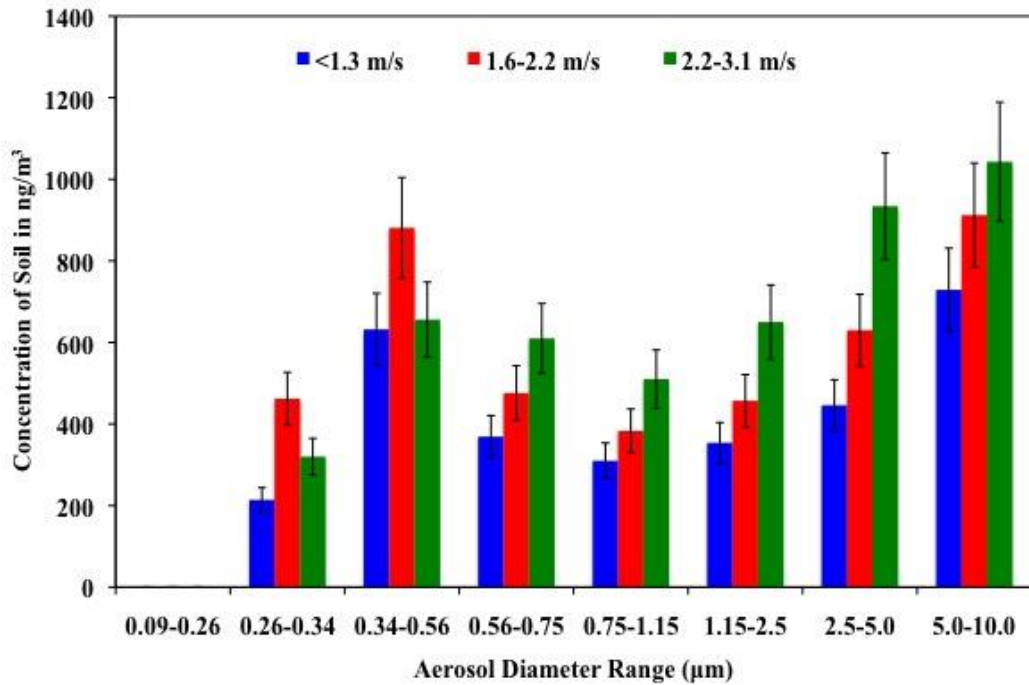
Figure 3-20. Bar graph of average soil concentrations as a function of wind speed for local wind events. Soil was defined using the IMPROVE soil algorithm formula. It can be seen from this figure that soil concentrations appear to increase in the larger size fractions with wind speeds and aerosol diameter size fractions. The lack of soil elements in the 0.09-0.26 micron size fraction should be noted.
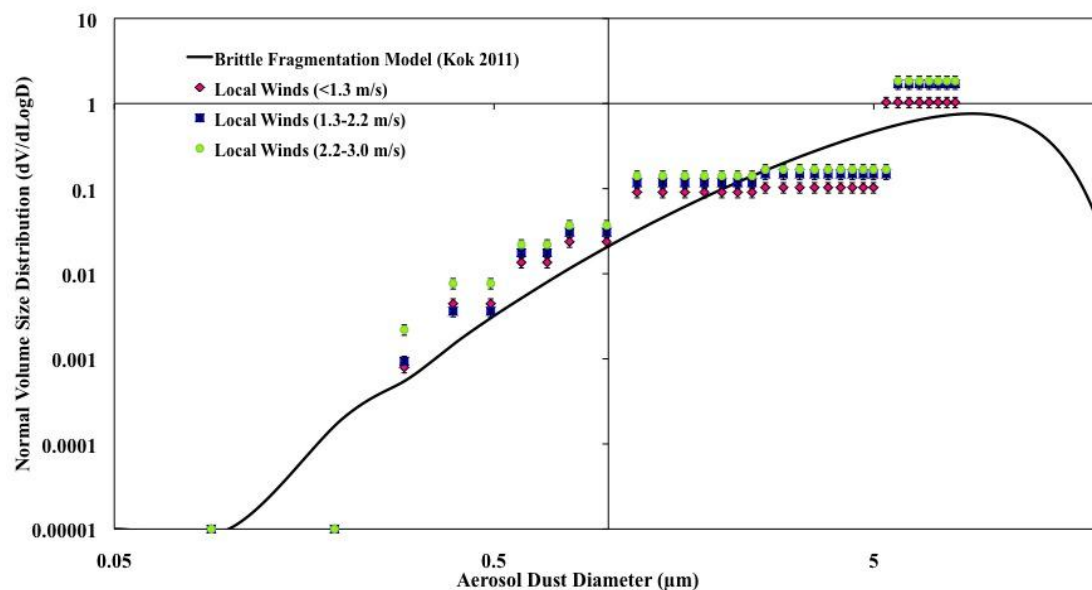
Figure 3-21. Iraqi wind data (local event) plotted against Kok's brittle fragmentation model (2011). Although there is an increase in the normal volume size distribution with increasing wind speed, the data correlates well to brittle fragmentation theory.
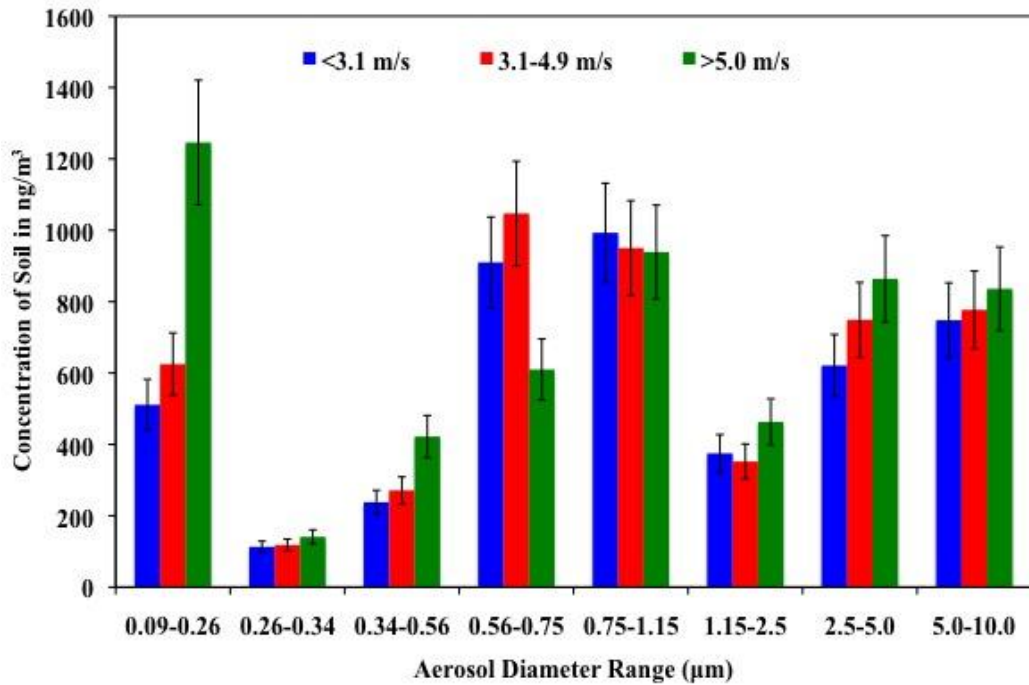
Figure 3-22. Bar graph of average soil concentrations as a function of wind speed for Shamal wind events. It can be seen from this figure that the two middle size fractions (0.56-0.75 and 0.75-1.15 microns) have the highest soil element concentrations. The prominent peaks in the 0.09 to 0.26 micron size fraction are of particular interest.
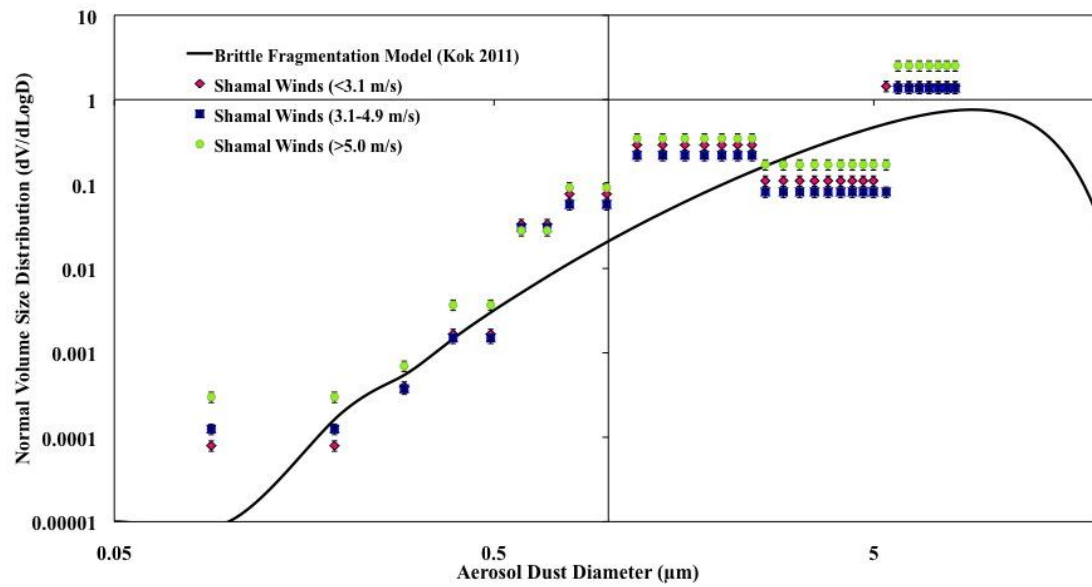
Figure 3-23. Iraqi wind data (Shamal event) plotted on Kok's brittle fragmentation model (2011). The uptick in the 0.09 to 0.26 micron size fraction is of interest as it deviates from Kok's model. Aside from this uptick and increases in normal volume size distribution with increasing wind speed, the data agrees well with the brittle fragmentation model.
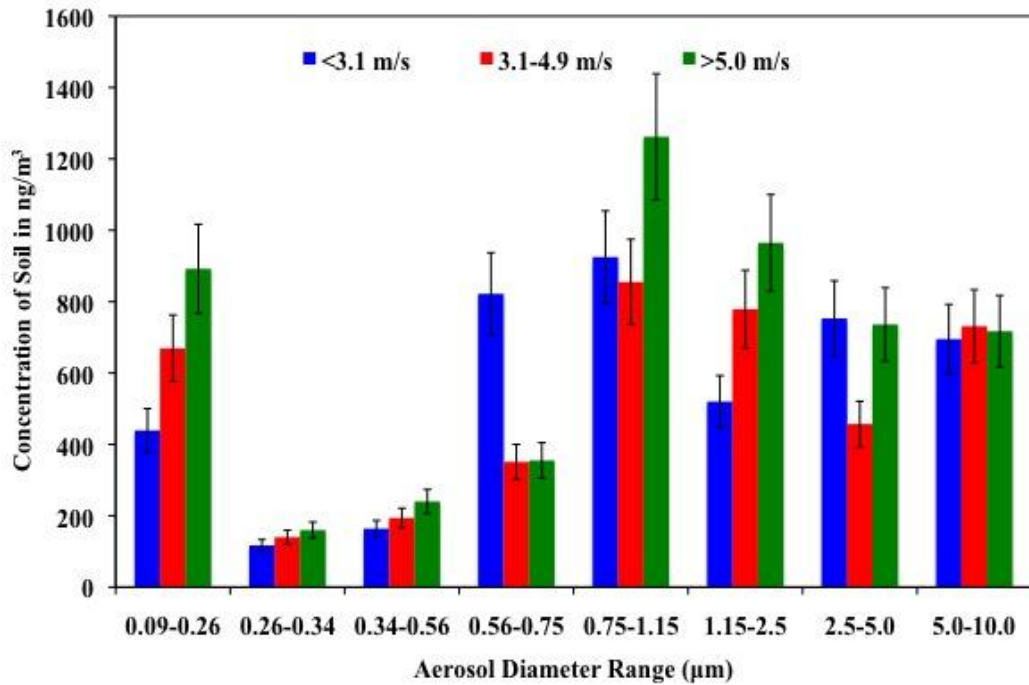
Figure 3-24. Bar graph of average soil concentrations as a function of wind speed for Kous wind events. It can be seen from this figure that the 0.75-1.15 size fraction has the highest soil element concentration. The prominent peaks in the 0.09 to 0.26 micron size fraction are of particular interest.
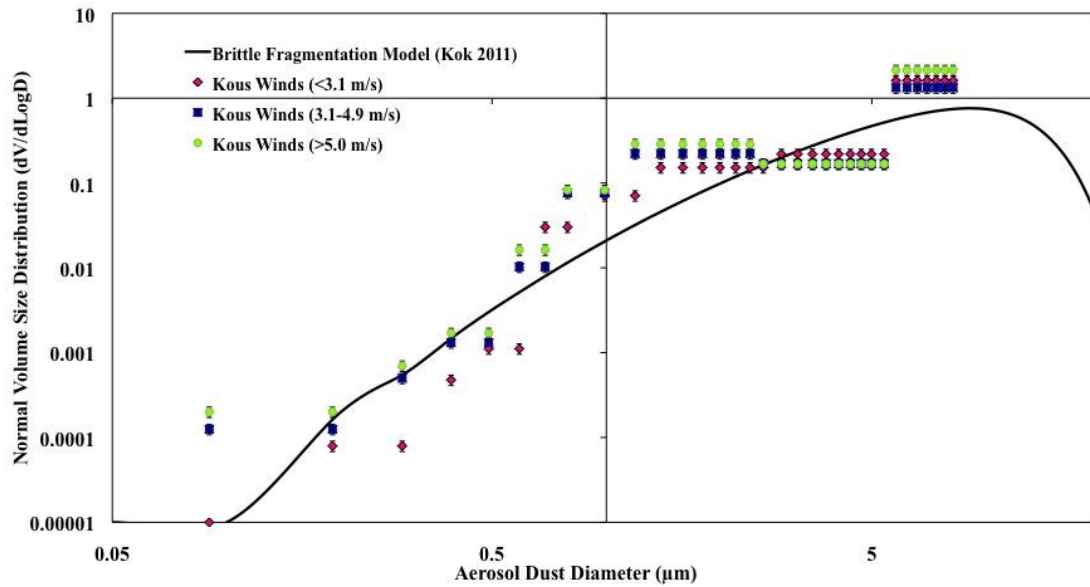
Figure 3-25. Iraqi Wind Data (Kous event) plotted on Kok's brittle fragmentation model (2011). The uptick in the 0.09 to 0.26 micron size fraction is of interest as it deviates from Kok's model. Aside from this uptick and increases in normal volume size distribution with increasing wind speed, the data agrees well with the brittle fragmentation model.
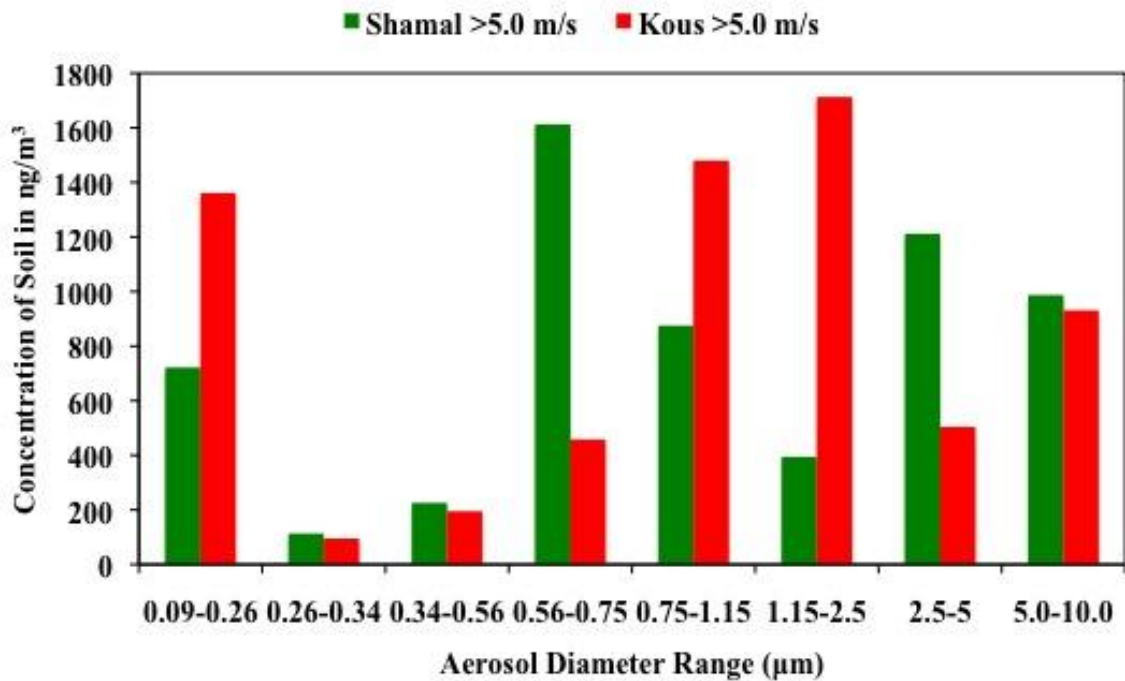
Figure 3-26. Bar graph of average soil concentrations as a function of wind speed for Shamal and Kous wind events. It can be seen from this figure that during this sampling campaign, the highest average soil concentration for the 0.56-0.75 micron size fraction occurred during Shamal winds, while the highest average soil concentration for the 1.15-2.5 micron size fraction occurred during Kous winds. The prominent peaks in the 0.09 to 0.26 micron size fraction are of particular interest.

3.8   Tables

Table 3-1. A comparison of the settling velocities and deposition times for particles of different sizes of lofted to the top of a 5500 m dust cloud.

Aerodynamic diameter range for DRUM size fractions (µm)	DRUM stage mid-point of aerodynamic diameter (µm)	Terminal settling velocity (m/s)	Time required for particle at lofted to the top of the dust cloud (5500 m) to reach the surface
5.0 - 10.0	7.5	1.72×10^{-2}	3.7 days
2.5 - 5.0	3.75	4.38×10^{-4}	145 days
1.15 - 2.5	1.83	1.09×10^{-4}	1.6 years
0.75 - 1.15	0.95	3.14×10^{-5}	5.6 years
0.56 – 0.75	0.66	1.61×10^{-5}	10.8 years
0.34 – 0.56	0.45	8.22×10^{-6}	21.2 years
0.26 – 0.34	0.40	6.73×10^{-6}	25.9 years
0.09 – 0.26	0.18	1.94×10^{-6}	90 years

3.9   References

Al-Bassam, K.S.; Huk, J. Metallic and industrial rocks and minerals. *In Geology of Iraq.* Jassim, S.Z.; Goff, J., Eds.; Dolin, Prague and Moravian Museum, Brno: Czech Republic. **2006**, 288-302.

Al-Dabbas, M.A.; Abbas, M.A.; Al-Khafaji, R.M. Dust storm loads analysis Iraq. Arabian Journal of Geosciences. **2012,** 5, 121-131. doi: 10. 1007/s12517-010-0181-7.

Al-Dabi, H.; Koch, M.; Al-Sarawi, M.; El-Baz, F. Evolution of sand dune patterns in space and time in northwestern Kuwait using LANDSAT images. Journal of Arid Environments. **1977**, 36, 15-24.

Al-Dawachi, B.M. Origin of some limestone and gypsum natural bridges at N. Iraq. Raf. Journal of Sciences. **2005**, 16(2), 26-34.

Alfaro, S. C.; Gomes, L. Modeling mineral aerosol production by wind erosion: Emission intensities and aerosol size distribution in source areas. Journal of Geophysical Research**. 2001,** 106, 18075-18084.

Al-Farrajii, F.A.H. Combating desertification in Iraq. United Nations Desertification Control Bulletin **1998**, 33, 2-10.

Al-Hurban, A.E.; Al-Ostad, A.N. Textural characteristics of dust fallout and potential effect on public health in Kuwait City and suburbs. Environment Earth Sciences. **2010**, 60(1), 169-181.

Al-Juboury, A.I.; McCann, T.   The middle Miocene Fatha (lower Fars) formation, Iraq. GeoArabia, Journal of the Middle East Petroleum Geosciences. **2008**, 13, 141-174.

Al-Khafaji, R.M.N. Effects of dust storms on some Iraqi territories, Ph.D. Thesis, College of Science, University of Baghdad. **2009**.

Ali, A.H. Wind regime of the Arabian Gulf. *In: The Gulf War and the Environment*. El-Baz, F.; Makharita, R.M., Eds.; Amsterdam, B.V. **1994**, 31-48.

Allen, M. D.; Raabe, O. G. Re-Evaluation of Millikan's Oil Drop Data for the Motion of Small Particles in Air. Journal of Aerosol Science. **1982**, 13, 537–547.

Andreae, M.O. Climatic effects of changing atmospheric aerosol levels. *In: World Survey of Climatology*. Future Climates of the World: A. Henderson-Sellers Ed.; Elsevier, Amsterdam. **1995**, 16, 341− 392.

Astrom, J.A. Statistical models of brittle fragmentation. Advances in Physics. **2006**, 5 (3-4), 247-278.

Astrom, J.A.; Ouchterlony, F.; Linna, R.P.; Timonen, J. Universal dynamic fragmentation in D dimensions. Physical Review Letters. **2004**, 92:245506.

Awadh, S.M. Geochemistry and mineralogical composition of the airborne particles of sand dunes and dust storms settled in Iraq and their environmental impacts. Environmental Earth Sciences. **2012**, 66 (8), 2247-2256. doi:10.1007/s/12665-011-1445-6.

Baddock, M.; Boskovic, L.; Strong, C.; McTainsh, G.; Bullard, J.; Agranovski, I.; Cropp, R. Iron-rich nanoparticles formed by aeolian abrasion of desert dune sand. Geochemistry Geophysics Geosystems. **2013**, 14, 3720–3729, doi:10.1002/ggge.20229.

Breed, C.; Grow, T. Morphology and distribution of dunes and sand seas observed by remote sensing. *In: A study of global sand seas.* McKee, E.D., Ed.; Washington, DC, USGPO. **1979**, 253-305.

Butler, H.J.; McTainsh G.H.; Hogarth, W.L. Simulations of spatial variability in particle-size emissions during wind erosion events. Earth Surface Processes and Landforms. **2012**, 37, 1362-1375.

Cahill, C.F.; Rinkleff, P.G.; Dehn, J.; Webley, P.W.; Cahill, T.A.; Barnes, D.E. Aerosol measurements from a recent Alaskan volcanic eruption: Implication for volcanic ash transport predictions. Journal of Volcanology and Geothermal Research. **2010**, 76-80.

Cahill, T.A.; Wakabayashi, P. Compositional analysis of size-segregated aerosol samples. *In: Measurement Challenges in Atmospheric Chemistry.* Newman, L., Ed.; American Chemical Society. **1993**, 211-228.

Carneiro, M.V.; Araújo, N.A.M.; Pähtz, T.; Herrmann, H.J. Midair collisions enhance saltation. Physical Review Letters. **2013**, 111, 058001. doi:10.1103/PhysRevLett.111.058001.

Clarke, A.D.; Collins, W.G.; Rasch, P.J.; Kapustin, V.N.; Moore, K.; Howell, S.; Fuelberg, H.E. Dust and pollution transport on global scales: aerosol measurements and model predictions. Journal of Geophysical Research. **2001**, 106, 32555–32569.

Countess, R.J.; Barnard, W.; Claiborn, C.; Gillette, D.; Latimer, D; Pace, T; Watson, J. Methodology for estimating fugitive windblown and mechanically resuspended road dust emissions applicable for Regional Air Quality Modeling; final report prepared for the Western Governors Association by Countess Environmental, Westlake Village, CA. **2001**.

d'Almeida, G.A.; Schütz, L. Number, mass and volume distributions of mineral aerosols and soils of the Sahara. Journal of Climate and Applied Meteorology. **1983**, 22, 233-243.

de Villiers, M.P.; van Heerden, J. Dust storms and dust at Abu Dhabi International Airport. Weather. **2007**, 62(12), 339-343.

Draxler, R.R.; Hess, G.D.   Description of the HYSPLIT_4 modeling system. NOAA Tech. Memo. ERL ARL-224, NOAA Air Resources Laboratory, Silver Spring, MD. **1997**, 24.

Draxler, R.R.; Hess, G.D. An overview of the HYSPLIT_4 modeling system of trajectories, dispersion, and deposition. Australian Meteorological Magazine. **1998**, **47**, 295-308.

Draxler, R.R.   HYSPLIT4 user's guide. NOAA Tech. Memo. ERL ARL-230, NOAA Air Resources Laboratory, Silver Spring, MD. **1999**.

Draxler, R.R.; Rolph, G.D. HYSPLIT (HYbrid Single-Particle Lagrangian Integrated Trajectory) Model [Online] **2013.** NOAA ARL READY Website (http://ready.arl.noaa.gov/HYSPLIT.php). NOAA Air Resources Laboratory, Silver Spring, MD.

El-Baz, F. Gulf War Disruption of the Desert Surface in Kuwait. *In: The Gulf War and the Environment*. El-Baz, F.; Makharita, R.M., Eds.; Amsterdam, B.V. **1994**, 31-48.

Engelbrecht, J.P.; McDonald, E.V.; Gilles, J.A.; Jayanty, R.K.M.; Casuccio, G.; Gertler, A.W. Characterizing mineral dusts and other aerosols from the Middle East − Part 1: Ambient sampling. Inhalation Toxicology. **2009**, 21, 297-326. doi:10.1080/08958370802464273.

Engelstaedter, S.; Washington, R.; Mahowald, N. Impact of changes in atmospheric conditions in modulating summer dust concentration at Barbados: A back-trajectory analysis. Journal of Geophysical Research, **2009,** 114, D17111.

Faure, G. Principles and Applications in Geochemistry, 2nd ed., Prentice Hall: New Jersey, **1998**, 46-51.

Foda, M.A., Khalaf, F.I.; Al-Kadi, A.S. Estimation of dust fallout rates in the northern Arabian Gulf. Sedimentology. **1985**, 32(4), 595-603. doi:10.1111/j.1365-3091.1985.tb00473.x.

Gillette, D.A.; Blifford, I.H.; Spencer, C.R. Measurements of aerosol size distributions and vertical fluxes of aerosols on land subject to wind erosion.   Journal of Applied Meteorology. **1972**, 11, 977-987.

Gillette, D.A.   On the production of soil wind erosion having the potential for long-range transport. Journal of Recherches Atmospheriques. **1974**, 8, 734-744.

Gilvarry, J.J.; Bergstrom, B.H. Fracture of brittle solids. 2. Distribution function for fragment size in single fracture (experimental). Journal of Applied Physics. **1961**, 32, 400–410.

Gomes, L.; Bergametti, G.; Coude-Gaussen, G.; Rognon, P. Submicron desert dusts: a sandblasting process. Journal of Geophysical Research. **1990**, 95, 13927-13935.

Ismail, S.A.; Arai, S.; Ahmed, A.H.; Shimizu, Y. Chromitite and peridotite from Rayat, northeastern Iraq, as fragments of Tethyan ophiolite. Island Arc. **2009**, 18, 175-183.

Jaenicke, R. Tropospheric aerosols. *In: Aerosol-Cloud-Climate Interactions*. Hobbs, P.V., Ed.; Academic Press. **1993**, pp. 1-27.

Jassim, S.Z.; Buday, T. Geology of Iraq. Jassim, S.Z.; Goff, J.C., Eds.; Dolin, Prague and Moravian Museum, Brno. **2006**.

Koh, G.; Wakely, L.D. Impact of gypsum on electromagnetic properties of desert soils. IEEE Geoscience and Remote Sensing Letters. **2011**, 8(6), 1051-1054. doi: 10.1109/LGRS. 2011.2154297

Kok, J.F. A scaling theory for the size distribution of emitted dust aerosols suggests climate models underestimate the size of the global dust cycle. Proceedings of the National Academy of Sciences. **2011a**, 108, 1016-1021.

Kok, J.F. Does the size distribution of mineral dust aerosols depend on the wind speed at emission? Atmospheric Chemistry and Physics. **2011b**, 11, 10149-10156.

Krueger, B.J.; Grassian, V.H.; Cowin, J.; Laskin, A. Heterogeneous chemistry of individual mineral dust particles from different dust source regions: The importance of particle mineralogy. Atmospheric Environment. **2004**, 38(36), 6253-6261. doi:10.1016/j.atmosenv.2004.07.010.

Lakes Environmental. http://www.weblakes.com/products/wrplot/index.html (accessed September 21, 2013).

Liaghat, S.; Moore, F.; Juni, M. The Kuh-e-Surmeh mineralization, a carbonate-hosted Zn-Pb deposit in the Simply Folded Belt of the Zagros Mountains, SW Iran. Mineralium Deposita. **1999**, 35, 72-78.

Membery, D.A. Low level wind profiles during the Gulf Shamal. Weather. **1983**, 38, 18-24.

Miller, M.; Gosar, M. Characterization of solid airborne particles in urban snow deposits from Ljubljana by means of SEM/EDS. Materials and Geoenvironment. **2009**, 56, (3), 266–282.

Misconi, H.; Navi, M. Medical geology in the Middle East. International Year of the Planet Earth. **2010**, 135-174. doi: 101007/978-90-481-3430-4_6.

Moore, K.G.; Clarke, A.D.; Kapustin, V.N.; Howell, S.G. Long-range transport of continental plumes over the Pacific Basin: Aerosol physiochemistry and optical properties during PEM-Tropics A and B. Journal of Geophysical Research: Atmospheres. **2003**, 108(D2), PEM 8-1-PEM8-27. doi:10.1029/2001JD001451.

Oddershede, L.; Dimon, P.; Bohr, J. Self-organized criticality in fragmenting. Physical Review Letters. **1993**, 71, 3107–3110.

Okin, G.S.; Gillette, D.A. Spatially explicit regional wind erosion and dust emission modeling: Incorporating large- and small-scale variability. *In: Proceedings of ICAR 5/ GCTE-SEN Joint Conference, International Center for Arid and Semiarid Land Studies (ICASALS).* Lee, J.A.; Zobeck, T.M., Ed.; Texas Tech University, Lubbock: ICASALS Publication. **2002**, 02-2, 256-260.

Raabe, O.G.; Braaten, D.A.; Axelbaum, R.L.; Teague, S.V.; Cahill, T.A. Calibration studies of the DRUM impactor. Journal of Aerosol Science. **1988**, 19(2), 183-195.

Radhi, M.; Box, G.P.; Mitchell, R.M.; Cohen, D.D.; Stelcer, E.; Keywood, M.D. Size-resolved mass and chemical properties of dust aerosols from Australia's Lake Eyre Basin, Atmospheric Environment. **2010,** 44, 3519-3528.

Reist, P. C. *Aerosol Science and Technology*. (2nd ed.). New York: McGraw-Hill, Inc. **1993**.

Rolph, G.D. Real-time Environmental Applications and Display sYstem (READY) [Online] **2013**. (http://ready.arl.noaa.gov). NOAA Air Resources Laboratory, Silver Spring, MD.

Saeed, T.M.; Hassam, A. Optical and physical characterization of "Iraqi Freedom" dust storm, a case study. Theoretical and Applied Climatology. **2010**, 104, 123-137.

Safar, M.I. Dust and dust storms in Kuwait. Meteorological Department of the Directorate General of Civil Aviation, Kuwait. **1985,** 212.

Schmaltz, J. Visible earth dust storm in Iraq, June 08, NASA Image, **2008**.

Seinfeld, J.H.; Pandis, S.N. *Atmospheric Chemistry and Physics: From Air Pollution to Climate Change*, 2nd ed.; J. Wiley, New York. **1998**.

Shahsavani, A.; Naddafi, K.; Haghighifard, N.J.; Mesdaghinia, A.; Yunesian, M.; Nabizadeh, R.; Arhami, M.; Yarahmadi, M.; Sowlat, M.H.; Ghani, M.; Jarahi, A.J.; Alimohamadi, M.; Motevalian, S.A.; Soleimani, Z. Characterization of ionic composition of TSP and PM10 during the Middle Eastern Dust (MED) storms in Ahvaz, Iran. Environmental Monitoring and Assessment. **2012**, 184:6683-6692 DOI 10.1007/s10661-011-2451-6.

Shao, Y.P.; Ishizuka, M.; Mikami, M.; Leys, J.F. Parameterization of size-resolved dust emission and validation with measurements. Journal of Geophysical Research: Atmospheres. **2011**, 116, D08203. doi:10.1029/2010JD014527.

Shi, Z.; Shao, L.; Jones, T.P.; Lu, S. Microscopy and mineralogy of airborne particles collected during severe dust storm episodes in Beijing, China. Journal of Geophysical Research: Atmospheres. **2005**, 110, D01303, doi:10.1029/2004JD005073

Sibrava, V. Geology of Iraq. Jassim, S.Z.; Goff, J.C., Ed.; Dolin, Prague and Moravian Museum, Brno. **2006**.

Sow, M.; Alfaro, S.C.; Rajot, J.L.; Marticorena, B. Size resolved dust emission fluxes measured in Niger during 3 dust storms of the AMMA experiment. Atmospheric Chemistry and Physics. **2009**, 9(12), 3881-3891. doi:10.5194/acp-9-3881-2009.

Tarbuck, E.J.; Lutgens, F.K.; Tasa, D.G. Earth: Matter and Mineral. *In: An Introduction to Geology. 11th ed.,* Dunway, A., Eds.; Upper Saddle River, NJ. **2013**, 81-115.

Weese, C.; Abraham, J. Potential Health Implications Associated with Particulate Matter Exposure in Deployed Settings in Southwest Asia. Inhalation Technology. **2009**, 21, 291-296.

Whitby, K.T.; Cantrell, B.K. Proceedings of the International Conference on Environmental Sensing and Assessment (ICESA), Institute of Electrical and Electronic Engineers (IEEE) 1976. Atmospheric aerosols: characteristics and measurement. **1976**, IEEE #75-CH 1004-1, ICESA paper 29-1, Washington, DC: IEEE. p. 6.

Wilkerson, W.D. Dust and sand forecasting in Iraq and adjoining countries. Air Weather Service TN-91/001. **1991**, 63.

Chapter 4 The Effect of Aerosol Loading on the Particle Size Separation of Brittle Minerals in

an 8-Stage DRUM Aerosol Impactor[1.]

4.1   Abstract

A calibration study was conducted on an 8-stage DRUM aerosol impactor to determine whether minerals subject to brittle fracture (calcium sulfate, sodium bicarbonate, and finely ground quartz) would fragment during impaction and to quantify the effects of high mass loading conditions on sample sizing. The amount of mass collected at predetermined points on the sample substrates was varied to determine if the ratios of aerosol mass between different stages remained constant under a wide range of mass loading conditions. The ratios remained constant as the mass loading increased implying that the minerals did not fragment during sampling. Mineral particles were not observed on the smallest size fraction (0.09-0.26 microns) under either 'wind' (4.1 m/s) or 'high wind' (8.3 m/s) conditions. This fact confirmed the particles were not breaking down into smaller particles than what was observed in the initial size distribution characterized by an optical particle counter. These findings suggest the increases in soil element concentrations on the DRUM stages collecting the smallest size fractions seen in data sets from Iraq and White Sands, NM, are due to actual single particles and not a product of particle fragmentation during sampling.

4.2   Introduction

A consensus exists among aerosol scientists about how atmospheric aerosols are formed. The basis for this understanding is summarized in a Seinfeld and Pandis (1998) diagram outlining a tri-modal distribution of typical aerosol growth patterns (Whitby and Cantrell, 1976).

[1.] Bell, J.M.; Cahill, C.F.; Egan, S.D. The effect of aerosol loading on the particle size separation of brittle minerals in an 8-Stage DRUM aerosol impactor. University of Alaska Fairbanks, Fairbanks, AK. In preparation for submission to the American Chemical Society, 2014.

Aerosols within this distribution range from the ultra-fine particles (<0.1 μm) of the transient nuclei or Aitken nuclei range, through the fine particles (0.1-2.5 μm) trapped within the Greenfield gap (Greenfield, 1957) of the accumulation mode, to the coarse particles (>2.5 μm) associated with natural (e.g., biological or geogenic) processes. Particles within the transient nuclei mode are typically combustion products that have undergone gas-to-particle conversions to form primary particles. These particles collide with each other and grow into particles of the sizes found in the accumulation mode. Ultimately, water vapor condenses onto accumulation mode particles causing them to be removed from the atmosphere via washout. Coarse particles form by different processes than finer particles; they are generated from larger source materials through grinding and other mechanical processes.

Atmospheric aerosols found within Iraq are predominately comprised of dust (Al-Hurban and Al-Ostad, 2010; Engelbrecht et al., 2009; Al-Dabbas et al., 2012; Misconi and Navi, 2010; Awadh, 2012; Shahsavani, et al., 2012). For the purposes of this paper, dust is defined as the silt-sized or clay-size soil particles lofted due to high velocity winds (Middleton and Goudie, 2001). Dust is usually associated with coarse particulate matter (Seinfeld and Pandis, 1998); however, it has been detected across all of the size fractions collected by DRUM aerosol impactors (Lundgren, 1967; Cahill et al., 1985; Raabe et al., 1988; Cahill and Wakabayashi, 1993; Wetzel et al., 2003; Collins et al., 2007) in Baghdad, Iraq. The DRUM aerosol impactor is a cascade impactor that continuously collects size (eight size fractions between 0.09 to 10 microns in aerodynamic diameter) and time-resolved aerosols (Lundgren, 1967; Cahill et al., 1985; Raabe et al., 1988; Cahill and Wakabayashi, 1993; Wetzel et al., 2003; Collins et al., 2007; Cahill et al., 2010). Of particular interest in the finest DRUM size fraction (0.09-0.26 μm) for

samples collected in Iraq is a peak in soil elements that occurred during high wind conditions. This peak is not consistent with a simple peak tailing of a soil size distribution. Seinfeld and Pandis (1998) noted that number distributions of desert soils tend to exhibit three overlapping modes at diameters of 0.01 microns or less, 0.05 microns, and 10 microns respectively. Although the occurrence of fine particles (>0.3 microns) has been reported (Alfaro and Gomes, 2001; Sow et al., 2009; Shao et al., 2011) and correlated to wind velocities, some models (Kok, 2011a; Kok, 2011b) suggest wind velocities have little role in this break down while others suggest it is a function of wind speed (Sow et al., 2009; Shao et al., 2011, Carneiro et al., 2013) and transport (Butler et al., 2012). Soil element concentrations are routinely detected in the finest fractions of the DRUM samplers deployed in Iraq. The frequency of dust peaks raises the question of whether the peaks are due to naturally occurring processes in the environment or the breakdown of larger soil particles during sampling.

Many studies (Mitchell and Pilcher, 1957; Lee et al., 1972; Whitby et al., 1974) argue about the level of certainty that cascade impactors, such as the DRUM aerosol impactor, have in representing the original particle captured. This concern is largely associated with the integrity of the original particle and whether fracturing occurs during loading as one particle collides with other particles, thereby breaking the original particle into smaller pieces that are caught in the sampler's air flow and deposited on later stages of the sampler. It is suggested (Gordon et al., 1974) that care should be taken when presenting data, as particle size from impaction on each stage can be misleading. Lundgren (1967) argues that problems associated with particle loss and inappropriately represented data (due to wall loss) can be effectively eliminated through the use of a coating and proper instrumental design and operations. The DRUM sampler uses Apiezon

L^{TM}- coated Mylar^{TM} sample substrates specifically to minimize the potential for particle bounce or removal of particles from the sample strip (Wesolowski et al., 1978; Cahill et al., 1979; Raabe et al., 1988; Bench et al., 2002).

It is the intent of this study to evaluate whether the brittleness of an aerosolized mineral may lead to particles fracturing during sampling. The likelihood that one mineral may resist the scratching of the other is determined by the Mohs scale of hardness which ranges from one to ten (Tarbuck et al., 2013). Gypsum is the defining mineral on the Mohs scale for hardness value two and has an absolute hardness of three. Calcite is the defining mineral for hardness value three, and has an absolute hardness of nine. Quartz is the defining mineral for hardness value seven and has an absolute hardness of 100. Specifically, we are evaluating whether soft minerals, such as hemihydrate gypsum ($CaSO_4 \bullet 0.5H_2O$) and calcite ($CaCO_3$), are more likely to flake or fragment into finer particles while passing through the sampler or colliding with other soft/brittle mineral particles already deposited on the sample substrate. Gypsum and calcite were chosen for analysis as they are major geological resources of Iraq (Bellen et al., 1959), are the predominate soft minerals found along Iraq's drainage paths and dried wetlands, which are major dust sources, and are defining minerals within the Mohs scale. Gypsum also comprises the 'white sands' of White Sands, NM, which have the largest known reserves of surface gypsum (Tarbuck et al., 2013) and are also a major source of dust aerosols in the southwestern United States. Calcite also was evaluated to further understand the behavior of soft minerals within the impactor and is also a common desert dust aerosol. Measurements from these two mineral types were compared to quartz, a common but far harder mineral that is more resistant to mechanical breakdown. The results from the sampler testing were compared with DRUM-sampled aerosol

datasets from White Sands, NM, and Baghdad, Iraq, to determine if the fine particles observed within those data sets are consistent with fine minerals breaking down in the sampler or if their formation was the result of naturally-occurring environmental processes.

4.3   Experimental

To determine whether impaction enhances the fragmentation of soft sedimentary minerals within the DRUM aerosol impactor, dry dispersed powders of anhydrous gypsum ($CaSO_4$) salts, sodium bicarbonate ($NaHCO_3$), and finely ground quartz (SiO_2) were collected under different simulated wind speed conditions and sampling durations using the 8-stage DRUM aerosol impactor in the laboratory. Table 4-1 provides a summary of the minerals used for analysis.

Anhydrous gypsum was chosen for this study because a study conducted by Yu and Brouwers (2011) suggests gypsum strength is reliant on the amount of hydration. As water evaporates the bonds between the gypsum crystals weaken, thereby weakening the crystalline structure and increasing the brittleness of the mineral. The use of anhydrous gypsum in the study would represent the worst-case brittleness scenario and be most representative of the impact brittle minerals have during bombardment.

$NaHCO_3$ was chosen for analysis due to the number of Nahcolite deposits within the oil shales of Turkey and Jordan (Dyni, 2006). Oil shales are the second largest fossil fuel in Turkey and are present as fine-grained sedimentary rocks (Altun et. al., 2006). Nahcolite is a brittle mineral (Mohs scale hardness of 2.5) that represents dusts transported to Iraq during Shamal winds that may become susceptible to fragmentation upon impact.

155

SiO$_2$ (silica) was chosen for analysis because it is a brittle mineral and the most abundant resource in the Earth's crust (Faure, 1998). Since SiO$_2$ may be represented as sand and quartz, the predominant mineral in desert dust, and there are varying quartz deposits in and around Iraq ample opportunities exists for SiO$_2$ to fragment. SiO$_2$ represents a significant amount of the dust lofted and transported to Iraq and has known brittle properties; therefore, its likelihood to fragment during bombardment was investigated. The methods used for the sampling and analyses of the minerals are described in the following sections.

4.3.1 8-stage DRUM Aerosol Impactor

The DRUM aerosol impactor (Figure 4-1) is a rotating Lundgren-type (1967) impactor with a flow rate of 16 L min^{-1} that continuously collects size and time-resolved aerosols (Cahill et al., 1985 Raabe et al., 1988; Cahill and Wakabayashi, 1993; Wetzel et al., 2003; Collins et al., 2007). The DRUM utilizes impaction to separate particles by aerodynamic diameter into 5.0-10.0, 2.5-5.0, 1.15-2.5, 0.75-1.15, 0.56-0.75, 0.34-0.56, 0.26-0.34, and 0.09-0.26 μm size fractions. These size cuts will decrease modestly as external wind speeds increase (Cahill and Barnes, 2009). Normally, the rotation rate of the drums gives the time resolution of the collected samples. In this study, the rotation of the DRUM was turned off so that the deposition time could be increased, thereby concentrating the aerosols collected on a given area. This allowed the effects of the additional deposition on top of previously impacted samples to be measured and compared to previously collected particles that were not subsequently impacted by additional particles. Apiezon L^{TM}-coated Mylar^{TM} was used to cover the rotating drums to prevent the loss of particles from bounce or rebound (Raabe et al., 1988). Surface coatings, such as Apiezon L^{TM}, are needed because the elastic properties of both the particle and the collecting surface are

high during impaction resulting in the tendency of particles to bounce off the surface (Lundgren, 1967; Vincent, 2007). This is problematic as some particles, especially solid, gritty ones such as soil particles, may fail to be retained on impact and may be deposited on smaller stages. Soils in the Middle East and other desert dust source areas are dry and fragile and thus may break into finer fractions as they collide against other particles in the DRUM aerosol impactor.

The samplers were calibrated with the size-cut methods outlined and published by Raabe et al. (1988), and the uniformity of a sample across the 1-cm high deposition area on each stage was shown to be consistent as demonstrated by Bench et al. (2002). Recent co-located field experiments by the U.C. Davis Delta Group also showed consistency between mass concentration measurements made by different DRUM aerosol impactors (Cahill et al., 2011).

4.3.2   Aerosol Generation

4.3.2.1 Sample Preparation

Sample preparation entailed adding dry-dispersed dusts of $NaHCO_3$, $CaSO_4$, and SiO_2, to the TSI Fluidized Bed Aerosol Generator (FBAG) sample reservoir. The $NaHCO_3$ and $CaSO_4$ did not require any preparation prior to use, as they were finely pulverized powders purchased from Baker Analyzed (Philipsburg, N.J.). The SiO_2 was ground into a fine powder with a rock grinder prior to use.

4.3.2.2 Aerosol Generator

Aerosols were generated using a TSI Fluidized Bed Aerosol Generator (FBAG) model 3400A with a bead purge of 10 L/min and an airflow rate of 2 L/min. Air was supplied through a high efficiency particulate air filter (HEPA) to the device at 25 psi of pressure to ensure a steady flow. The copper bead bath in the FBAG was purged before introducing a new compound into

157

the system by flushing the reservoir with air for 30 minutes before filling the reservoir with new material. The FBAG was equilibrated for 1 hour to ensure sample delivery resulted in a consistent aerosol output. An optical particle sizer (OPS) was used to determine the particle size distributions of the aerosolized samples and the consistency of the aerosol generation.

4.3.3 Methodology

To simulate the movement of air and aerosols past the DRUM impactor by a wind, the inlet of the impactor was placed in the middle of a 12" wide Sonnotube (Figure 4-2) and air was pulled in a cross-stream past the inlet cap. A HEPA filter was positioned upstream of the sampler's inlet and a vacuum was pulled downstream of the inlet to create an up to 12.4 m/s flow of clean, HEPA-filtered air through the tube and past the inlet. The 'wind' velocities were measured using a LPM Air flow meter. A wind velocity of 8.28 m/s is representative of the Shamal and Kous windy days experienced in Iraq. A TSI Optical Particle Sizer (OPS), model 3330, was used to sample and record in real time the aerosol size distribution (17 bins between 0.3 to 10 microns) created by the FBAG. To do this, the OPS sampling line was placed in the Sonnotube between the injection port for the FBAG and the inlet for the DRUM. This allowed the clean air to dilute the aerosols from the FBAG upstream from the OPS sampling line and the DRUM's inlet. The diluted aerosol stream moved downstream through the Sonnotube, across the OPS sampling line and then across the DRUM's sampling inlet, thus providing the same size distribution and concentration to the OPS as the DRUM. In addition, the OPS was flushed with HEPA-cleaned air in between runs to remove residual aerosols from the inlet tube before the next sampling run. Sample collection durations included 5-hour, 8-hour, 12-hour and 20-hours durations. After each run, the substrate-coated drums in the DRUM impactor were rotated to

provide separation between the different sample deposits. After the completion of all sampling runs, the Mylar® DRUM strips were removed and placed on slide frames in preparation for mass concentration analysis using the β-gauge.

4.3.4   Mass Concentration Analysis

A DRUMAir β-gauge was used to measure the total mass of aerosols collected during sampling (Courtney et al., 1982; Chueinta and Hopke, 2001). The analysis is conducted by beta particle attenuation.

4.4.   Results

4.4.1   Experimental Results

4.4.1.1 Particle Fragmentation Tests

Particle fragmentation studies were conducted on aerosolized particles of $CaSO_4$, $NaHCO_3$, and SiO_2 collected by an 8-stage DRUM aerosol impactor. In accordance with our OPS measurements of $NaHCO_3$ and $CaSO_4$, (Figure 4-3 and Figure 4-4, respectively) dust concentrations decreased in each successive fraction until they can no longer be read by the OPS finest fraction for $NaHCO_3$, which represents particles 0.3-0.374 microns. The OPS detected low concentrations of fine (0.3 microns) $CaSO_4$ aerosols (Figure 4-4). Figure 4-5 bins the OPS data for $CaSO_4$ into size fractions equivalent to those measured by the DRUM. In general, concentration decreases with each successive stage.

Table 4-2 provides the effective mass concentration of $CaSO_4$ collected under different lengths of time to simulate the effect of higher ambient mass concentrations during a normal 3-hour sampling period. The mass concentration increased with longer run times, with the greatest mass being collected during the 20-hour run. Both $NaHCO_3$ and $CaSO_4$ particles were detected

on stages 1-6, which represent particles with aerodynamic diameters ranging between 0.34 to 10 μm. The table demonstrates that mineral dust generated by mechanical grinding mechanisms can readily be detected on stages with aerodynamic diameters smaller than the 2.5 μm, which is commonly thought of as the breakpoint between mechanically generated and combustion-related aerosols. There was no distinguishable mass on stage 7 of the DRUM. The OPS showed a low mass concentration of particles (0.13 ug/m^3) in this size range, but the deposited mass was below the maximum detection limit (MDL) for the beta gauge. The lack of particles on the DRUM stages corresponding to particle sizes smaller than those observed using the OPS means that these particles are not breaking down or bouncing in the sampler, even during periods with large mass loadings present on the substrate.

To confirm that samples are not breaking down within the sampler, Figure 4-6 shows the difference in loading becomes greater as fractions become smaller within the DRUM impactor. It should be noted the mass concentration ratio between stages 3 and 8 are not apparent as there was not sufficient mass on stage 8 to be considered. It is for this reason a peak cannot be seen for this ratio. Higher concentrations of CaSO$_4$ are noted on stage 3 (1.15-2.5 microns) than on stage 2 (2.5-5.0 microns) as a more uniform concentration of pulverized material occurs across the 1.15-2.5 micron range. Additionally, it is noted that as time progresses the FBAG does not consistently produce the same number of particles as during the initial measurement. Figure 4-7 shows decreasing particle numbers as sampling time increases. This may be due to the failure of the bead chain to pick up the same number of particles as the chain hollows out a track through the sample in the sample chamber. To minimize this problem it was ensured that the sample

160

chamber always had ample sample prior to and through each run so that gravity would cause the particles above the chain to be fill in the hollowed out area around the chain.

The quartz samples were not reproducibly analyzed by the β-gauge. It appears the electrostatic properties of quartz fragments interfered with the transfer of electrons between the source and detector for the β-gauge. Therefore, no quantitative measurements of the mass of quartz particles were made. However, the charging anomaly does indicate whether there are quartz particles present on a stage. According to this evidence, quartz particles deposit on stage 8. The OPS, however, cannot size particles smaller than 0.3 microns, so the initial size distribution cannot be determined for the small particles. Given that quartz is harder than the other minerals, it is unlikely that the quartz fractured when the other particles did not so it is probable that the quartz on stage 8 is due to particles initially of that size. Figure 4-8 shows that the smallest particles entering the sampler, as measured by the OPS, could be below 0.3 microns in size because there are particles in the size fraction immediately above the OPS cutoff.

4.4.1.2 Wind Speed Sampling Tests

The $CaSO_4$ and SiO_2 aerosols collected by the DRUM aerosol impactor under simulated 'high wind' conditions did not change from the 'wind' case. That is, although the aerosols were injected into a larger volume of air and moved through the testing apparatus more quickly, there was no evidence of fragmentation upon impaction or loss of larger particles due to aerosol inlet impacts. Figure 4-9 depicts the size distribution of aerosols collected during the high wind-speed tests. The size distribution is consistent with what resulted from the low-wind test described above.

4.4.1.3 Comparison with other Data Sets

Field campaigns conducted in Baghdad, Iraq, using DRUM aerosol impactors routinely detect dust within the finest size fractions (0.09-0.26 microns). The time series of aluminum (Al), calcium (Ca), silicon (Si), magnesium (Mg) and iron (Fe) in Figure 4-10 depicts the elemental mass concentrations for dust in stage 6 (0.34-0.56 microns) during a period from 02/13/09 to 03/05/09 in Iraq. Iraq is an arid desert with soils enriched in brittle minerals (Bellen, 1959) so there was concern that these aerosols were due to particle bounce and fragmentation in the sampler. However, the results from the laboratory study suggest the high concentration of soil elements on this stage are indeed due to environmental production mechanisms and not particle bounce and fragmentation under high aerosol loading conditions.

A field campaign conducted at White Sands Missile Range, New Mexico, using an 8-stage DRUM aerosol impactor to study the production of aerosols as a function of meteorology during springtime (windy, dusty) conditions. The field data from White Sands was used as a comparison to Iraq because the sand dunes are dominated by gypsum, the soils range from fine silt to coarse sand, and winds bring about the lofting of significant amounts of dust. The presence of gypsum particles on stage 6 (0.34 to 0.56 µm), stage 7 (0.26 to 0.34 µm), and stage 8 (0.09 to 0.26 µm), shown in Figure 4-11 (Cahill et al., 2005), of the White Sands Missile Range data was used in this study as a field measurement comparison to the experimental data. These aerosols are significant in that they demonstrate the total mass of particles within the smallest size fractions of the DRUM impactor. The presence of gypsum in these finest fractions suggests geogenic dusts may routinely fractionate to sizes not previously believed to result from mechanical processes. The results of the study above and from Cahill et al. (2005) are consistent

with this study and show that these small size fractions are real and that there is no evidence of mechanical break down of the aerosols within the sampler.

Figure 4-12 provides a ratio between DRUM stages 5 (1.15-0.75μm), 6, (0.75-0.56), 7 (0.56-0.34), and 8 (0.26-0.09 μm) from the White Sands Missile Range study. As partitioning occurs between each successive stage (5 to 6, 5 to 7, and 5 to 8) a greater concentration difference is seen and a substantial decrease in concentration exists between stages 5 and 8. This would suggest particles are not fragmenting within the sampler. Therefore, the field measurements collected from White Sands, NM further suggests samples are not fragmenting within the DRUM impactor and that the presence of fine and ultrafine soil particles (<2.5 μm) is a result of fragmentation resulting from environmental geogenic processes.

4.5. Conclusion

A calibration study was conducted on an 8-stage DRUM aerosol impactor to determine whether brittle minerals (calcium sulfate, sodium bicarbonate, and finely ground quartz) were likely to fragment during impaction and to quantify the effects of high mass loading conditions on sample sizing. The purpose of this study was to determine if inconsistencies observed with field data could be explained via instrumental design flaws or whether geological conditions exist that result in the enhanced presence of very fine-grained geogenic aerosols.

Laboratory results show that particles are not fragmenting in the DRUM aerosol impactor across the range of mass loadings despite different wind conditions. The mass concentrations decrease in each successive stage for the smaller size fractions as expected, implying that there are no small particle production mechanisms occurring in the sampler. Additionally, the dust

concentrations on the DRUM stages were consistent with the particle distributions measured using the OPS, so no particle loss or production was occurring in the inlet and sampler.

The results of the Iraqi field campaign and field measurements collected from White Sands, NM are consistent with this study and show no evidence of mechanical breakdown of the aerosols within the sampler. Further, the results imply the presence of fine and ultrafine soil particles (<2.5um) observed in field samples is a result of production from environmental geogenic processes. This suggests the DRUM cascade impactor is functioning as designed and its size-cut calibrations are consisted with Raabe et al. (1998).

Future studies to confirm the effectiveness of the DRUM aerosol impactor as a quantitative aerosol collection device would verify the uniformity of the samples across the 1 cm high sample deposit through scanning electron microscopy (SEM). Elemental mass could be then evaluated and validated using synchrotron x-ray fluorescence analysis to confirm the results. The additional analyses could provide specific information on the behavior of quartz particles during sampling.

4.6   Acknowledgements

4.7   Figures
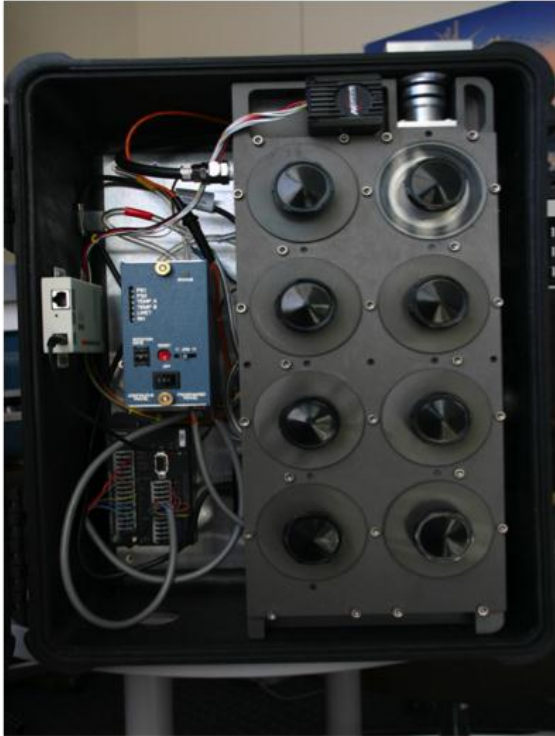
Figure 4-1. Photograph of a Davis rotating drum unit for monitoring (DRUM) aerosol impactor.

Figure 4-2. Schematics of the instrumental set-up. The inlet of the DRUM aerosol impactor was placed in the middle of a 12" wide Sonnotube to simulate a cross-stream of air.
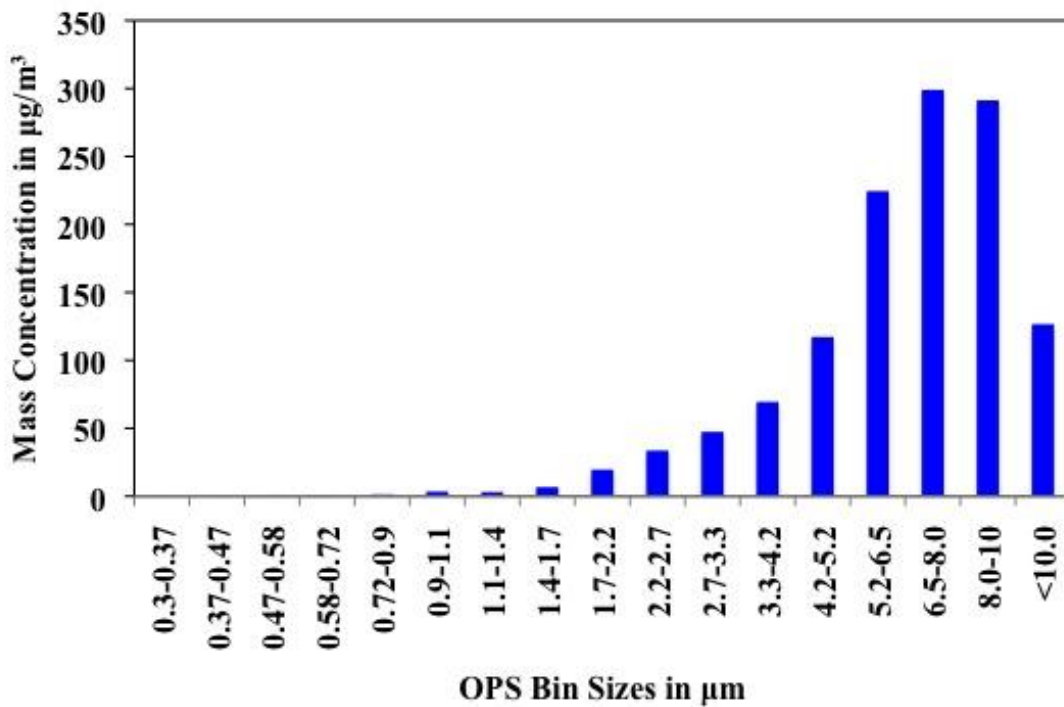
Figure 4-3. Optical Particle Sizer (OPS) measured the size distribution of $NaHCO_3$ produced by the aerosol generator. The finest size measured was 0.374 microns.
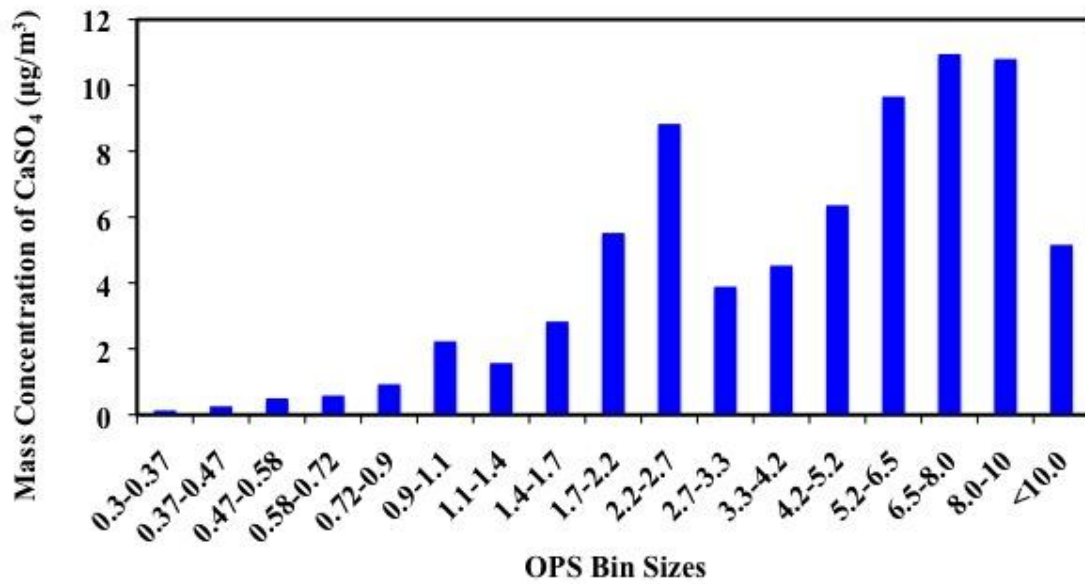
Figure 4-4. Optical Particle Sizer measured the size distribution of $CaSO_4$ produced by the aerosol generator.   The finest size measured was 0.3 microns.
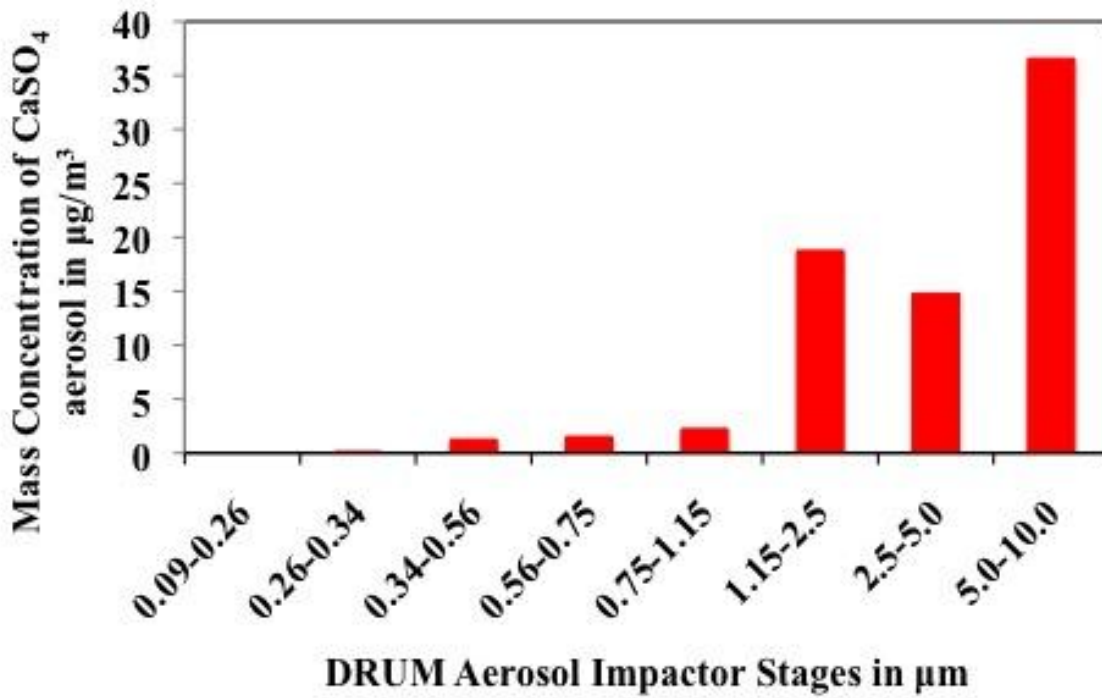
Figure 4-5. OPS size bins were combined to fit within the DRUM aerosol impactor stages. The finest measurable size fraction was stage 7 (0.26-0.34 microns).
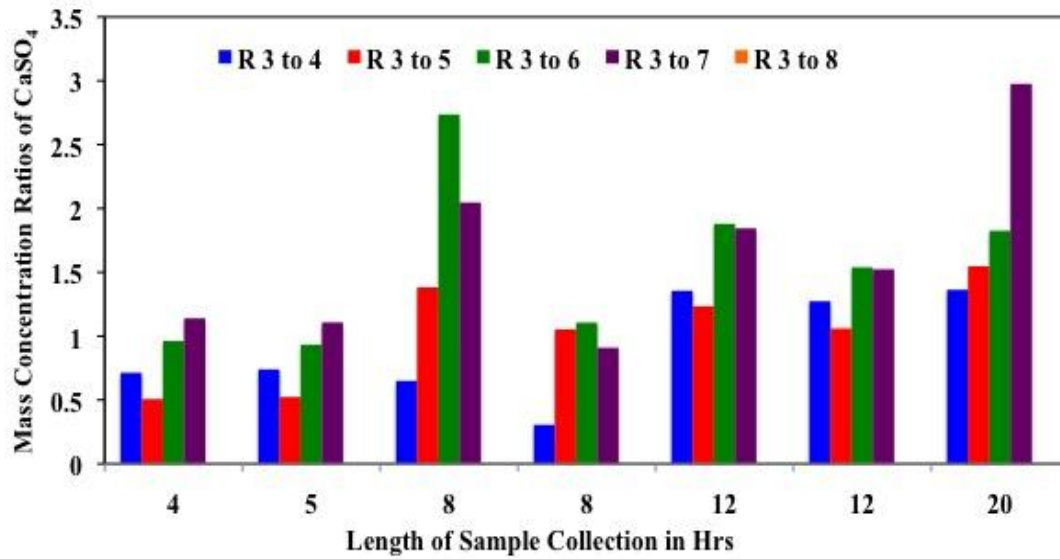
Figure 4-6. Mass concentration ratios between the DRUM impactor's size fractions 3 (1.15-2.5), 4 (0.75-1.15), 5 (0.56 -0.75 μm), 6 (0.34-0.56 μm), 7 (0.26 – 0.34μm), and 8 (0.09 – 0.26 μm). It should be noted that no peak appears for ratio stages 3 to 8. Stage 8 did not have sufficient mass to be considered.
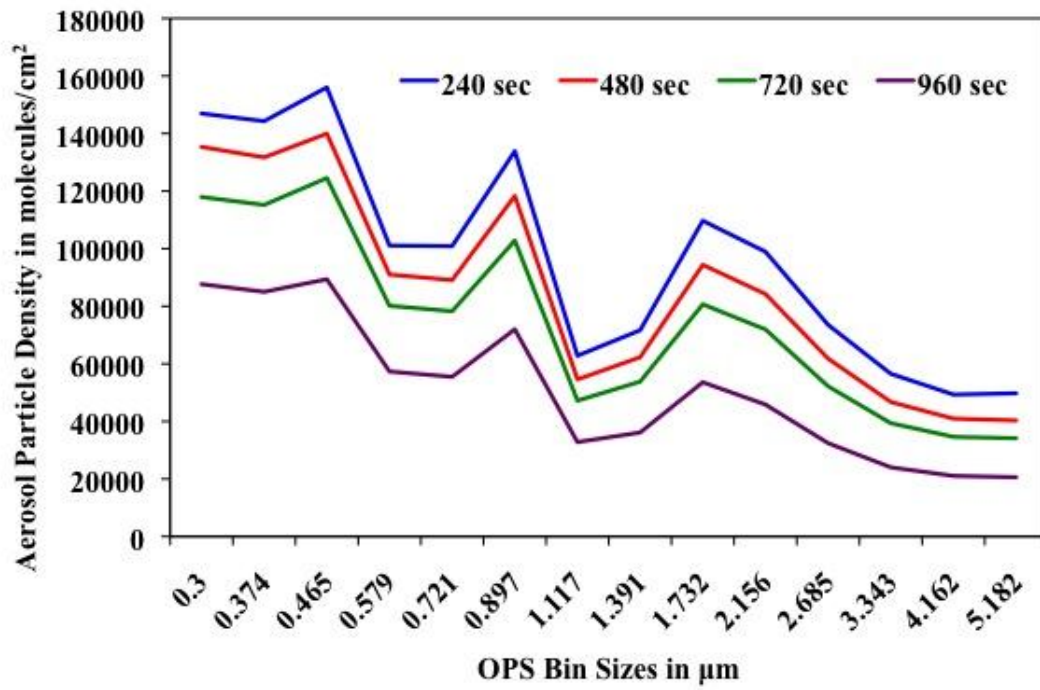
Figure 4-7. A decrease of particles are generated by the FBAG over time.
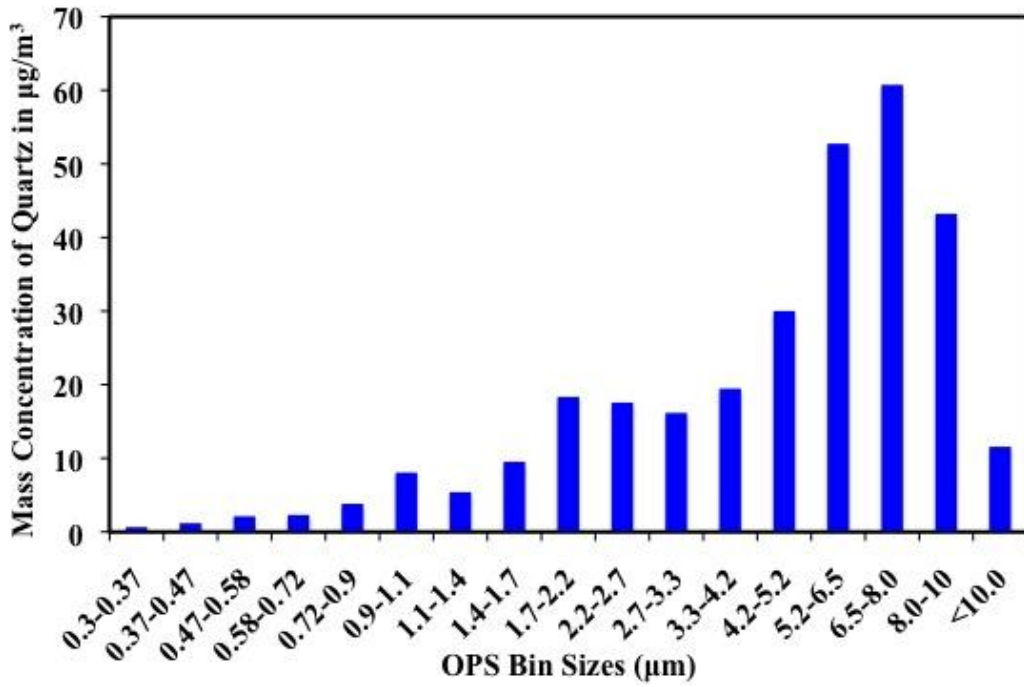
Figure 4-8. Optical Particle Sizer determined the mass concentration in each OPS bin range for quartz.
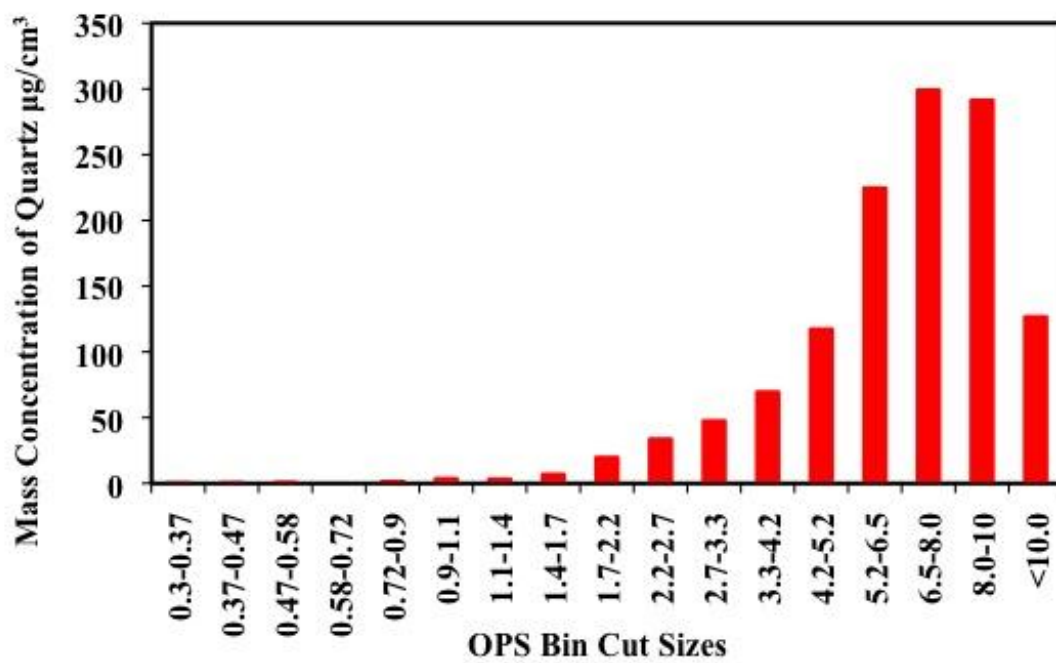
Figure 4-9. Optical Particle Sizer determined the mass concentration in each OPS bin range for quartz under high wind conditions.
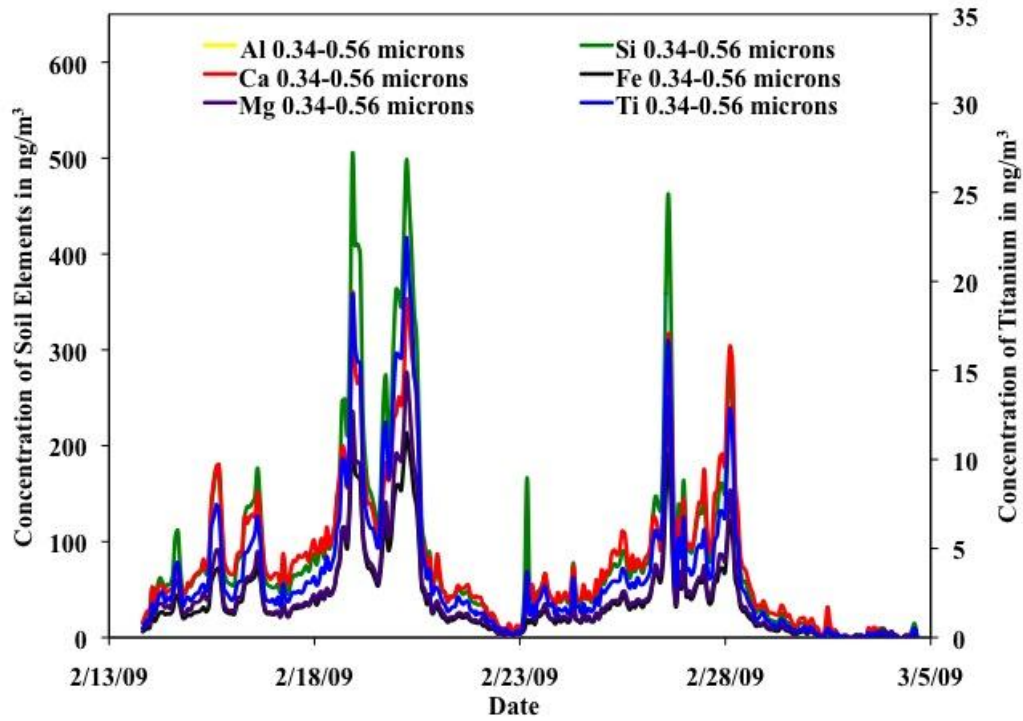
Figure 4-10. Time series of the soil elements Al, Si, Ca, Mg, Ti, and Fe in the 0.34-0.56 micron size fraction. The concentration of Ti is on the secondary axis. This figure shows the presence of soil within the fine aerosols.
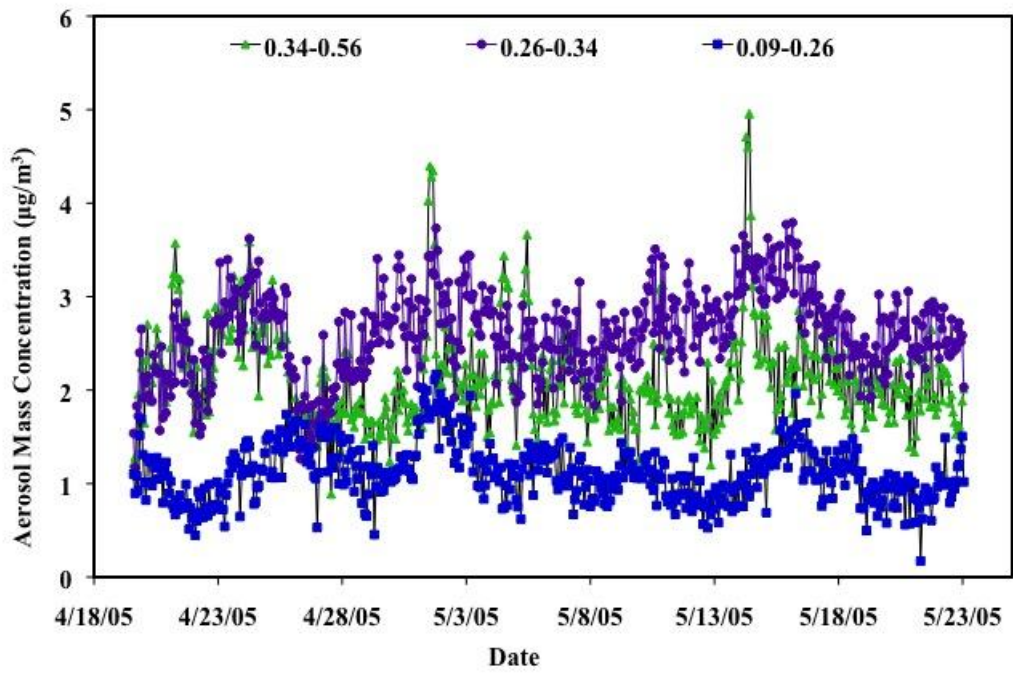
Figure 4-11. Aerosol mass concentration for 0.09 to 0.56 μm aerosols collected by the DRUM sampler at Space Harbor, White Sands, NM (Cahill et al., 2005).
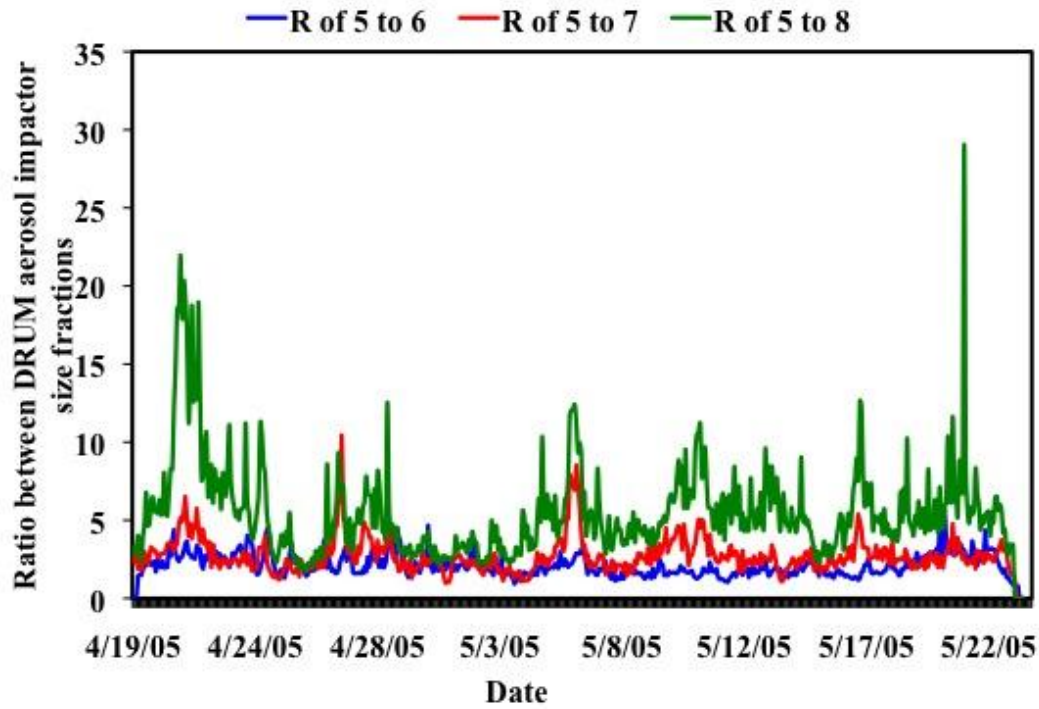
Figure 4-12. This figure shows the ratios between stages 5 (0.56 -0.75 μm), 6 (0.34-0.56 μm), 7 (0.26 – 0.34μm), and 8 (0.09 – 0.26 μm) for aerosol samples collected by the DRUM sampler from Space Harbor.

4.8   Tables

Table 4-1. Chemical summary information for minerals analyzed.

Substrate	Mineral Name	Chemical Composition	Mass (g/mol)	Density (g/cm^3)	Moh Hardness
Calcium sulfate	Gypsum	$CaSO_4$	136.15	2.96	2
Sodium bicarbonate	Nahcolite	$NaHCO_3$	84.01	2.2	2.5
Silicon dioxide	quartz	SiO_2	60.09	2.65	7

Table 4-2. Mass concentrations of CaSO$_4$ aerosols on stages 3-8 (0.09-2.5 microns) in laboratory tests. The finest fraction of detectable aerosols range from 0.26 – 0.34 µm.

Sample Duration (hr)	Aerosol DRUM Stages Mass Concentration (µg/m^3)					
	0.09-0.26	0.26-0.34	0.34-0.56	0.56-0.75	0.75-1.15	1.15-2.5
5	ND	3.76	9.6	ND	ND	14.8
8	ND	5.6	ND	11.3	24.2	39.3
20	ND	5.5	15	44.5	57.5	72.5
5	ND	3.5	9.5	ND	9.9	24
8	ND	4.4	ND	7.8	20.8	35
12	ND	8	ND	17	30.6	45

4.9   References

Al-Dabbas, M.A.; Abbas, M.A.; Al-Khafaji, R.M.   Dust storm loads analysis Iraq.   Arabian Journal of Geosciences. **2012,** 5, 121-131. doi: 10. 1007/s12517-010-0181-7.

Al-Hurban, A.E.; Al-Ostad, A.N.   Textural characteristics of dust fallout and potential effect on public health in Kuwait City and suburbs.   Environmental Earth Sciences. **2010**, 60(1), 169-181.

Alfaro, S.C.; Gomes, L.   Modeling mineral aerosol production by wind erosion: Emissions intensities and aerosol size distribution in source areas.   Journal of Geophysical Research: Atmospheres. **2001**, 106 (D16), 18075-18084.

Altun, N. E.; Hiçyilmaz, C.; Hwang, J.Y.; Suat Bağci, A.; Kök, M. V.   Oil shales in the world and Turkey; reserves, current situation and future prospects: a review (PDF).   *In: Oil Shale. A Scientific-Technical Journal*; Estonian Academy Publishers. **2006**; 23(3), 211–227. ISSN 0208-189X.

Awadh, S.M.   Geochemistry and mineralogical composition of the airborne particles of sand dunes and dust storms settled in Iraq and their environmental impacts.   Environmental Earth Sciences. **2012**, 66(8), 2247-2256. doi:10.1007/s/12665-011-1445-6.

Bellen, R.C.; Van Dunnington, H.V.; Wetzel, R; Morton, D.   Lexique Stratigraphique Intern. Asie. Iraq. Intern. Geol. Conger. Comm. Stratigr. **1959**, 3, 10a, 333.

Bench, G.; Grant, P.; Ueda, D.; Cliff, S.; Perry, K.D.; Cahill T.A.   The use of STIM and PESA to measure profiles of aerosol mass and hydrogen content, respectively, across mylar rotating drums impactor samples.   Aerosol Science and Technology. **2002**, 36, 642-651.

Butler, H.J.; McTainsh, G.H.; Hogarth, W.L.   Simulations of spatial variability in particle-size emissions during wind erosion events.   Earth Surface Processes and Landforms. **2012**, 37(13), 1362-1375.

Cahill, T.A.; Barnes, D.E.; Velarde, R.; Gill, T.   Tracking sources of fugitive dust at Nipomo Mesa, California. In: Ascough II, J.C.; Flanagan, D.C.; Nieber, J.L., Eds.; American Society of Agricultural and Biological Engineers (ASABE) - International Symposium on Erosion and Landscape Evolution. **2011**, 147-155.

Cahill, C.F.; Rinklef, P.G.; Dehn, J.; Webley, P.W.; Cahill, T.A.; Barnes, D.E.   Aerosol measurements from a recent Alaskan volcanic eruption: Implication for volcanic ash transport predictions. Journal of Volcanology and Geothermal Research. **2010**, 76-80.

Cahill, T. A.; Barnes, D. E. Comparison of Fine Mass, UC Davis DRUM versus FRM, at the Air Resources Board 13th and T Street Site. Final Report to the California ARB, Sacramento, CA. **2009**.

Cahill, C.F.; Yee, Y.; Gill, T.E.; Ruiz, A.; Emmert, S.P.; Cahill, T.A.; Wilson, F.; Ellison, E. Springtime dust aerosols at White Sands Missile Range, New Mexico. Eos. Transactions American Geophysical Union. 86(52), Fall Meeting Supplement. **2005**, Abstract P22B-02.

Cahill, T.A.; Goodart, C.; Nelson, J.W.; Eldred, R.A.; Nasstrom, J.S.; Feeney, F.J. Design and evaluation of the DRUM impactor. In: *Proceedings of the International Symposium on Particulate and Multiphase Processes*. Ariman, T.; Veziroglu, T. Eds.; Hemisphere Publishing Corporation. **1985**, 2, 319-325.

Cahill, T.A.; Wakabayashi, P. Compositional analysis of size-segregated aerosol samples. *In: Measurement Challenges in Atmospheric Chemistry*. Newman, L., Ed.; American Chemical Society. **1993**, 211-228.

Cahill, T.A.; Eldred, R.A.; Barone, J.; Ashbaugh, L. Ambient Aerosol Sampling with Stacked Filter Units. Federal Highway Administration, Washington, D.C. **1979**.

Carneiro, M.V.; Araújo, N.A.M.; Pähtz, T.; Herrmann, H.J. Midair collisions enhance saltation. Physical Review Letters. **2013**, 111, 058001. doi:10.1103/PhysRevLett.111.058001.

Chueinta, W.; Hopke, P.K. Beta gauge for aerosol mass concentrations. Aerosol Science and Technology. **2001**, 35(4), 840-843.

Collins, R.L.; Fochesatto, J.; Sassen, K.; Webley, P.W.; Atkinson, D.E.; Dean, K.; Cahill, C.F.; Mitzutani, K. Predicting and validating the motion of an ash cloud during the 2006 eruption of Mount Augustine Volcano, Alaska, USA. Journal of the National Institute of Information and Communications Technology. **2007**, 54(1/2), 17-28.

Courtney, W.; Shaw, R.W.; Dzubay, T.G. Precision and accuracy of a B-Gauge for aerosol mass determinations. Environmental Science and Technology. **1982**, 16, 236-239.

Dyni, J.R. Geology and resources of some world oil-shale deposits: U.S. Geological Survey Scientific Investigations Report 2005-5294. **2006**, 42. [Online] World Wide Web: http://www.usgs.gov/sir/2006/5294.

Engelbrecht, J.P.; McDonald, E.V.; Gillies, J.A.; Jayanty, R.K.M.; Casuccio, G.; Gertler, A.W. Characterizing mineral dusts and other aerosols from the Middle East – Part 1: Ambient sampling, Inhalation Toxicology. **2009**, 21, 297-326. doi:10.1080/08958370802464273.

Faure, G. Principles and Applications in Geochemistry, 2nd ed., Prentice Hall: New Jersey, **1998**, 46-51.

Gordon, G.E.; Gladney, E.S.; Ondov, J.M.; Conry, T.; Zoller, W.H. Problems with the use of cascade impactors. Proceedings of the Annual National Science Foundation Trace Contaminants Conference (National Science Foundation) 1973. Pub. **1974**, 138-145.

Greenfield, S. Rain scavenging of radioactive particulate matter from the atmosphere. Journal of Meteorology. **1957**, 14, 115–125.

Kok, J.F. A scaling theory for the size distribution of emitted dust aerosols suggests climate models underestimate the size of the global dust cycle. Proceedings of the National Academy of Sciences of the United States of America. **2011a**, 108(3), 1016-1021.

Kok, J.F. Does the size distribution of mineral dust aerosols depend on the wind speed at emission? Atmospheric Chemistry and Physics. **2011b**, 11 10149-56.

Lee, R.E.; Goranson, S.S.; Enrione, R.E.; Morgan G.B. National air surveillance cascade impactor network-II. Size distribution measurements of trace metal components. Environmental Science and Technology. **1972**, 6, 1025-1030.

Lundgren, D.A. An Aerosol Sampler for Determination of Particle Concentration as a function of Size and Time. Journal of the Air Pollution Control Association. **1967**, 17, 225-229.

Middleton, N.J.; Goudie, A.S. Saharan dust: sources and trajectories: Transactions of the Institute of British Geographers, New Series. **2001**, 26 (2), 165-181.

Misconi, H.; Navi, M. Medical geology in the Middle East. International Year of the Planet Earth. **2010**, 135-174. doi: 101007/978-90-481-3430-4_6.

Mitchell, R.J.; Pilcher, J.M. Design and calibration of an improved cascade impactor for size analysis of aerosols. 5th AEC AIR Cleaning Conference, 24-27 June, 1957, Office of Technical Services. Washington D.C., 67-83. **1957**.

Raabe, O.G.; Braaten, D.A.; Axelbaum, R.L.; Teague, S.V.; Cahill, T.A. Calibration studies of the DRUM impactor. Journal of Aerosol Science. **1988**, 19 (2), 183-195.

Seinfeld, J.H.; Pandis, S.N. *Atmospheric Chemistry and Physics: From Air Pollution to Climate Change*, 2nd ed.; J. Wiley, New York. **1998.**

Shahsavani, A.; Naddafi, K.; Haghighifard, N.J.; Mesdaghinia, A.; Yunesian, M.; Nabizadeh, R.; Arhami, M.; Yarahmadi, M.; Sowlat, M.H.; Ghani, M.; Jarahi, A.J.; Alimohamadi, M.; Motevalian, S.A.; Soleimani, Z. Characterization of ionic composition of TSP and PM10 during the Middle Eastern Dust (MED) storms in Ahvaz, Iran. Environmental Monitoring and Assessment. **2012**, 184 (11), 6683-6692. doi: 10.1007/s10661-011-2451-6.

Shao, Y.P.; Ishizuka, M.; Mikami, M.; Leys, J.F. Parameterization of size-resolved dust emission and validation with measurements. Journal of Geophysical Research: Atmospheres. **2011**, 116, D08203. doi:10.1029/2010JD014527.

Sow, M.; Alfaro, S.C.; Rajot, J.L.; Marticorena, B. Size resolved dust emission fluxes measured in Niger during 3 dust storms of the AMMA experiment. Atmospheric Chemistry and Physics. **2009**, 9 (12), 3881-3891. doi:10.1016/j.atmosres.2011.08.010.

Tarbuck, E.J.; Lutgens, F.K.; Tasa, D.G. Earth: Matter and Mineral. *In: An Introduction to Geology. 11th ed.,* Dunway, A., Eds.; Upper Saddle River, NJ. **2013**; 81-115.

Vincent, J.H. Aerosol Sampling: Science, Standards, Instrumentation, and Applications. 1st ed.; John Wiley and Sons, Ltd. The Atrium, Southern Gate, Chichester, West Sussex PO19 8SQ, England. **2007**.

Wesolowski, J.J.; Alcocoet, A.; Appel, B.R. The validation of the Lundgren impactor. Hutchinson Me-morial volume on the ACHEX studies in California. **1978**.

Wetzel, M.A.; Shaw, G.E.; Slusser, J.R.; Borys, R.A.; Cahill, C.F. Physical, chemical, and ultraviolet radioactive characteristics of aerosol in Central Alaska. Journal of Geophysical Research. **2003**, 108 (D14), 4418, doi:10.1029/2002D003208.

Whitby, K.T.; Charlson, R.E.; Wilson, W.E.; Stevens, R.K. The size of suspended particle matter in air. Science. **1974**,183, 1098-1100.

Whitby, K.T.; Cantrell, B.K. Proceedings of the International Conference on Environmental Sensing and Assessment (ICESA), Institute of Electrical and Electronic Engineers (IEEE) 1976. Atmospheric aerosols: characteristics and measurement. **1976**, IEEE #75-CH 1004-1, ICESA paper 29-1, Washington, DC: IEEE. p. 6.

Yu, Q.L.; Brouwers, H.J.H. Microstructure and mechanical properties of β-hemihydrate produced gypsum: An insight from its hydration process. Construction and Building Materials, **2011**, 25, 3149–3157.

Chapter 5 Conclusion

This dissertation describes the results from a sampling campaign in Baghdad, Iraq, designed to collect continuous high temporal resolution aerosol size and composition data for use in epidemiological studies. The studies that comprise this dissertation address the limitations of previous studies conducted in the same region. To overcome inherent problems associated with one day in six sampling techniques and limited size segregation, an 8-stage DRUM aerosol impactor was used in this study to obtain 1.5 hour resolution mass concentration, particle size (between 0.09 and 10 microns in aerodynamic diameter), and elemental composition data during three week sampling campaigns. The results of these analyses are described in the following sections.

5.1   Sources of Iraqi Aerosols

Results from the sources and source regions study (Chapter 2) demonstrate that Iraqi aerosols result from numerous natural and anthropogenic sources. Aerosols containing lead and sulfur result from local fossil fuel combustion, smelting operations, the continued use of leaded fuel, and the lofting and transport of Pb enriched soil/deposits and gypsum-laden dusts. The presence and accumulation of V, in the absence of wind drainage, is a good indicator of local fossil fuel combustion, smelting, and mining activities. Bromine (Br) and S appearing together serve as an indicator of sea salts and when Br appears with Pb it correlates to anthropogenic source emissions of leaded fuel and smelting activities. Elemental soil ratios were consistent across all aerosol size fractions and matched the elemental abundances found in the earth's crust. The discovery of the crustal elemental abundances in particles in the finest size fractions means there are geogenic crustal particles in the finest size fractions and that current hypotheses for dust

185

particle generation need to be revised to include an Aiken nuclei generation mechanism for soil particles. The ambient particulate Pb concentrations routinely exceed the U.S. National Ambient Air Quality Standards (NAAQS) for lead, which implies that there may be adverse health effects associated with breathing the Iraqi aerosol.

5.2   Geological Findings and Brittle Fragmentation

Elemental analyses, SEM images of individual particles, meteorological analyses, and a brittle fragmentation model were used to determine the sources and production mechanisms for the ultra-fine dust aerosols found in this study. As described in Chapter 2, the presence of high concentrations of soil aerosols in the finest size fraction (0.09-0.26 μm in aerodynamic diameter) was surprising because most hypotheses about the generation of soil particles do not produce particles of this size. The meteorological analyses in Chapter 3 determined the fine particles only occurred under windy conditions. This implied the source of these particles was not a result of local anthropogenic source emissions, which are higher under still air conditions. Wind roses, HYSPLIT meteorological backwards trajectories, and the aerosol composition show that although there are differences between the aerosols impacting the site during Shamal and Kous wind conditions, the finest size fraction of soil aerosols is produced under both Shamal and Kous wind conditions. The conclusion from these results is that a mechanism exists for the production of Aitken mode geogenic particles from desert surfaces.

The soil data collected during this study agree with Kok's (2011a) brittle fragmentation hypothesis during low wind situations; however, the high mass concentration of soil particles in the finest size fraction produced during high wind situations, does not agree with Kok's brittle fragmentation hypothesis. Therefore, brittle fragmentation, which is hypothesized to be

independent of wind speed, may provide one mechanism for generating the small crustal particulates observed in the data, but it is not the only explanation. The data presented in this study show wind velocity plays a significant role in the fragmentation process and fine particle production. The combination of hypotheses put forward in recent papers by Carneiro et al. (2013) and Butler et al. (2012) could explain the deviation from the brittle fragmentation model because they describe a fine particle production model in high wind, dust storm conditions that would lead to additional particle break down during particle transport in a dust plume. These hypotheses are worthy of further testing to determine in they can explain the size distributions observed in the Camp Victory aerosol data.

5.3   Aerosol Loading of Brittle Minerals on the 8-Stage DRUM Impactor

To ensure that particles seen in the finest size fractions (Chapters 2 and 3) were not produced as a result of particle breakdown in the DRUM aerosol impactor during sampling, a laboratory calibration study was conducted (Chapter 4) on an 8-stage DRUM aerosol impactor. The purpose of this study was to prove that brittle minerals (calcium sulfate, sodium bicarbonate, and finely ground quartz) representative of mineral types found in Iraq would not fragment during impaction and to quantify the effects of high mass loading conditions on particle sizing. The study specifically examined whether the high concentrations of soil particles in the finest size fraction observed in the Iraqi samples could be explained via instrumental design flaws.

Laboratory results show that particles are not fragmenting in the DRUM aerosol impactor across the range of mass loadings despite different wind conditions. The mass concentrations decrease in each successive stage for the smaller size fractions as expected, implying that there are no small particle production mechanisms occurring in the sampler. Additionally, the dust

concentrations on the DRUM stages were consistent with the particle distributions measured using the OPS, so no particle loss or production was occurring in the inlet and sampler.

The results of the Iraqi field campaign and field measurements collected from White Sands, NM are consistent with this study and show no evidence of a mechanical break down of the aerosols within the sampler. Further, the results imply that the presence of fine and ultrafine soil particles (<2.5 μm) in the field samples is a result of production from environmental geogenic processes. This suggests the DRUM cascade impactor is functioning as designed and its size-cut calibrations are consisted with Raabe et al. (1988).

5.4   Future Work

The production of ultra-fine particles found within desert dust storms seem to result from a combination of several factors that should be investigated further. Specifically studies could evaluate how entrained particles interact with other particles and whether this interaction results in finer particle production. The role of midair collisions and their relationship to the strength and duration of the dust cloud could be examined further to quantify their effects on fragmentation. Studies should address whether midair collisions and increased travel distances can account for the size distributions observed in the data collected during this study.

Future studies can confirm the effectiveness of the DRUM aerosol impactor as a quantitative aerosol collection device and verify the uniformity of the samples across the 1 cm high sample deposit through scanning electron microscopy (SEM). Then elemental mass could be evaluated and validated using synchrotron x-ray fluorescence analysis to confirm the results. The additional analysis could provide specific information on the behavior of quartz particles during sampling.

188

The unique and valuable data set presented in this thesis should be used to assess future potential adverse health effects associated with the inhalation of the Iraqi aerosols. The concentrations of lead and other elements suggest that there may be long-term impacts from soldiers' exposure to the Iraqi air. Epidemiologists should combine the results of the elemental analysis with information on soldiers' health and exposure to Iraqi air. If correlations between specific aerosol components and morbidity are discovered, the causality of the relationship can be investigated and steps to mitigate the effects can be explored and implemented. Hopefully, the results of these studies will lead to new ways to protect U.S. soldiers and civilians from the dangers of ambient aerosols.

5.5 References

Abdalmogith, S.S.; Harrison, R.M. The use of trajectory cluster analysis to examine the long-range transport of secondary inorganic aerosols in the UK. Atmospheric Environment. **2005**, 39, 6686-6695.

Alfaro, S.C.; Gomes, L. Modeling mineral aerosol production by wind erosion: Emissions intensities and aerosol size distribution in source areas. Journal of Geophysical Research: Atmospheres. **2001**, 106 (D16), 18075-84.

Al-Hurban, A.E.; Al-Ostad, A.N. Textural characteristics of dust fallout and potential effect on public health in Kuwait City and suburbs. Environment Earth Sciences. **2010**, 60(1), 169-181.

Ali, A.H. Wind regime of the Arabian Gulf. *In: The Gulf War and the Environment*. El-Baz, F. and Makharita, R.M. Eds.; Amsterdam, B.V. **1994**, 31-48.

Astrom, J.A. Statistical models of brittle fragmentation. Advances in Physics. **2006**, 5(3-4), 247-278.

Astrom, J.A.; Ouchterlony, F.; Linna, R.P.; Timonen, J. Universal dynamic fragmentation in D dimensions. Physical Review Letters. **2004**, 92:245506.

Astrom, J.; Timonen, J. Fragmentation by crack branching. Physical Review Letters. **1997**, 78 3677-3680

Auger, J.; Kunstmann, J.M; Czyglik, F. Decline in semen quality among fertile men in Paris during the past 20 years. New England Journal of Medicine. **1995**, 332, 281-285.

Awadh, S.M. Geochemistry and mineralogical composition of the airborne particles of sand dunes and dust storms settled in Iraq and their environmental impacts. Environmental Earth Sciences. **2012**, 66(8), 2247-2256. doi:10.1007/s12665-011-1445-6.

Barberie, S.R.; Cahill, A.; Cahill, C.F.; Cahill, T.M.; Iceman, C.R.; Barnes, D.E. UC Davis XIPline ("zipline") end-station at the Stanford Synchrotron Radiation Lightsource: Development and experimental results. Nuclear Instruments and Methods in Physics Research Section A: Accelerators, Spectrometers, Detectors and Associated Equipment. **2013**, 729(21), 930-933.

Bates, D.J. Health indices of the adverse effects of air pollution: The question of coherence. Environmental Research. **1992**, 59, 336-49.

Bell, M.L.; Davis, D.L. Reassessments of the lethal London fog of 1952: Novel indicators of acute and chronic consequences of acute exposure to air pollution. Environmental Health Perspectives. **2001**, 109(3), 389-394.

Bench, G.; Grant, P.; Ueda, D.; Cliff, S.; Perry, K.; Cahill T. The use of STIM and PESA to measure profiles of aerosol mass and hydrogen content, respectively, across mylar rotating drum impactor samples. Aerosol Science and Technology. **2002**, 36, 642-651.

Bem, H.K.; Bou-Rabee, F. Environmental and health consequences of depleted uranium use in the 1991 Gulf War. Environment International. **1997**, 30, 123-134.

Benoff, S.; Hurley, I.R.; Barcia, M.; Mandell, F.S; Cooper, G.W.; Hershlag, A. A potential role for cadmium in the etiology of varicocele-associated infertility. Fertility and Sterility. **1997**, 67(2), 336-347.

Brimblecombe, P. History of air pollution. *In: Composition, Chemistry and Climate of the Atmosphere*. Singh, H.B., Ed.; Van Nostrand Reinhold, New York. **1995**, 1-18.

Buringh, P. Soils and Soil Conditions in Iraq. Republic of Iraq. Ministry of Agriculture. Directorate General of Agricultural Research and Projects. **1963**.

Butler, H.J.; McTainsh, G.H.; Hogarth, W.L. Simulations of spatial variability in particle-size emissions during wind erosion events. Earth Surface Processes and Landforms. **2012**, 37(13), 1362-1375.

Byers, R.K.; Lord, E.E. Late effects of lead poisoning on mental development. The American Journal of Diseases of Children. **1943**, 66, 471-494.

Cahill, C.F.; Rinkleff, P.G.; Dehn, J.; Webley, P.W.; Cahill, T.A.; Barnes, D.E. Aerosol measurements from a recent Alaskan volcanic eruption: Implication for volcanic ash transport predictions. Journal of Volcanology and Geothermal Research. **2010**, 76-80.

Cahill, C.F. Technical Proposal. Department of defense enhanced particulate matter surveillance program (EPMSP). Prepared to investigate technologies and design and to fabricate instrumentation for rapid characterization of airborne threats. University of Alaska, Fairbanks, AK. **2009**.

Cahill, C.F. Asian Aerosol Transport to Alaskas during ACE-Asia. Journal of Geophysical Research. **2003**, 108 (D23), 8664, doi:10.1029/2002JD003271.

Cahill, T.A.; Cliff, S.S.; Perry, K.D.; Jimenez-Cruz, M.P.; McHugo, S.A. Size and time resolved anthropogenic components of aerosols via synchrotron x-ray fluorescence: application to Asian aerosol transport. *In Abstracts, Amer. Geophys. Union 1999 Fall Mtg, December 13-17, 1999, San Francisco, California*. American Geophysical Union. **1999**.

Cahill, T.A.; Goodart, C.; Nelson, J.W.; Eldred, R.A.; Nasstrom, J.S.; Feeney, F.J. Design and evaluation of the DRUM impactor. In: *Proceedings of the International Symposium on Particulate and Multiphase Processes*. Ariman, T.; Veziroglu, T., Eds.; Hemisphere Publishing Corporation. **1985**, 2, 319-325.

Cahill, T.A.; Wakabayashi, P. Compositional analysis of size-segregated aerosol samples. *In: Measurement Challenges in Atmospheric Chemistry.* Newman, L., Ed.; American Chemical Society. **1993**, 211-228.

Carneiro, M.V.; Araújo, N.A.M.; Pähtz, T.; Herrmann, H.J. Midair collisions enhance saltation. Physical Review Letters. **2013**, 111, 058001. doi:10.1103/PhysRevLett.111.058001.

Chueinta, W.; Hopke, P.K. Beta Gauge for Aerosol Mass Measurement. Aerosol Science and Technology. **2001**, 35(4), 840-843.

Clarke, A.D.; Collins, W.G.; Rasch, P.J.; Kapustin, V.N.; Moore, K.; Howell, S.; Fuelberg, H.E. Dust and pollution transport on global scales: aerosol measurements and model predictions. Journal of Geophysical Research. **2001**,106, 32555–32569.

Collins, R.L.; Fochesatto, J.; Sassen, K.; Webley, P.W.; Atkinson, D.E.; Dean, K.; Cahill, C.F.; Mitzutani, K. Predicting and validating the motion of an ash cloud during the 2006 eruption of Mount Augustine Volcano, Alaska, USA. Journal of the National Institute of Information and Communications Technology. **2007**, 54(1/2), 17-28.

Cong, Z.; Kang, S.; Liu, X.; Wang, G. Elemental composition of aerosols in the Nam Co region, Tibetan Plateau, during summer monsoon season. Atmospheric Environment. **2007**, 41(6), 1180-1187.

Cullen, M.R.; Robins, J.M.; Eskenazi, B. Adult inorganic lead intoxication: Presentation of 31 new cases and a review of recent advances in the literature. Medicine (Baltimore). **1983**, 62, 221-247.

Davis D.L. Air pollution risks to children: A global environment health problem. Environmental Manager. **2000**, 31-37.

Dockery, D.W.; Pope III, C.A. Acute respiratory effects of particulate air pollution. Annual Review of Public Health. **1994**, 15, 107-132.

Dockery, D.W.; Speizer, F.E.; Stram, D.O.; Ware, J.H.; Spengler, J.D. Effects of inhalable particles on respiratory health of children. American Review of Respiratory Disease. **1989**, 139, 587-594.

Draxler, R.R.; Hess, G.D. An overview of the HYSPLIT_4 modeling system of trajectories, dispersion, and deposition. Australian Meteorology Magazine. **1998**, 47, 295-308.

Dzubay, T.G.; Hines, L.E.; Stevens, R.K. Particle bounce errors in cascade impactors. Atmospheric Environment. **1976**, 10, 229-234.

Engelbrecht, J.P.; McDonald, E.V.; Gilles, J.A.; Jayanty, R.K.M.; Casuccio, G.; Gertler, A.W. Characterizing mineral dusts and other aerosols from the Middle East − Part 1: Ambient sampling. Inhalation Toxicology. **2009**, 21, 297-326. doi:10.1080/08958370802464273.

Evelyn, J. Fumifugium. *In: The writings of John Evelyn*. Boydell and Brewer. Woodbridge. **1995**.

Escudero, M.; Stein, A.; Draxler, R.R.; Querol, X.; Alastuey, A.; Castillo, S.; Avila, A. Determination of the contribution of northern Africa dust source areas to PM_{10} concentrations over the Central Iberian Peninsula using Hybrid Single Particle Langragian Integrated Trajectory model (HYSPLIT) model. Journal of Geophysical Research: Atmospheres (1984-2012). **2006**, 111 (D8), 27.

Federal Register. Rules and Regulations. **2006**, 71(200), 61236-61328.

Fineberg, J.; Marder, M. Instability in dynamic fracture. Physics Reports. **1999**, 313, (1-2), 1-108.

Firket, J. Fog along the Meuse Valley. Transactions of the Faraday Society. **1936**, 32, 1192-1197.

Foda, M.S.; Salama, H.S.; Selim, M. Factors affecting growth physiology of Bacillus thuringiensis. Applied Microbiology and Biotechnology. **1985**, 22, 50-52.

Friedlander, G.; Kennedy, J.W.; Macias, E.; Miller, J. M. Nuclear and Radiochemistry, 3rd ed., John Wiley & Sons, New York. **1981**, 222.

Gillette, D.A. On the production of soil wind erosion having the potential for long-range transport. Journal of Recherches Atmospheriques. **1974**, 8, 734-744.

Hamdan, F. The ecological crisis in Lebanon. *In: Lebanon's second republic: prospects for the twenty-first century.* Ellis, K., Ed.; Gainesville: University Press of Florida: **2002**, 175-187.

Hopke, P. Contemporary threats and air pollution. Atmospheric Environment. **2009**, 43, 87-93.

Husar, R.B.   Atmospheric Particulate Mass Monitoring with a β Radiation Detector. Atmospheric Environment. **1974**, 8, 183-188.

ICRP-72. International commission on Radiological Protection Annals: Part 4. Inhalation dose coefficients.   Age dependent.   Doses to members of the public from intake of radionuclieds. **1995**, 25(3-4).

Inhorn, M.C.; King, L.; Nriagu, J.O.; Kobeissi, L.; Hammond, N.; Awwad, J.; Abu-Musa, A.A.; Hannoun, A.B. Occupational and environmental exposure to heavy metals: risk factors for male infertility in Lebanon? *Reproductive Toxicology*. [Online] **2008**, 25, 203-212.

Inhorn, M.C. Middle Eastern masculinities in the age of new reproductive technologies: male infertility and stigma in Egypt and Lebanon. Medical Anthropology Quarterly. **2004**, 18, 162-82.

Katsouyanni, K.; Zmirou, D.; Spix, C.; Sunyer, J.; Schouten, J.P.; Pönkä, A.; Anderson, H.R.; Le Moullec, Y.; Wojtyniak, B.; Vigotti, M.A.; Bacharova, L.   Short-term effects of air pollution on health: A European approach using epidemiological time-series data. European Respiratory Journal. **1995**, 8, 1030-1038.

Kennedy, K. Burn pits provoked concerns from start, health official says. Navy Times (August 17, 2009). [Online] kellykennedy@militarytimes.com (accessed March 17, 2010).

Kok, J.F. A scaling theory for the size distribution of emitted dust aerosols suggests climate models underestimate the size of the global dust cycle. Proceedings of the National Academy of Sciences. **2011a**, 108, 1016-1021.

Kok, J.F. Does the size distribution of mineral dust aerosols depend on the wind speed at emission? Atmospheric Chemistry and Physics. **2011b**, 11, 10149-10156.

Lawson, D.R. Impaction surface coatings: Inter-comparison and measurements with cascade impactors. Atmospheric Environment. **1979**, 14, 195-199.

Li. J.; Okin, G.; Epstein, H. Effects of enhanced wind erosion on surface soil texture and characteristics of windblown dusts. Journal of Geophysical Research-Biogeosciences. **2009**, 114 G02003.

Linna, R.P.; Astrom, J.A.; Timonen, J. Unconstrained periodic boundary conditions for solid-state elasticity. Computer Physics Communications. **2004,** 158, 26.

Lyles, M.B. Naval Institute for Dental and Biomedical Research. Personal communication. **2011**.

Malm, W.C.; Sisler, J.F.; Huffmon, D.; Eldred, R.A.; Cahill, T.A. Spatial and Seasonal trend in particle concentration and optical extinction in the United States. Journal of Geophysical Research. **1994**, 99. doi:10.1029/93JD02916.

McGowan, H.; Clark, A. Identification of dust transport pathways from Lake Eyre. Atmospheric Environment. **2008**, 42(29), 6915-6925.

Membery, D.A. Low level wind profiles during the Gulf Shamal. Weather. **1983**, 38, 18-24.

Ministry of Health. Mortality and Morbidity during the London fog of December 1952. Reports on Public Health and Medical Subjects No 95, London: London Ministry of Health. **1954**.

Misconi, H.; Navi, M. Medical geology in the Middle East. International Year of the Planet Earth. **2010**, 135-174. doi: 101007/978-90-481-3430-4_6.

Moore, K.G.; Clarke, A.D.; Kapustin, V.N.; Howell, S.G. Long-range transport of continental plumes over the Pacific Basin: Aerosol physiochemistry and optical properties during PEM-Tropics A and B. Journal of Geophysical Research. **2003**, 108(D2), 8236, doi:10.1029/2001JD001451.

National Oceanic and Atmospheric Administration. www.ncdc.noaa.gov/oa/climate/afghan/iraq-narrative.html (accessed Jan 29, 2014).

Nemery, B.; Hoet, P.H.M; Abderrahim, N. The Meuse Valley Fog of 1930: An Air Pollution Disaster. Lancet. **2001**, 357, 704-708.

Nickling, W.G.; McTanish, G.H.; Leys, J.F. Dust emission from the Channel Country of western Queensland, Australia Zeitschrift for Geomorphologic Supplement. **1999**, 116, 1-17.

Owens, A. Synchrotron light sources and radiation detector meteorology. Nuclear Instruments and Methods In Physics Research Section A. **2012**, 1-12. doi:10.1016/ j.nima.2011.11.077

Pack, D.H.; Ferber, G.J.; Heffter, J.L.; Telegadas, K.; Angell, J.K.; Hoecker, W.H.; Machta, L. Meteorology of long-range transport. Atmospheric Environment. **1978**, 12, 425-444.

Pecharsky, V.K.; Zavalij, P.Y. Fundamentals of Powder Diffraction and Structural Characterization of Materials. 2nd ed.; Publisher: Springer Publishers. **2009**, 110-119.

Pope III, C.A.; Burnett, R.T.; Thun, M.J.; Calle, E.E.; Krewski, D.; Ito, K.; Thurston, G.D. Lung cancer, cardiopulmonary mortality, and long-term exposure to fine particulate air pollution. Journal of American Medical Association. **2002**, 287, 1132-1141.

Pope III, C.A.; Bates, D.V.; Raizenne, M.E. Health effects of particulate air pollution: Time for reassessment? Environmental Health Perspectives. **1995**, 103(5) 472-480.

Priest, ND. Toxicity of depleted uranium. Lancet. **2001**, 357, 244-246.

Raabe, O.G.; Braaten, D.A.; Axelbaum, R.L.; Teague, S.V.; Cahill, T.A. Calibration studies of the DRUM impactor. Journal of Aerosol Science. **1988**, 19(2), 183-195.

Reid, J.; Reid, E.; Walker, A.; Piketh, S.; Cliff, S.; Mandoos, A.; Tsay, S.C.; Eck, T. Dynamics of southwest Asian dust particle size characteristics with implications for global dust research. Journal of Geophysical: Research-Atmospheres. **2008**, 113(D14), D14212.

Schwartz, J.; Dockery, D.W.; Neass, L.M. Is Daily Mortality Associated Specifically with Fine Particles? Journal of the Air and Waste Management Association. **1996**, 46, 927-936.

Schwartz, J.; Marcus, A. Air pollution and daily mortality: A review and meta-analysis. Environmental Research. **1994**, 64, 36-52.

Schrenk, H.H.; Heimann, H.; Clayton, G.D.; Galafer, W.M.; Wexler, H. Air Pollution in Donora, PA: Epidemiology of the Unusual Smog Episode of October 1948, Preliminary Report. Public Health Bulletin No. 306. Washington, DC U.S. Public Health Service. **1949.**

Scott, J.A. Fog and Deaths in London, December 1952. Public Health Reports. **1953**, 68. 474-479.

Seaton, A.; MacNee, W.; Donaldson, K.; Godden, D. Particulate air pollution and acute health effects. Lancet. **1995**, 345, 176-78.

Serour, G.I. Bioethics in reproductive health: a Muslim's perspective. Middle East Fertility Society Journal. **1996**, 1, 30–35.

Sharon, E.; Fineberg, J. The Micro-Branching Instability and the Dynamic Fracture of Brittle Materials. Physics Review. **1996**, B54, 7128-7139.

Shao, Y. A model for mineral dust emission. Journal of Geophysical Research. **2001**, 106, 20239–20254.

Sheehy, J. Enhanced Particulate Matter Surveillance in USCENTCOM, Presentation #6077. Presented at the 11th Annual Force Health Protection Conference, Albuquerque, New Mexico, August 9-15, **2008**.

Sibrava, V. Geology of Iraq. Jassim, S.Z.; Goff, J.C., Eds.; Dolin, Prague and Moravian Museum, Brno. **2006**.

Sow, M.; Alfaro, S.C.; Rajot, J.L.; Marticorena, B. Size resolved dust emission fluxes measured in Niger during 3 dust storms of the AMMA experiment. Atmospheric Chemistry and Physics. **2009**, 9(12), 3881-3891. doi:10.5194/acp-9-3881-2009.

Stohl, A. Computation, accuracy and applications of trajectories − a review and bibliography. Atmospheric Environment. **1998**, 32(6), 947-966.

Telisman, S.; Cvitkokic, J.J.; Pizent, A. Semen quality and reproductive endocrine function in relation to biomarkers of lead, cadmium, zinc, and copper in men. Environmental Health Perspectives. **2000**, 108, 45-53.

Thoppil, P.; Hogan, P. Persian Gulf response to winter Shamal event. Deep Sea Research I. **2010**, 57, 947-955.

Thurston, G.O.; Ito, K.; Kinney, P.L.; Lippmann, M. A multi-year study of air pollution and respiratory hospital admissions in three New York state metropolitan area: Results for 1998 and 1989 summers. Journal of Exposure Analysis and Environmental Epidemiology. **1992**, 2, 429-450.

Uno, I.; Wang, I.; Chiba, I.; Chun, Y.; Gong, S.; Hara, Y.; Jung, E.; Lee, S.; Liu, M.; Mikami, M.; Music, S.; Mickovic, S.; Satake, S.; Shao, Y.; Song, Z.; Sugimoto, N.; Tanaka, T.; Westphal, D. Dust model intercomparison (DMIP) study over Asia: overview. Journal of Geophysical Research. **2006**, 111, D12213. doi: 10.1029/2005JD006575.

US AEPI. Health and environmental consequences of depleted uranium use in the US Army. US Army Environmental Policy Institute. Technical Report. Georgia Institute of Technology, Atlanta. **1995a**.

U.S. Environmental Protection Agency. www.epa.gov/air/caa/ (accessed January 29, 2014).

U.S. Environmental Protection Agency. www.epa.gov/air/criteria.html (accessed January 29, 2014).

USACHPPM RD 230. Environmental health risk assessment and chemical exposure guidelines for deployed military personnel. Technical Guide 230 [Online] **2013**. http://phc.amedd.army.mil/PHC%20Resource%20Library/TG230.pdf (accessed Jan. 10, 2014)

Vincent, J.H. Aerosol Sampling: Science, Standards, Instrumentation, and Applications. 1st ed.; John Wiley and Sons, Ltd. The Atrium, Southern Gate, Chichester, West Sussex PO19 8SQ, England. **2007**.

Weese, C. Strategies to assess health outcomes associated with particulate matter in the CENTCOM AOR, Presentation # 6082. Presented at the 11th Annual Force Health Protection Conference, Albuquerue, New Mexico, August 9-15, **2008**.

Wetzel, M.A.; Shaw, G.E.; Slusser, J.R.; Borys, R.A.; Cahill, C.F. Physical, chemical, and ultraviolet radioactive characteristics of aerosol in Central Alaska. Journal of Geophysical Research. **2003**, 108 (D14), 4418. doi:10.1029/2002D003208.

Yang, P.; Gao, B.C.; Baum, B.A.; Hu, Y.X.; Wiscombe, W.J.; Mishchenko, M.I.; Winker, D.M.; Nasiri, S.L. Asymptotic solutions for optical properties of large particles with strong absorption. Applied Optics. **2001**, 40, 1532-1547. doi:10.1364/AO.40.001532.

Yin, D.; Nickovic, S.; Sprigg, W. The impact of using different land cover data on wind-blown desert dust modeling results in the southwestern United States. Atmospheric Environment. **2007**, 41, 2214–2224.